

**THE EXPERIMENTAL BEHAVIOR OF STEEL FIBER REINFORCED POLYMER
RETROFIT MEASURES**

by

Patrick Lucien Minnaugh

Bachelor of Science in Civil Engineering, University of Pittsburgh, 2006

Submitted to the Graduate Faculty of
the School of Engineering in partial fulfillment
of the requirements for the degree of
Master of Science

University of Pittsburgh

2006

UNIVERSITY OF PITTSBURGH

SCHOOL OF ENGINEERING

This thesis was presented

by

Patrick Lucien Minnaugh

It was defended on

October 4, 2006

and approved by

Dr. Amir Koubaa, Academic Coordinator and Lecturer,
Department of Civil and Environmental Engineering

Dr. Piervincenzo Rizzo, Assistant Professor,
Department of Civil and Environmental Engineering

Dr. Kent A. Harries, Assistant Professor,
Department of Civil and Environmental Engineering
Thesis Advisor

Copyright © by Patrick Lucien Minnaugh

2006

EXPERIMENTAL BEHAVIOR OF STEEL FIBER REINFORCED POLYMER RETROFIT MEASURES

Patrick Lucien Minnaugh, M.S.

University of Pittsburgh, 2006

Four 10" (254 mm) deep, 6" (152 mm) wide and 186" (4730 mm) long concrete beams having three #4 longitudinal steel reinforcing bars as primary flexural reinforcement, were retrofitted with steel fiber-reinforced polymer (SFRP). A commercially available 4.75 in. (121 mm) wide, 0.048 in. (1.2 mm) thick unidirectional steel fiber reinforced strip system was used along with a commercially available adhesive system. One beam was tested monotonically under simply supported conditions to failure. Three identical beams were tested under midpoint cyclic loading until fatigue-induced failure or 2,000,000 cycles. Any beam that survived 2,000,000 cycles was tested monotonically to failure. Results of the tests were compared to beams that were retrofitted with an equivalent amount of carbon fiber reinforced polymer (CFRP) as determined by the axial stiffness of the material.

The monotonic test revealed that the SFRP specimen showed comparable behavior when compared to the CFRP companion specimens in terms of ultimate load and deflection, general yield load, and deflection ductility. The SFRP specimen was shown to compare poorly in terms of debonding strain. One fatigue specimen achieved 2,000,000 cycles and was subsequently tested monotonically to failure. The behavior of the SFRP system degraded only slightly in terms of each parameter considered; thus it was apparent that SFRP systems may perform well under fatigue conditions. Debonding strains for the SFRP were still shown to be very low, indicating

that the guidance for the mitigation of CFRP specimens may not be appropriate to apply directly to SFRP specimens.

Two of the retrofit fatigue specimens failed due to fatigue-induced rupture of the internal reinforcement prior to achieving 2,000,000 cycles. Observations include stress range drift and degradation of secant stiffness with cycling. Reinforcing bar stresses at the final cycle were noted to increase significantly from the initial cycle. The SFRP was noted to increase the secant stiffness of the retrofit specimens and slow the rate of decay of stiffness when compared to the control fatigue specimen. When results were compared to the CFRP companion specimens, it was apparent that SFRP is an acceptable retrofit and is in some ways superior in terms of fatigue.

TABLE OF CONTENTS

NOMENCLATURE.....	XIII
1.0 INTRODUCTION AND LITERATURE REVIEW.....	1
1.1 INTRODUCTION	1
1.2 OBJECTIVE	2
1.3 SCOPE OF REPORT	3
1.4 LITERATURE REVIEW	3
1.4.1 Description of SFRP Material.....	4
1.4.1.1 Bonding Matrix.....	5
1.4.2 Mechanical Anchorage	6
1.4.3 Use of SFRP U-wraps	7
1.4.4 Geometry of SFRP Retrofit.....	7
1.4.4.1 Different Cord Types.....	7
1.4.4.2 Applying FRP Materials in Varying Widths and Layers	8
1.4.5 SFRP vs. CFRP	10
1.4.6 Field Applications of SFRP	10
1.4.6.1 SFRP Use on Double-Tee Prestressed Concrete Beams.....	10
1.4.6.2 SFRP Use on Reinforced Concrete Bridge.....	11
1.4.6.3 SFRP Use in Restoration of Historic Theatre	12

1.4.7	SFRP Use in Blast Resistant Design	12
1.4.8	Conclusions from Reeve (2005).....	13
1.4.9	Conclusions from Zorn (2006).....	15
2.0	EXPERIMENTAL PROGRAM.....	22
2.1	REINFORCED CONCRETE BEAM TEST SPECIMENS	22
2.2	RETROFIT MEASURES	23
2.3	APPLICATION OF SFRP TO THE TEST SPECIMENS	25
2.3.1	Concrete Surface Preparation	25
2.3.2	Preparation of the Retrofit Material.....	25
2.3.3	Application of the Retrofit Material	26
2.4	SPECIMEN DESIGNATION.....	27
2.5	TEST SETUP	28
2.6	INSTRUMENTATION	29
2.7	TEST PROCEDURE.....	30
2.7.1	Selection of Fatigue Load Levels	31
2.7.2	Fatigue Run-out Specimens	32
2.8	SUMMARY OF COMPARABLE TESTS	33
3.0	TEST RESULTS AND TYPICAL SPECIMEN BEHAVIOR.....	40
3.1	TEST RESULTS.....	40
3.2	SPECIMEN BEHAVIOR	44
3.2.1	Specimen SC	44
3.2.2	Specimen S4F	45
3.2.3	Specimen S4.75F	45

3.2.4	Specimen S5.5F	46
4.0	DISCUSSION OF EXPERIMENTAL RESULTS.....	62
4.1	COMPARISON OF MONOTONIC TEST SPECIMENS	62
4.2	COMPARISON OF FATIGUE TEST SPECIMENS	65
4.2.1	Stress Range “Drift”	66
4.2.2	Secant Stiffness.....	67
4.3	COMPARISON OF FATIGUE RUN-OUT SPECIMENS.....	68
4.3.1	Effect of Fatigue Cycling on Debonding Strain	69
4.3.2	Effect of Fatigue Cycling on Other Parameters.....	69
4.4	PREDICTED DEBONDING BEHAVIOR	70
5.0	SUMMARY, CONCLUSIONS, AND RECOMMENDATIONS	82
5.1	SUMMARY OF TEST PROGRAM	82
5.2	CONCLUSIONS.....	83
5.2.1	Debonding of SFRP	86
5.3	RECOMMENDATIONS	87
APPENDIX A		89
REFERENCES.....		94

LIST OF TABLES

Table 2.1 Measured concrete and reinforcing steel material properties.	34
Table 2.2 Manufacturer reported material properties of CFRP and SFRP.	34
Table 2.3 Manufacturer reported material properties of adhesive systems used.	34
Table 2.4 Cycle numbers (N) at which data was recorded.....	35
Table 2.5 Stress range (S) and cycles to failure (N) observations and predictions.....	36
Table 2.6 Matrix of comparable specimens.	36
Table 3.1 Summary of Fatigue Data.	47
Table 3.2 Summary of Monotonic Data.....	49
Table 4.1 Analysis of key results summary for monotonic and runout specimens.....	74
Table 4.2 Measures of fatigue behavior.....	74
Table A.1 Summary of Key Results from Reeve (2005).	90
Table A.2 Summary of Key Results from fatigue tests of Zorn (2006).....	91
Table A.3 Summary of Key Results from run-out monotonic tests of Zorn (2006).....	93

LIST OF FIGURES

Figure 1.1 Example of fatigue conditioning deterioration of CFRP	17
Figure 1.2 Different arrangements of the steel wires	17
Figure 1.3 SFRP sheets.	18
Figure 1.4 Epoxy vs. grout, nail anchorage, and multiple layers	18
Figure 1.5 Load vs. deflection comparison for U-wrap specimen	19
Figure 1.6 Differences in changing SFRP width vs. adding SFRP layer	19
Figure 1.7 Example of end peel debonding	20
Figure 1.8 Use of SFRP on double T prestressed beams.	20
Figure 1.9 Typical bridge span stiffening with use of SFRP	21
Figure 1.10 Results of retrofitted slabs after blast.	21
Figure 2.1 Test specimen details	37
Figure 2.2 Retrofit details.	37
Figure 2.3 SFRP sheet and cord	38
Figure 2.4 Test set-up	38
Figure 2.5 Instrumentation for specimens	39
Figure 3.1 Test Specimens SC and C	50
Figure 3.2 Specimens S4F, SC, and C	50

Figure 3.3 Specimens S4.75F, SC, and C.	51
Figure 3.4 Specimens S5.5F, SC, and C.	51
Figure 3.5 Midspan deflection accumulation curves.	52
Figure 3.6 Strain accumulation curves for Specimen S4F (shifted vertically 2000 $\mu\epsilon$).	52
Figure 3.7 Strain accumulation curves for Specimen S4.75F (shifted vertically 2000 $\mu\epsilon$).	53
Figure 3.8 Strain accumulation curves for Specimen S5.5F (shifted vertically 2000 $\mu\epsilon$).	53
Figure 3.9(a) Load-strain behavior for Specimen SC (shifted horizontally).	54
Figure 3.9(b) Test Specimen SC – North strain gages (9), (10), and (5).	55
Figure 3.9(c) Test Specimen SC – South strain gages (8), (11), and (12).	56
Figure 3.10 Load-strain behavior for Specimen S4F (shifted horizontally).	57
Figure 3.11 Shear crack of Specimen SC (east side).	58
Figure 3.12 Debonding at toe of shear crack, Specimen SC (west side).	58
Figure 3.13 Shear crack on Specimen S4F (west side).	59
Figure 3.14 Debonding at toe of shear crack, Specimen S4F (west side).	59
Figure 3.15 Specimen S4.75F after reinforcing bar rupture (west side).	60
Figure 3.16 Fatigue-induced reinforcing bar rupture, Specimen S4.75F.	60
Figure 3.17 Specimen S5.5F after reinforcing bar rupture (west side).	61
Figure 3.18 Fatigue-induced reinforcing bar rupture, Specimen S5.5F.	61
Figure 4.1 Load vs. deflection for monotonic tests.	75
Figure 4.2 SFRP vs. CFRP, general yield load.	75
Figure 4.3 SFRP vs. CFRP, maximum load capacity.	76
Figure 4.4 SFRP vs. CFRP, deflection at maximum load.	76
Figure 4.5 SFRP vs. CFRP, ductility deflection.	77

Figure 4.6 SFRP vs. CFRP, strain at apparent initiation of debonding.	77
Figure 4.7 S-N data determined at $N=2$ and $N=N_f$ for SFRP and CFRP.....	78
Figure 4.8 S-N data for SFRP specimens with database compiled by Zorn (2006).	78
Figure 4.9 SFRP vs. CFRP, effect on fatigue stress range at $N = 2$	79
Figure 4.10 S-N data comparing different adhesives.....	79
Figure 4.11 Stiffness degradation with fatigue cycling for SFRP specimens.....	80
Figure 4.12 SFRP vs. CFRP, stiffness degradation with fatigue cycling.	80
Figure 4.13 Load vs. deflection for all runout specimens.....	81
Figure 4.14 Strain vs. E_{ftf}	81

NOMENCLATURE

Abbreviations

ACI	American Concrete Institute
AO	Adhesion Optimized
CEB	Comité Euro-International du Beton
CFRP	carbon fiber-reinforced polymer
FIC	flexure intermediate crack-induced debonding
FIRR	fatigue-induced reinforcing steel rupture
FRP	fiber-reinforced polymer
GFRP	glass fiber-reinforced polymer
LVDT	linear variable displacement transducer
RC	reinforced concrete
SIC	shear intermediate crack-induced debonding
SFRG	steel fiber-reinforced grout
SFRP	steel fiber-reinforced polymer

Notation

a	shear span of beam
A_c	concrete cross-sectional area
A_f	FRP cross-sectional area
A_s	steel reinforcement cross-sectional area

b	width of RC member (tension face)
b_{cfrp}	width of CFRP strip
b_f	width of FRP strip
b_{sfrp}	width of SFRP strip
E	modulus of elasticity
E_{cfrp}	CFRP modulus of elasticity
E_f	FRP modulus of elasticity
E_s	steel modulus of elasticity
E_{sfrp}	SFRP modulus of elasticity
f_c	compressive concrete strength
f_c'	28 day concrete compressive strength
f_{fu}	ultimate capacity of FRP
f_{fub}	allowable stress in FRP to mitigate debonding
f_u	ultimate strength of steel reinforcement
f_y	yield strength of steel reinforcement
h	depth of concrete section
k_b	factor accounting for b_f/b in design
k_L	factor accounting for $L_b < L_{b\text{max}}$ in design
L	beam clear span length
L_b	provided anchorage bond length
$L_{b\text{max}}$	effective anchorage bond length
M	applied moment at midspan
N	fatigue cycle number
N_f	fatigue failure cycle
n	number of plies of FRP
P	applied load at midspan

S	stress range in reinforcing steel
t_a	adhesive thickness
t_{cfrp}	CFRP thickness
t_f	FRP thickness
t_{sfrp}	SFRP thickness
α	empirical constant
ϵ_{fu}	<i>in situ</i> rupture strain of FRP
ϵ_{fub}	strain in FRP when debonding occurs
κ_m	ACI 440.2R strain reduction factor
$\rho_{equivalent}$	equivalent steel ratio
ρ_s	steel reinforcement ratio

This dissertation was completed using US units throughout except where noted. The following “hard” conversion factors were used:

$$1 \text{ inch} = 25.4 \text{ mm}$$

$$1 \text{ kip} = 4.448 \text{ kN}$$

$$1 \text{ ksi} = 6.895 \text{ MPa}$$

Reinforcing bar sizes are given using the designation cited in the appropriate reference. In the report, a bar designated with a “#” followed by a number refers to a standard inch-pound designation used in the United States (e.g.: #7). The number refers to the diameter of the bar in eighths of an inch. A bar designated with an “M” after the number refers to the standard metric designation. The number refers to the nominal bar diameter in mm (e.g.: 20M).

ACKNOWLEDGMENTS

Hardwire LLC

Fox Industries Engineered Products

1.0 INTRODUCTION AND LITERATURE REVIEW

1.1 INTRODUCTION

Repair and retrofit of structures will be an increasingly important issue as infrastructure continues to age and deteriorate. More options are becoming available for those structures for which it is more economical to retrofit than to demolish. Fiber reinforced polymer (FRP) composite materials have come to the forefront as promising materials and systems for structural retrofit.

Steel fiber reinforced polymer (SFRP) composite materials have recently been introduced as an alternative to glass and carbon fiber reinforced polymer (GFRP and CFRP) composite materials (Hardwire, 2002). There are many benefits to using SFRP over GFRP or CFRP. Significantly, the steel cords that make up SFRP have some inherent ductility. Also, when cementitious grout is used rather than epoxy as the bonding agent, the SFRG can exhibit excellent fire endurance properties (Casadei et al., 2005a). Similar to GFRP and CFRP, SFRP has the advantage of being relatively lightweight in comparison to steel plates, making it relatively easy to install.

1.2 OBJECTIVE

The purpose of this thesis is to investigate and gather more information regarding the behavior of surface bonded steel fiber reinforced polymer (SFRP) retrofit methods for reinforced concrete members subject to monotonic and fatigue loading conditions. This study focuses on flexure/shear intermediate crack-induced debonding (FIC/SIC) of the bonded SFRP from the concrete substrate, also known as mid-span debonding.

The results of this study will be compared with companion specimens having bonded CFRP retrofits tested previously by Reeve (2005) and Zorn (2006). These companion specimens were retrofitted with CFRP having an equivalent axial stiffness to the SFRP considered herein. The companion theses have already shown how the established consensus for mitigating debonding of CFRP systems is insufficient. This thesis represents a step toward considering SFRP in a manner similar to G/CFRP for structural retrofit.

Many retrofit applications can be subject to transient or fatigue loads. Previous studies conducted by Harries (2005) have shown the deleterious effects of fatigue loading on the behavior of concrete specimens retrofitted with FRP, and specifically on the performance of the bond layer (FRP-adhesive-concrete). Deterioration has been seen in cases where the stress level in the CFRP was as low as 4% of its capacity (Harries and Aidoo, 2005). This effect is shown in Figure 1.1 where the ACS curve is a monotonically loaded specimen and the ACF curve is an identical CFRP-strengthened specimen that has been subject to 2 million cycles of fatigue loading at a level resulting in a CFRP stress of $0.04f_u$, where f_u is the strength of the CFRP. The fatigue behavior of bonded SFRP may also be of concern. This study is believed to be the first to address fatigue-induced degradation of SFRP performance.

1.3 SCOPE OF REPORT

This thesis presents the experimental results of the monotonic and fatigue performance of reinforced concrete beams strengthened with steel fiber reinforced polymer (SFRP) strips bonded with an epoxy resin. The outline of this thesis is as follows:

- Chapter 1 presents a review of related research involving the use of SFRP as a retrofit material.
- Chapter 2 presents a detailed explanation of the experimental program. The beam fabrication and SFRP application are described in this chapter. The method for testing each beam monotonically or in fatigue is outlined in this chapter.
- Chapter 3 presents the results from the experimental program.
- Chapter 4 presents a discussion of the results of the experimental program. A comparison with companion specimens retrofitted with carbon fiber reinforced polymer (CFRP) tested by Reeve (2005) and Zorn (2006) is also presented.
- Chapter 5 presents a summary, conclusion, and recommended future research endeavors.

1.4 LITERATURE REVIEW

As current infrastructure ages, and load demand continues to increase, both rehabilitation (restoring to original capacity) and strengthening measures must be made. Fiber reinforced polymer (FRP) materials have been successfully used for rehabilitation and strengthening efforts for the past two decades. Recently, a new form of FRP: steel fiber reinforced polymer (SFRP), has been introduced as an alternative to more conventional carbon or glass fiber reinforced

polymers (C/GFRP). This literature review focuses on research investigating the use and performance of SFRP. The companion theses, Reeve (2005) and Zorn (2006) present reviews of issues affecting FRP bond to concrete and the fatigue performance of concrete beams retrofitted with FRP materials, respectively. The conclusions of these companion theses that consider the use of CFRP are summarized later in this chapter.

1.4.1 Description of SFRP Material

SFRP materials are composed of ultra high strength steel fibers embedded in a polymeric matrix. The fibers are of a very small diameter so that the steel can have the microstructure of pearlite. The result is a high tensile strength steel, up to eleven times stronger than typical steel plate (Hardwire, 2002). The fibers are similar to the steel cords used as reinforcement in automotive tires.

Individual fibers are wrapped together into cords of different configurations and twist angles (Figure 1.2). The configuration and twist angle depend on the intended application. Fibers are wrapped at low twist angles when balanced compressive and tensile strengths are required. Often an additional fiber is wrapped around the straighter inner fibers at a higher twist angle to affect a better mechanical bond with the resin system. The low twist angle of the primary fibers results in a system in which there are more openings for the resin to penetrate. Fibers can be wrapped at high twist angles for optimum tensile strain and improved ductility (Hardwire, 2002).

The cords can be coated in a variety of ways. Brass can be used when the main concern is aesthetics. An Adhesion Optimized (AO) Brass coating is used in the present applications. AO coating is a titanium-based priming system that can increase bond performance of epoxies up to

500% (Hardwire, 2002). Zinc can also be used as a coating when enhanced corrosion resistance or high surface reactivity is needed (Hardwire, 2002).

Cords are subsequently arranged into continuous sheets (Figure 1.3) that are available in 12 inch (305 mm) widths (Hardwire, 2002). The cords are held together using a scrim, or net, of polyester yarns (Figure 1.3(b)). The result is a fabric-like material that can be bent without any material degradation.

1.4.1.1 Bonding Matrix

The steel-cord sheets can be bonded using either an epoxy resin system or with cementitious grout. For the purpose of this review, SFRP refers to the product which is bonded with epoxy, and SFRG refers to product bonded with grout. It is believed (Casadei et al., 2005a) that the use of SFRG results in a higher fire rating, which has been a common criticism of retrofit schemes that use an epoxy system. Additionally, the construction industry is more familiar with using grout, so a designer may feel more confident that the SFRG retrofit will be installed properly.

Casadei et al. (2005a) report that interfacial failure modes are more dependent on the bonding material used than on fiber type (steel or carbon). Their study showed that debonding occurred earlier when grout was used in comparison to using epoxy resin (Figure 1.4). Behavior was similar up to yielding of the internal steel, but at ultimate, the SFRP exhibited a mid-span deflection 23% larger than the SFRG. It was reported that strength increases were larger when epoxy was used rather than grout. These results can be largely attributed to the superior adhesion properties of epoxy over cementitious grout.

Pecce et al. (2006) reported that beams retrofitted with SFRG showed a less stiff behavior under serviceability conditions than beams retrofitted with SFRP. When a low-density steel fiber

tape was used with grout, it gave a low tension-stiffening effect. When Pecce et al. compared code formulations for crack width and deflections with experimental values, they determined that the epoxy resin system showed a scatter that is generally comparable to that observed in unstrengthened beams. When grout was used, nonconservative results were found in comparing experimental and code-prescribed values.

Wobbe et al. (2004) reported similar results. A beam retrofitted with SFRP reached a maximum load of 22.5 kips (99 kN), while a beam retrofitted with an equivalent amount of SFRG reached only 21 kips (92.5 kN). This demonstrates the trend that strength increases are larger when using epoxy. This is, again, likely due to the improved bond behavior between the retrofit and original substrate concrete. Wobbe et al. did not, however, report any indication that strengthening with epoxy increases ductility.

1.4.2 Mechanical Anchorage

A successful method to anchor SFRP/G would have a great impact on mitigating observed problems with debonding. Prota et al. (2006) conducted tests on SFRG that used nail anchors for additional mechanical anchorage. It was shown that the nail anchors did not significantly affect performance or ductility. The SFRP/G failed in bearing at the nail locations due to the lack of a transverse link to distribute the local stress concentration at the anchor location. Similarly, Pecce and Manfredi (2005) report that when nails were distributed along a beam retrofitted with SFRG, there was no effect on cracking phenomenon.

1.4.3 Use of SFRP U-wraps

Plate end delamination (PE) is a common failure mechanism for SFRP specimens (Figeys et al., 2005). A study performed by Kim et al. (2005) attempted to delay PE delamination through the use of SFRP U-wraps. A U-wrap is a strip of SFRP bent such that it is in the shape of a U and bonded transversely to the exact shape of the beam, “clamping” the longitudinally applied SFRP. It was concluded that transverse reinforcement like the U-wrap could delay the PE delamination failure. A specimen with the U-wrap was able to resist 15.47 kips (68.83 kN) of applied force, while equivalent specimens without the retrofit were only able to resist 13.32 kips (59.23 kN) and 13.44 kips (59.77 kN) respectively (Figure 1.5). Kim et al. conclude that U-wraps could also be used to reduce shear deformations that are induced by diagonal cracking. An example of U-wraps being used on a large scale specimen is discussed later.

1.4.4 Geometry of SFRP Retrofit

This section discusses the difference in performance of different cord types of SFRP and differences in applying the SFRP in layers.

1.4.4.1 Different Cord Types

The study performed by Casadei et al. (2005a) compared the performance of beams retrofitted with SFRP having different cord types. The different types used were 3X2 cord and 12X cord (see Figure 1.2). Hardwire LLC reports that a 3X2 cord consists of three straight fibers wrapped by two fibers at a high twist angle, and for the purpose of this study, was arranged in a high-density tape. The 12X steel cord consists of two fibers twisted together in

twelve strands, with one wire twisting around to form a bundle. For this study, it was considered a medium-density tape. Both arrangements were reported to have increased the capacity of the beam. The stiffening effects, however, were very different. The 3X2 retrofit significantly stiffened the beam. It was reported that the wider the width of the SFRP tape, the stiffer the beam would become. The 12X retrofit was unable to provide any significant stiffening. The authors report that this is due to the macrostructure of the tape. This is an example of why it is important to choose the right type of SFRP material.

1.4.4.2 Applying FRP Materials in Varying Widths and Layers

Casadei et al. (2005a) also reported on the differences of applying SFRP materials in layers. It was reported that a specimen retrofitted with two layers of 5.9 in. (150 mm) wide 3X2 SFRP material exhibited the same behavior as a specimen retrofitted with only one layer having the same width up to the point of general yield of the specimen (Figure 1.6). While the eventual increase in strength was 16% in comparison to using one layer of the same width, it should be noted that using one layer of 11.8 in. (300 mm) SFRP material increased strength (over the two layers at 5.9 in.) by 40% and stiffened the beam significantly more (Figure 1.6). This observation is generally consistent with FRP applications where single wide layers are more efficient than multiple less-wide layers.

The same study also investigated 12X SFRG materials in layers. When one layer was used, it was reported that the 12X tape provided no significant stiffening effect to the beam regardless of the adhesive system used (epoxy or grout). It was reported that adding a second layer did stiffen the beam in comparison to using one layer. The authors concluded, however, that the 12X tape was ineffective at reducing crack widths and stiffening the flexural element.

It was reported by Pecce et al. (2006) that crack widths became smaller when the width of the SFRP/G was increased. Using multiple layers was less effective at decreasing the crack widths.

Wobbe et al. (2004) reported that SFRP materials could be installed in multiple layers to improve ultimate strength. The beams in their study showed that using two layers of SFRP increased strength 17% in comparison to using one layer. It appears as though the flexural stiffness of the member was increased slightly, but the authors make no conclusions on this topic.

In four point bending tests performed by Figeys et al. (2005), a different result was seen. This is due to the failure mechanism of plate end (PE) debonding, or delamination (Figure 1.7). The span of each of the beams in this study was 59.1 in. (1500 mm). The SFRP was cut such that there would be either 3.9 in. (100 mm) or 9.8 in. (250 mm) of unbonded length adjacent each support. For a specimen retrofitted with one layer of SFRP material, Figeys et al. predicted that delamination would occur at 17.3 kips (77 kN). The actual failure loads were 18.0 kips (80 kN) and 20.2 kips (90 kN), both in PE delamination. When a second layer of SFRP was added, the prediction was that delamination would occur at 16.2 kips (72 kN). The test results confirmed this trend, as the actual failure load at delamination was 16.9 kips (75 kN). This shows the importance of considering all potential failure mechanisms when using SFRP as a retrofit. The actual bending capacity of the specimen was predicted to increase as more layers of SFRP were added. However, adding more material causes the stress concentrations at the end of the external reinforcement to increase. As a result, the PE failure mechanism occurs at a lower load (Figeys et al., 2005).

1.4.5 SFRP vs. CFRP

Casadei et al. (2005a) compared the use of SFRP to CFRP as a retrofit measure for concrete beams. They conclude that CFRP was more effective than SFRP in terms of ultimate strength. Due to its inherent ductility, however, SFRP performed better than CFRP in terms of achieving a higher ultimate deflection. It should be noted that the axial stiffnesses of the SFRP and CFRP retrofit measures were not equivalent in this study. Pecce et al. (2006) report that when the reinforcement percentage is the same and epoxy is used as the bonding agent, steel cords and carbon fibers give very similar results.

Direct shear tests performed by Figeys et al. (2005) revealed more comparisons between SFRP and CFRP. SFRP was bonded to concrete prisms, and direct shear tests were performed. Failure was always in the concrete. The conclusion was that elements bonded with SFRP seemed to be stronger and stiffer when compared to similar elements strengthened with CFRP.

1.4.6 Field Applications of SFRP

The following examples illustrate efforts made to validate the use of SFRP on large scale applications.

1.4.6.1 SFRP Use on Double-Tee Prestressed Concrete Beams

A study performed by Casadei et al. (2005b) investigates the use of SFRP materials as a retrofit measure for precast prestressed concrete double-tee beams. The beams were from a decommissioned parking garage in Bloomington, Indiana. A total of three beams were tested. Beam DT-C was the control beam, Beam DT-1 was a beam strengthened with one ply of SFRP,

and Beam DT-2U was strengthened with two plies of SFRP, which were then anchored at each end with U-wraps of SFRP. In this case, the U-wrap was actually two overlapping L-shaped wraps applied from opposing sides. The epoxy resin used for all applications in this study was SikaDur 330. The plies were of a medium density SFRP.

Beam DT-C failed due to the lower reinforcing strand rupturing. The capacity of Beam DT-1 was 12% higher than that of Beam DT-C (Figure 1.8). The failure mechanism of Beam DT-1 was debonding of the SFRP that started at mid-span and progressed towards the supports, until complete detachment occurred (FIC or SIC). The capacity of Beam DT-U2 was 26% higher than that of Beam DT-C. The failure mechanism was the lower reinforcing strand rupturing, followed by SFRP rupturing at the location of the U-wraps.

From the tests, Casadei et al. were able to conclude that SFRP is effective as a retrofit to improve flexural capacity of large scale double-tee prestressed concrete beams. Due to concrete still being attached to the SFRP laminate after debonding, it was concluded that the epoxy resin SikaDur 330 was capable of creating an adequate bond. The authors observed that the U-wraps were effective in preventing complete detachment of the SFRP. However, there was no beam tested with two plies of SFRP without any U-wraps, so it was not concluded that they achieved a higher flexural capacity. The authors also confirmed that SFRP is easy to install in the field.

1.4.6.2 SFRP Use on Reinforced Concrete Bridge

A project still being investigated by Lopez and Nanni (2005) involves the use of SFRP materials to strengthen one span of a three span bridge in Dallas County, MO. The span is 42.3 feet (12.9 m) and the deck width is 23.6 ft (7.2 m). SFRP was placed on the soffit of both the girders and the deck to provide flexural reinforcement. SFRP was also applied in U-wraps for shear reinforcement on the girders.

The authors report that in-situ load tests reveal that the retrofit resulted in a marginal decrease in deflection (Figure 1.9). Therefore, the retrofitted system was slightly stiffer than the original structure. It was recommended that the load posting for the bridge could be removed, although it remains at this time. The authors are committed to continue to perform load tests on the bridge for another five years to study any degradation of performance. The results will also be used to calibrate design factors. This study shows the importance of field verification for the use of SFRP materials.

1.4.6.3 SFRP Use in Restoration of Historic Theatre

SFRP has been used in rehabilitation efforts at the Hippodrome Theatre in Baltimore. Gallagher (2005) points out that while work on the theatre was originally aesthetic in nature, it became apparent that concrete in the balcony had become badly deteriorated. The risers needed protection from cracking due to movement under loading. SFRP was placed in L-wraps on the risers to address the problem. Gallagher claims that it is the first commercial use of SFRP. It is evidence that SFRP can be an economical and successful alternative to typical rehabilitation efforts.

1.4.7 SFRP Use in Blast Resistant Design

SFRP materials show promise in protecting structural elements from blast loads. A study conducted by Lu et al. (2006) uses a displacement based design (DBD) methodology to test the blast-resistant capacity of reinforced concrete slabs (Figure 1.10). Performance of a control slab exposed to a blast load was compared to the performance of retrofitted slabs. The authors concluded that slabs should be retrofitted on both sides to protect sufficiently against realistic

blast loads. It was observed that slabs retrofitted on only one side were severely damaged, due largely to the effects of negative pressure following the initial positive pressure of the blast. It was also concluded that while retrofitting on both sides can resist appropriate threat levels, the shear capacity of the slab which was largely unaffected by the retrofit measures proved to be a weak link.

According to Hardwire (2002), SFRP can also be used with wood products to protect against impact loading such as that from projectiles in a hurricane or tornado. The U.S. military has interest in using SFRP to armor vehicles and buildings against blasts and small arms fire. Hardwire claims that SFRP is an economical alternative to standard ballistic armor having equal performance.

1.4.8 Conclusions from Reeve (2005)

Reeve (2005) tested a number of beams that serves as companion specimens to the present work. The following are conclusions that were drawn from the work of Reeve.

The concrete beams tested by Reeve are identical to the beams in the present work. The beams were retrofitted with different widths and geometries of CFRP. Each width and geometry was bonded with a high modulus and a low modulus adhesive. All tests were monotonic to failure. The unretrofit monotonic control specimen for the present work was also tested by Reeve.

Reeve observed that general yield and maximum loads increase as the retrofit material area was increased. The rate of increased capacity, however, decreased as more retrofit material was used. It was observed that deflection capacity decreased as wider strips, and therefore more area of retrofit material, were used.

Reeve considered two cases where 2 in. (51 mm) of CFRP material was used. In one case, one strip of the full 2 in. (50.8 mm) width was used. In the other case, two strips of 1 in. (25.4 mm) each, separated by a 2 in. (51 mm) gap were used. The conclusion was that multiple thinner strips are preferable to fewer wider strips due to the observation that they resulted in a high load capacity as well as greater deflection capacity. These specimens, having 2 in. wide CFRP retrofits, are the ones that will serve as the companion specimens to those reported in this thesis.

It was concluded that specimens with the low modulus adhesive had higher general yield and maximum loads. The deflections at general yield and at maximum load were also observed to be higher. The modulus of the adhesive used in the present work falls between that of the low and high modulus adhesives considered by Reeve, which themselves only varied by a factor of two.

Reeve concluded that the ACI equation intended to mitigate debonding failure by limiting allowable strain in the FRP material (ACI 2002) is generally non-conservative. The strains were overestimated by a factor of two for the high modulus adhesive and somewhat less so for the low modulus adhesive. Reeve recommends that the best model to predict FIC/SIC debonding is that proposed by Teng et al. (2004). This model was appropriately conservative for the low modulus adhesive, but was still slightly non-conservative for the high modulus adhesive. Reeve recommends that the nature of the adhesive should be included in the calculations for limiting strain.

Reeve was able to effectively mitigate end peel debonding by extending the CFRP to just short of the supports. The present work also extended the SFRP to just short of the supports. Key results from the specimens tested by Reeve are provided in Table A1 of Appendix A.

1.4.9 Conclusions from Zorn (2006)

Zorn (2006) tested specimens that were identical to those tested by Reeve (2005). The retrofit schemes were also identical, using the same CFRP geometries and two adhesives. Zorn, however, tested specimens to fatigue failure, or 2,000,000 cycles, whichever came first. If the full 2,000,000 cycles were reached, a monotonic run-out test to failure was performed.

It was concluded that stress range drift should be considered when designing a bonded retrofit that will perform in fatigue conditions. Stress ranges were seen to increase from 4% to 16% from the second fatigue cycle to the final fatigue cycle (defined by failure or 2 million cycles).

The secant stiffness of the beams generally degraded at a rate proportional to the fatigue life of the specimen. Degradation was essentially the same for all retrofit schemes and adhesive types. Zorn concluded that sound bond was maintained during fatigue cycling for all specimens.

As the amount of CFRP increased, the stress range of the internal reinforcing bars decreased. This reduction in stress range resulted in an increase in fatigue life. It is concluded that the data from the fatigue tests fits within the expected scatter of fatigue data, as well as within the existing bonded retrofit database compiled by Zorn.

Contrary to intuition, Zorn discovered that the performance of the lower modulus adhesive degraded at a greater rate than that of the higher modulus adhesive. Additionally, fatigue cycling of the low modulus adhesive had detrimental effects on the debonding strains. Debonding strains in the low modulus adhesive run-out specimens were much lower than their companion monotonic specimens reported by Reeve (2005). This degradation was not observed for the high modulus specimens. Zorn concludes that the adhesive type should be included in calculating the expected debonding strain under fatigue conditions.

The fatigue conditioned run-out specimens tested by Zorn displayed only marginal effects on parameters such as ductility, ultimate capacity, maximum deflection, and general yield in comparison to their monotonic companion specimens. Key results from the fatigue and monotonic run-out specimens tested by Zorn are provided in Tables A2 and A3 of Appendix A, respectively.

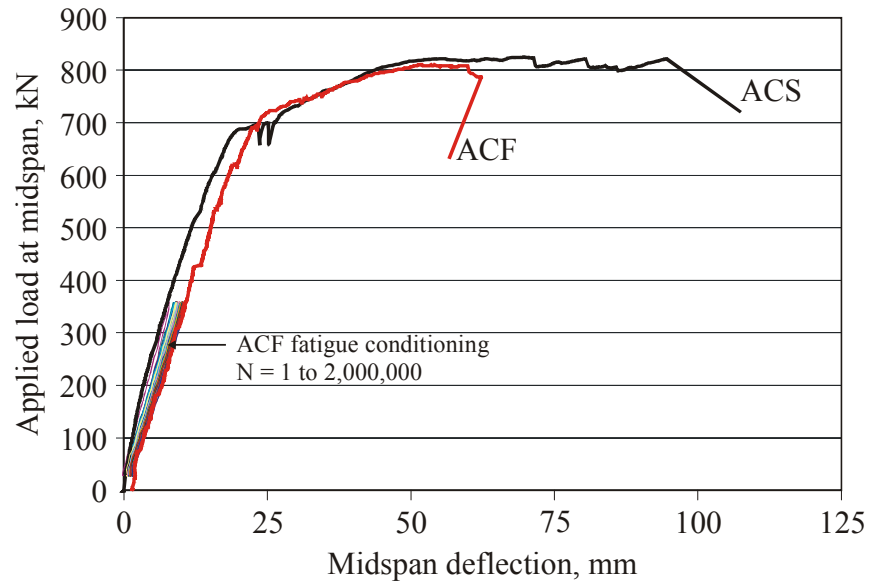


Figure 1.1 Example of fatigue conditioning deterioration of CFRP (Harries and Aidoo, 2005).

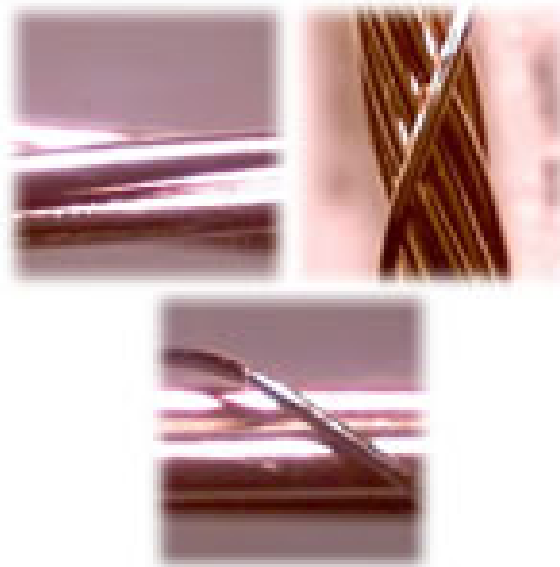
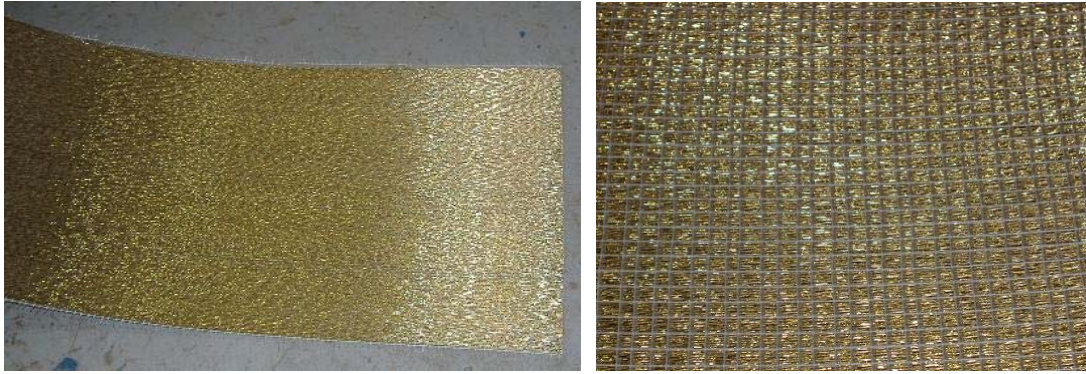


Figure 1.2 Different arrangements of the steel wires. Top left shows 3x2 cord type, top right shows 12X cord type, and bottom shows 3SX cord type. (Hardwire, 2002)



(a) Sheet of SFRP

(b) Polyester scrim on back of SFRP

Figure 1.3 SFRP sheets.

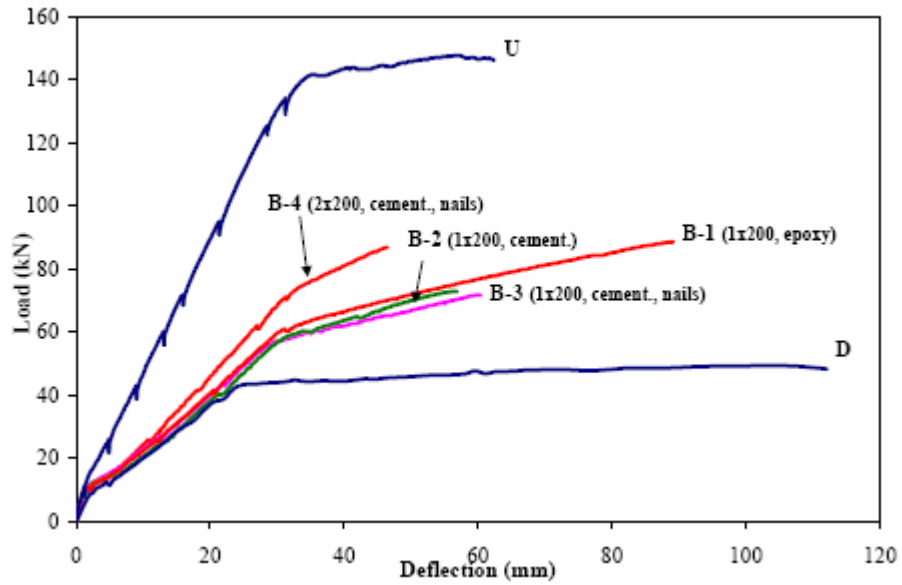


Figure 1.4 Epoxy vs. grout, nail anchorage, and multiple layers.
(Casadei et al, 2005a)

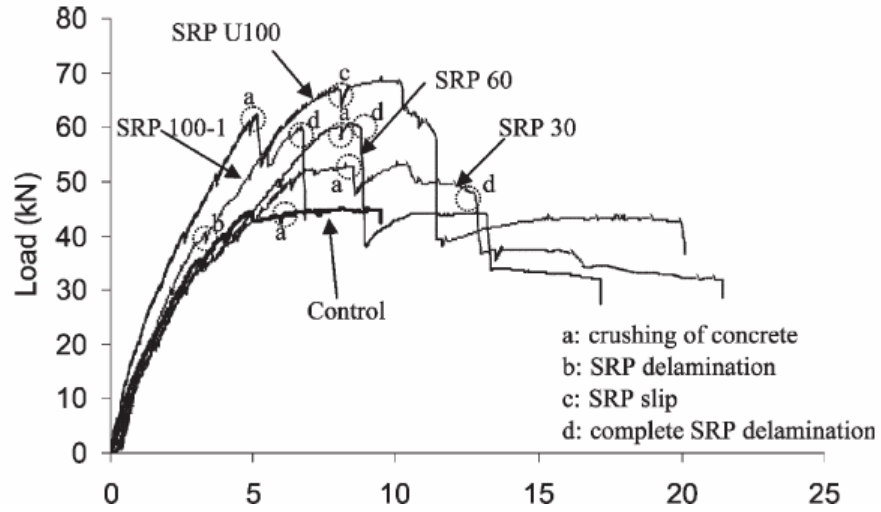


Figure 1.5 Load vs. deflection comparison for U-wrap specimen.
(Kim et al. 2005)

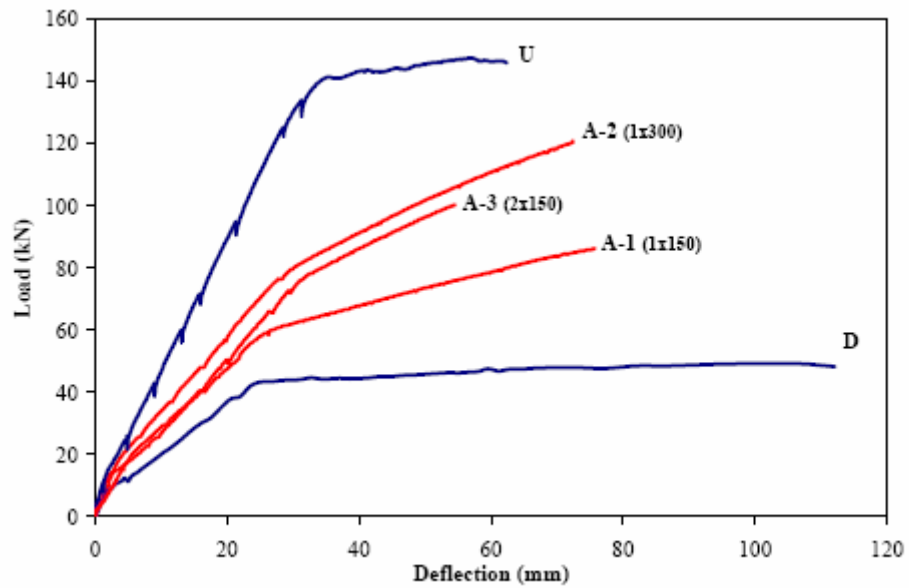


Figure 1.6 Differences in changing SFRP width vs. adding SFRP layer.
(Casadei et al., 2005a)



Figure 1.7 Example of end peel debonding (Figeys et al., 2005).

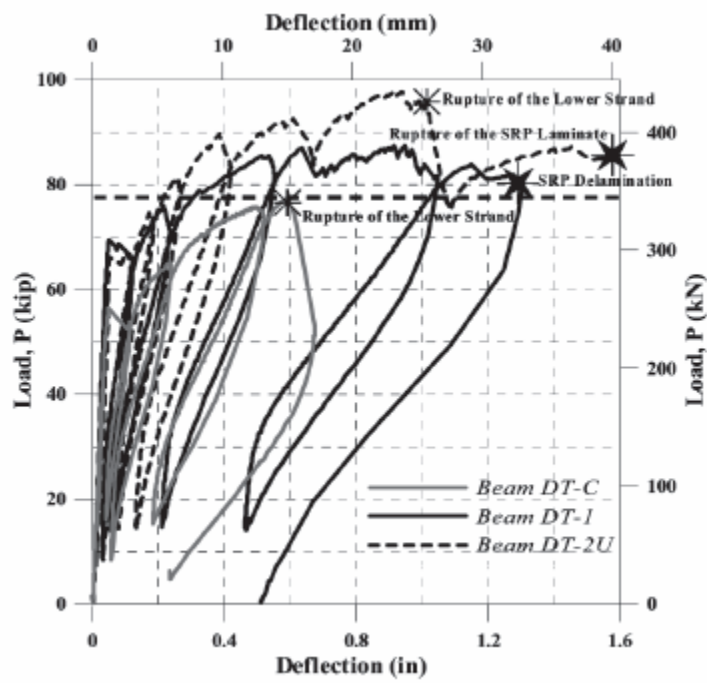


Figure 1.8 Use of SFRP on double T prestressed beams. (Casadei et al., 2005b)

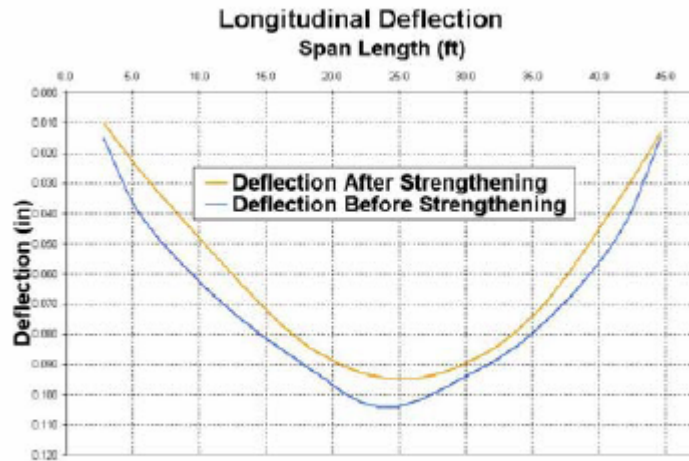


Figure 1.9 Typical bridge span stiffening with use of SFRP. (Lopez and Nanni, 2005)



Figure 1.10 Results of retrofitted slabs after blast. Top picture shows slab retrofitted on one side, bottom two pictures show slab retrofitted on both sides. (Lu et al., 2006).

2.0 EXPERIMENTAL PROGRAM

This chapter reports the details of the experimental program. Test setup and instrumentation details are also presented in Reeve (2005) and Zorn (2006) and repeated here for completeness and clarity.

2.1 REINFORCED CONCRETE BEAM TEST SPECIMENS

Twenty-four identical reinforced concrete beams were cast. Beams had a height of 10 in. (254 mm), a width of 6 in. (152 mm), and an overall length of 186 in. (4730 mm). The concrete had a measured 28-day compressive strength, f_c' , equal to 3384 psi (23.3 MPa). Maximum coarse aggregate size was 1.5 in. (37 mm). Three #4 reinforcing bars were used as the primary longitudinal flexural reinforcement. This resulted in a reinforcing ratio of 1.0%. Two #3 bars were provided in the compression zone of the beam. The compression bars were necessary to ensure that the beams would not crack under their self weight when they were inverted for the application of the retrofit materials. The #4 bars had a measured yield strength of 62.2 ksi (429 MPa) and a tensile strength of 96.8 ksi (667 MPa). Concrete and reinforcing steel material properties are reported in Table 2.1. Details of the concrete beam specimens are shown in Figure 2.1.

Of the twenty-four beams, sixteen were retrofitted with carbon fiber reinforced polymer (CFRP) composite strips. Eight of those sixteen were tested monotonically to failure (as reported by Reeve, 2005). The other eight were tested under fatigue loading to failure or 2 million cycles (as reported by Zorn, 2006). The beams that remained intact after 2 million cycles of fatigue loading were referred to as “fatigue-conditioned” specimens and subsequently loaded monotonically to failure (Zorn, 2006). An additional two beams were used as unretrofitted control specimens, one tested monotonically (Reeve, 2005) and one tested in fatigue (Zorn, 2006). Finally, four of the beams were retrofitted with steel fiber reinforced polymer (SFRP) strips; these are the focus of this thesis.

All beams were allowed to cure in their forms for seven days before being stripped and stored in ambient laboratory conditions. The beams were allowed to cure in ambient conditions for more than 56 days before they were inverted for retrofit applications.

2.2 RETROFIT MEASURES

The four SFRP specimens had an identical retrofit measure. This can be seen in Figure 2.2. The 3x2-23-12 SFRP retrofit material used was supplied by Hardwire LLC. The SFRP designation indicates that each strip is made of cords comprised of five individual wire fibers. Three of the fibers are straight, while two are wrapped around the three at a high twist angle. The fibers making up each cord were of high carbon steel with a micro-fine brass or AO-brass (Adhesion Optimized) coating (Hardwire, 2002). The strip used is comprised of 23 such cords per inch width (9 cords per cm width). Table 2.2 provides geometric and material properties of

the SFRP. Figure 2.3 shows a photograph of an individual cord and the entire 12 in. (305 mm) wide SFRP strip.

The strip width of 4.75 in. (121 mm) was selected such that the axial stiffness of the resulting retrofit was essentially equivalent to comparable CFRP retrofits tested previously by Reeve (2005) and Zorn (2006). That is:

$$E_{CFRP}t_{CFRP}b_{CFRP} = E_{SFRP}t_{SFRP}b_{SFRP} \quad (2.1)$$

$$(22500ksi)(0.055in)(2.0in) = (10952ksi)(0.048in)b_{SFRP}$$

As shown in Table 2.2, the axial stiffness, EA, of 2 in. (51 mm) wide CFRP is 2475 kips (11009 kN) while that of 4.75 in. (121 mm) of SFRP is 2497 kips (11107 kN).

Fox Industries epoxy adhesive FX-776 was used to bond the SFRP as recommended by Hardwire LLC. The manufacturer-reported material properties of the adhesive system is given in Table 2.3.

The specimens prepared for this study were compared with equivalent specimens having CFRP retrofits tested previously by Reeve (2005) and Zorn (2006). The CFRP retrofit material used in these companion studies studies was Fyfe UC strips. Two adhesive systems were used in the companion work: Sikadur 23 (designated “L”) and Sikadur 30 (“H”). Manufacturer-reported material properties for the CFRP and adhesive systems are provided in Tables 2.2 and 2.3, respectively. Two comparable CFRP strip arrangements are considered: a single 2 in. (51 mm) wide strip located in the middle of the beam soffit (H2 and L2 specimens) and 2 – 1 in. (25 mm) wide strips having 2 in. (51 mm) clear space between them centered on the beam soffit (L2x1 and H2x1 specimens). Each configuration was prepared using both the Sikadur 23 (L) and Sikadur 30 (H) adhesives. The arrangement of retrofit strips for all concrete specimens is shown in Figure 2.2.

2.3 APPLICATION OF SFRP TO THE TEST SPECIMENS

The retrofitting process was not begun on any of the beams until the substrate concrete was at least 56 days old. This allowed the concrete to cure long enough to be able to be handled and inverted, as well as to dry out the surface region of the concrete where the retrofit material was to be applied. The strips were applied to the tension face (soffit) of all the beam specimens with the exception to the control specimens. Four beams were retrofitted with SFRP, while sixteen were retrofitted with CFRP. Only those beams with configurations discussed in Section 2.2 and shown in Figure 2.2 are discussed in this thesis.

2.3.1 Concrete Surface Preparation

The surface of the concrete to which the SFRP or CFRP is applied had to be prepared before any retrofit measures could begin. The beams were inverted so the soffit was facing upwards. The surface was prepared with an angle grinder that had a wire wheel attachment to remove all laitance and dirt from the soffit. Compressed air was used to remove concrete dust and dirt that had settled on the beam. This ensured that a sound bond would form between the concrete surface and the retrofit material. The final beam surface resembled ICRI Concrete Surface Profile 3 (ICRI, 1997).

2.3.2 Preparation of the Retrofit Material

The SFRP was precut into strips 172 in. (4369 mm) long and 4.75 in. (121 mm) widths. The lengths were such that they would extend to just short of the supports during testing. Cutting

the high strength SFRP is difficult; recommended shear types can be found at www.hardwirellc.com. The SFRP strips were stored such that they were protected from dust, dirt, and moisture. The CFRP specimens were cut to length using aviation shears and cut longitudinally with a straight razor as needed. The CFRP was stored such that it was protected from dust, dirt, and mechanical damage (Zorn, 2006).

2.3.3 Application of the Retrofit Material

With the beam inverted and the concrete surface prepared, the retrofit process could begin. The four beams retrofitted with SFRP used FX-776 epoxy. The two-part epoxy was mixed according to the manufacturer's specification: 4 parts resin to 1 part hardener by weight. The epoxy was applied within the specified pot life of the epoxy system. Plastic spatulas and paint rollers were used to apply a layer of epoxy on the soffit of the beam. Once the entire surface had a layer of epoxy, an SFRP strip was laid down on top and centered on the width of the beam. Pressure was applied to the strips using fingertips and blocks of wood to remove any voids and allow the epoxy to seep through the porous mesh of steel cords. Once the strip was pressed down and impregnated sufficiently, a final layer of epoxy was applied to the top.

It is noted that the SFRP has a glass fiber mesh on one side. This is intended to serve as a medium of keeping the epoxy from dripping in overhead applications. Contrary to the Hardwire recommendations, the SFRP was inadvertently installed with this mesh facing the concrete. Discussions with Hardwire revealed that the orientation of the mesh does not affect the behavior of the system. Indeed, it is proposed that by installing the mesh in the adhesive line, a more uniform adhesive thickness may be obtained as the mesh serves as a uniform spacer. A detailed description of the CFRP application can be found in Reeve (2005) and Zorn (2006).

2.4 SPECIMEN DESIGNATION

The four test specimens retrofitted with SFRP were designated as follows:

PQR

Where P indicates the retrofit measure used:

S = SFRP retrofit with FX-776 epoxy as described above

Where Q stands for the applied load range:

4.00 = 4 kip (17.79 kN) fatigue load range

4.75 = 4.75 kip (21.13 kN) fatigue load range

5.5 = 5.5 kip (24.47 kN) fatigue load range

C = SFRP monotonically tested control specimen

And R indicates the loading type:

Blank = Monotonic loading

F = Fatigue loading as described in Section 2.7

Thus, for example, the S4F specimen indicates that the beam was retrofitted with SFRP using the FX-776 epoxy and was tested under fatigue loading having a 4 kip load range.

The designation for the CFRP specimens discussed in this work (tested by Reeve (2005) and Zorn (2006)) are as follows:

XYZ

Where X stands for the epoxy system:

C = Unretrofit control beam

H = High-modulus epoxy (Sikadur 30)

L = Low-modulus epoxy (Sikadur 23)

Where Y stands for the CFRP strip width and configuration:

2 = 2 in. (51 mm) wide strip

2x1 = two 1 in. (25 mm) wide strips

And Z indicates loading type:

Blank = Monotonic loading (tested by Reeve 2005)

F = Fatigue loading (tested by Zorn 2006)

For example, the H2x1F specimen is a beam with two 1 in. strips adhered to the soffit of the beam using the high modulus adhesive (Sikadur 30) and tested under fatigue loading. It is noted that all fatigue loading cycles for the CFRP specimens ranged from 1 kip (4.45 kN) to 5 kips (22.24 kN) resulting in a 4 kip (17.79 kN) range.

2.5 TEST SETUP

All beams were tested under mid-point bending. One SFRP specimen was tested under monotonically increasing load to failure, while the remaining three were tested under various fatigue loading conditions. An MTS hydraulic actuator with a capacity of 50 kips (222 kN) and a stroke of 4 in. (102 mm) was used to apply the load. The beams were supported over a clear span of 178.25 in. (4527 mm). At the supports, the beams rested on 3 x 6 x ½ in. (76 x 152 x 13 mm) neoprene pads having a durometer hardness of 65-75. The neoprene pads rested on top of 3/8 in. (9 mm) thick steel plates which subsequently rested on steel rollers resulting in simply supported reaction conditions. A similar neoprene pad was used at mid-span, where the load was applied. The neoprene pad was necessary to minimize local crushing of the concrete, as significant damage could result from a steel-to-concrete interface during cyclic loading. The test set-up is shown in Figure 2.4.

2.6 INSTRUMENTATION

The beams had slightly different instrumentation depending on the type of loading. Each of the four beams were instrumented with four electrical resistance strain gages located on the middle #4 reinforcing bar. The gages were spaced at 12 in. (305 mm) center-to-center and were centered on mid-span. Therefore, two gages were 18 in. (457 mm) from mid-span, and two were 6 in. (152 mm) away, one in each direction (Figure 2.5). The mid-span vertical deflection was measured with a draw wire transducer as shown in Figure 2.5.

All specimens had electrical resistance strain gages on the external surface of the SFRP strips. The fatigue specimens had an additional four gages located in locations coincident with the gages on the internal #4 reinforcing bar. The monotonic specimen SC had a total of eight gages placed on the SFRP. Six were placed at a distance of 18 in. (457 mm) from mid-span, three on each side. The remaining two were placed at a distance of 6 in. (152 mm) away from mid-span, one on each side as shown in Figure 2.5. In this manner, the gage locations corresponded to the gages placed on the internal reinforcing bar. The locations with three strain gages transversely across the SFRP allowed investigation of the distribution of strain transversely across the SFRP width.

The MTS hydraulic actuator was equipped with a 50 kip (222 kN) load cell. All instruments were connected to a Vishay System 5100 data acquisition system. The controller was an MTS FlexTest SE hydraulic servo-controller. Data was recorded at 2 samples per second for all monotonic tests and 50 samples per second for all recorded cycles of the fatigue tests. Essentially identical instrumentation schemes were used for the companion CFRP-retrofit specimens as described by Reeve (2005) and Zorn (2006)

2.7 TEST PROCEDURE

All beams were tested in mid-point bending. They were simply supported over a 178.25 in. (4527 mm) span. Of the four SFRP-retrofit beams, one specimen (SC) was tested under monotonically increasing load to failure. All monotonic tests (SC and those reported by Reeve (2005): C, L2, H2, L2x1 and H2x1) were performed under displacement control at a constant rate of 0.13 in./minute (3.4 mm/min).

The remaining three SFRP-retrofit beams were tested under a cyclic loading condition to failure or two million cycles at a frequency not exceeding 1.7 Hz. All cyclic tests were conducted in load control. The three fatigue tests each had a unique stress range. Specimen S4F had an applied mid-span load that cycled from 1 kip (4.45 kN) to 5 kips (22.24 kN) in a sinusoidal wave form. Specimen S4.75F had an applied mid-span load cycled from 1 kip (4.45 kN) to 5.75 kips (25.58 kN). Specimen S5.5F had an applied mid-span load cycled from 1 kip (4.45 kN) to 6.5 kips (28.91 kN). All CFRP-retrofit specimens reported (those reported by Zorn (2006): CF, L2F, H2F, L2x1F and H2x1F) were tested in a similar manner although the load was cycled from 1 kip (4.45 kN) to 5 kips (22.24 kN) in all cases. Testing proceeded twenty-four hours a day, seven days a week, to ensure that tests would be completed in a reasonable amount of time. This also did not allow the beam to exhibit any damage recovery between cycling periods. The frequency was slowed to 1.2 Hz during cycles in which data was recorded (see below) to ensure that the quality of the data would remain high.

The upper limit of the frequency was determined by quality of the sustained control of the loading. For Specimen S4F, the test could be run at 1.7 Hz and still accurately load the beam from 1 to 5 kips. For Specimens S4.75F and S5.5F, the frequency was reduced to 1.5 Hz. It was observed that higher frequencies would not accurately maintain the load at the required peaks

and valleys due to the greater absolute deflection required for each cycle. The upper limit for the frequency was only used when data was not being taken. Specimen S5.5F was unique in that the test needed to be slowed down at night to ensure that it would not cycle too often before the next data scan. It was run at a frequency of 0.5 Hz during the night to ensure that data could be taken at an appropriate interval the next morning.

Due to the fact that each of the fatigue specimens was expected to have a different fatigue life, the interval at which data was recorded was different for each test. For Specimen S4F, the target was to take data at intervals not exceeding 100,000 cycles. For Specimens S4.75F and S5.5F, due to the expected reduced fatigue life, this target was similarly reduced to 50,000 and 25,000 cycles respectively. Table 2.4 provides the actual cycle numbers (N) at which data was recorded for each specimen, including the companion CFRP specimens tested by Zorn (2006). The unretrofit control specimen CF was unintentionally loaded to failure at cycle 329,324 cycles due to an equipment malfunction.

2.7.1 Selection of Fatigue Load Levels

The fatigue loading scheme used was selected based on the measured reinforcing bar strains from the original monotonic control Specimen C reported by Reeve (2005) as well as from Specimen SC. The target reinforcing bar strain range for the study conducted by Zorn (2006) was 1200 $\mu\epsilon$. This equates to a target stress range (S) of 34.8 ksi (240 MPa) in the reinforcing steel. The lower limit was chosen to be 1 kip (4.45 kN) to represent a constant dead load on the beam. After analyzing the data from Specimen C, it was determined that an upper limit of 5 kips (22.24 kN) was necessary to achieve the desired strain range. This stress range was chosen so that for the unretrofit control specimen, the fatigue life would be between $N =$

100,000 and $N = 1,000,000$. Specimen S4F used this same stress range so it may be directly compared to the specimens tested by Zorn (2006). Additionally, it was predicted that S4F would reach $N = 2,000,000$ cycles, and allow a run-out test to be performed to assess the effects of fatigue conditioning as described in Section 2.7.2.

Using data from Specimen SC, as well as representative S-N relationships, stress ranges were chosen for the other two fatigue specimens. The target fatigue life for Specimen S4.75F was $N = 1,000,000$. This resulted in a target strain range of $1410 \mu\epsilon$, or a stress range of 40.9 ksi (282 MPa). The upper applied load was found to be 5.75 kips (25.58 kN) to achieve this stress range. The target fatigue life for Specimen S5.5F was $N = 500,000$. This resulted in target strain range of $1664 \mu\epsilon$, or a stress range of 48.2 ksi (333 MPa). The upper applied load was found to be 6.5 kips (28.91 kN) for Specimen S5.5F. The equations used as guidance in estimating the fatigue life of each specimen were those proposed by Mallet (1991), Tilly and Moss (1982), CEB/FIB (1990) and Helgason and Hanson (1974). The target and actual fatigue life of all of the SFRP specimens and selected specimens from Zorn (2006) are shown in Table 2.5.

2.7.2 Fatigue Run-out Specimens

Specimen S4F did not exhibit a fatigue-induced reinforcing bar rupture (FIRR) or other failure after two million cycles of fatigue loading. The fatigue loading was then stopped and the beam was subsequently loaded monotonically to failure. The procedure for the monotonic test is the same as that described for Specimen SC. Specimen S4F is thus classified as a fatigue-conditioned specimen, and is comparable to the monotonic tests performed by Reeve (2005) and the fatigue-conditioned specimens reported by Zorn (2006).

2.8 SUMMARY OF COMPARABLE TESTS

The SFRP tests reported here are comparable in a variety of ways to those reported by Reeve (2005) and Zorn (2006). As described in Section 2.2, the SFRP details were selected to result in essentially similar values of retrofit axial stiffness as described in Equation 2.1. Table 2.6 provides a matrix of these comparables.

All of the specimens listed in Table 2.6 have the same axial stiffness ($E_{frp}t_{frp}b_{frp}$) regardless of retrofit scheme. Therefore, Table 2.6 displays which specimens underwent comparable testing procedures.

Table 2.1 Measured concrete and reinforcing steel material properties.

Specimen	28 Day Concrete Strength	Age at Time of Beam Test	Reinforcing Steel
	psi (MPa)	days	ksi (MPa)
CF	$f'_c = 3384$ (23.3)	175	E = 30000 (206842) $f_y = 62.2$ (429) $f_u = 96.8$ (667)
S4F		312	
SC		327	
S5.5F		333	
S4.75F		341	

Table 2.2 Manufacturer reported material properties of CFRP and SFRP.

Property	ASTM test method	SFRP Strip	CFRP Strip
cord architecture		3 straight surrounded by two twisted	
cord diameter, in. (mm)		0.035 (0.89)	
cord area, in ² (mm ²)		0.00096 (0.62)	
cords per inch width (per cm width)		23 (9)	
tensile strength, ksi (MPa)	D3039	164 (1132)	405 (2792)
tensile modulus (E), ksi (MPa)	D3039	10952 (75512)	22500 (155138)
elongation at rupture	D3039	0.014	0.018
perpendicular strength, psi (MPa)	D3039	not reported	negligible
strip thickness (t), in. (mm)		0.048 (1.2)	0.055 (1.4)
strip width used in this study (b), in. (mm)		4.75 (121)	2 (51)
axial stiffness (EA = Etb), kips (kN)		2497 (11107)	2475 (11009)

Table 2.3 Manufacturer reported material properties of adhesive systems used.

Property	ASTM test method	FX-776	Sikadur 23	Sikadur 30
tensile strength, ksi (MPa)	D638	4.5 (32)	2.0 (14)	3.6 (25)
tensile modulus, ksi (MPa)	D638	not reported	323 (2227)	650 (4482)
elongation at rupture	D638	0.025	0.063	0.01
modulus of rupture, ksi (MPa)	D790	not reported	4.8 (33)	6.8 (47)
tangent modulus of elasticity, ksi (MPa)	D790	575 (3964)	471 (3247)	1700 (11721)
shear strength, ksi (MPa)	D732	not reported	3.0 (21)	3.6 (25)
bond strength, ksi (MPa)	C882	not reported	2.6 (18)	3.2 (22)
compressive strength, ksi (MPa)	D695	not reported	5.2 (36)	8.6 (59)
compressive modulus, ksi (MPa)	D695	not reported	128 (883)	390 (2689)

Table 2.4 Cycle numbers (N) at which data was recorded.

CF ¹	S4F	S4.75F	S5.5F	L2F ¹	L2x1F ¹	H2F ¹	H2x1F ¹
1	1	1	1	1	1	1	1
4	2-100	2-100	2-100	28	42	60	33
41	105	101	138	30	68	208	201
53	244	230	207	100	200	500	506
80	505	525	501	203	514	1000	1003
203	1006	1006	1005	503	1000	2002	2002
503	5301	2001	2406	1000	2000	5002	5000
1003	14002	3059	4222	2002	5002	10000	12345
2004	18011	5016	5522	5000	20006	17536	22263
5004	24003	8333	10817	9005	49921	48309	41728
10003	31113	11756	13720	26175	93754	76518	74672
23000	40805	15817	18604	53644	129884	105945	105084
25003	50011	18652	24861	97371	186508	127367	134019
50001	133118	22469	29423	139081	243456	174010	180804
80630	152010	26318	53876	171802	286524	193373	221546
100003	185409	37301	71800	198997	333084	244356	263148
118835	207001	62465	82151	252293	387071	288365	330456
150008	276506	82712	102700	306074	447695	309744	383080
163210	316516	128309	112051	339047	472642	332931	408711
175016	364889	137003	135612	394505	478203	363267	457917
200003	438905	169000	152003	448168		384397	491206
232341	506736	213413	175119	516204		456885	543094
250005	579033	241815	198851	548306		499343	587368
260560	607851	268710	217952	614758		530053	634543
263864	639702	314700	238758	649379		584658	680704
288703	712505	355265	262401	678344		634809	727082
288795	787622	381800	286306	718318		683506	770932
288869	870302	427305	305882	796748		725006	795840
319910	924451	458106	307334	850088		769108	857770
319940	1008831	474901	308007	932773		829105	888616
319972	1075518	493453	308650	999057		870311	921602
320754	1158550	527271		1104642		900472	956056
	1226701	559805		1104779		929177	1010641
	1307004	588205		1153058		981210	1046631
	1380035	635753		1208866		1026397	1091782
	1454009	656654		1233708		1064437	1150133
	1515814	689671		1270711		1128006	1195622
	1603210	740400		1313465		1191770	1249275
	1662206	740803		1331586		1213229	1308834
	1718115	742511		1370787		1244102	1339340
	1780505	743210		1428332			1395821
	1855904	745600		1480351			1440043
	1929408	747000		1497354			1469580
	1999510	750556		1513597			1522985
	2000000	753050		1551888			1582672

Table 2.4 (continued)

CF ¹	S4F	S4.75F	S5.5F	L2F ¹	L2x1F ¹	H2F ¹	H2x1F ¹
		754950		1589683			1626337
		757500		1613127			1682752
		761500		1644243			1737853
		764000		1698454			1774778
		765900		1778638			1820072
				1838827			1882516
				1882825			1928895
				1924840			1965616
				2000000			1966273
							1998684
							2000000

¹Tests performed by Zorn (2006)

Table 2.5 Stress range (S) and cycles to failure (N) observations and predictions.

	Target Fatigue Life (cycles)	Initial ϵ range ($\mu\epsilon$)	Initial S (ksi)	Observed N
Target for CF	<1,000,000	1200	34.8	NA
CF ¹	<1,000,000	1203	34.9	>329324 ²
S4F	>2,000,000	1195	34.7	2000000
S4.75F	1,000,000	1410	40.9	689671
S5.5F	500,000	1664	48.3	286306
L2F ¹		1035	30.0	2000000
L2x1F ¹		1036	30.0	447695
H2F ¹		996	28.9	1128006
H2x1F ¹		1101	31.9	2000000

¹Tests performed by Zorn (2006)

²Specimen CF loaded to failure due to an equipment malfunction

Table 2.6 Matrix of comparable specimens.

Comparable	Control specimen	SFRP specimen(s)	CFRP specimen(s)
Monotonic loading	C	SC	H2, L2, H2x1, L2x1
Fatigue loading	CF	S4F	H2F, L2F, H2x1F, L2x1F
Fatigue-conditioning		S4F	L2F, H2x1F
Fatigue loading of SFRP	S4F	S4.75F and S5.5F	

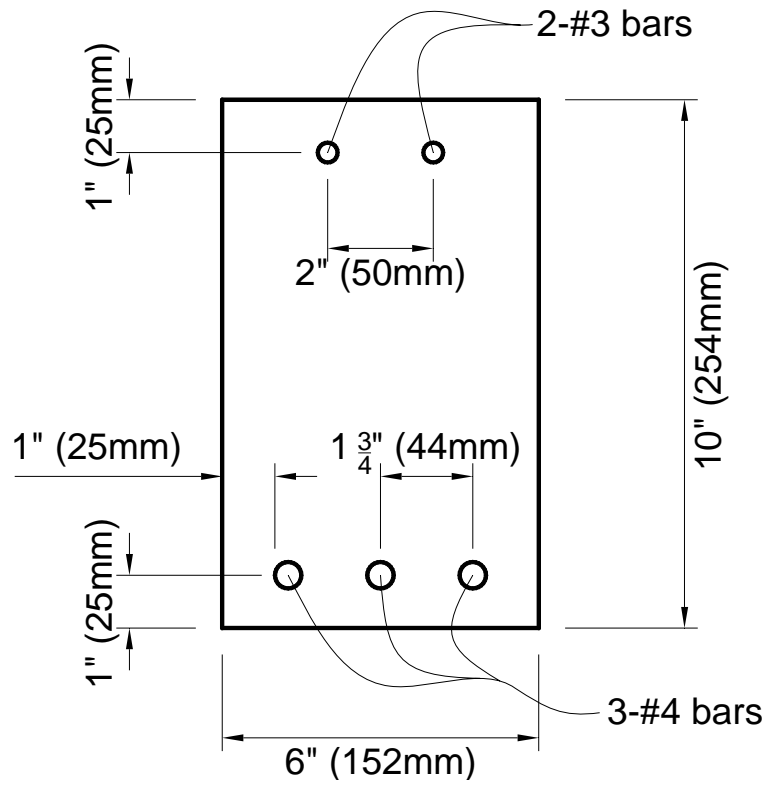


Figure 2.1 Test specimen details.

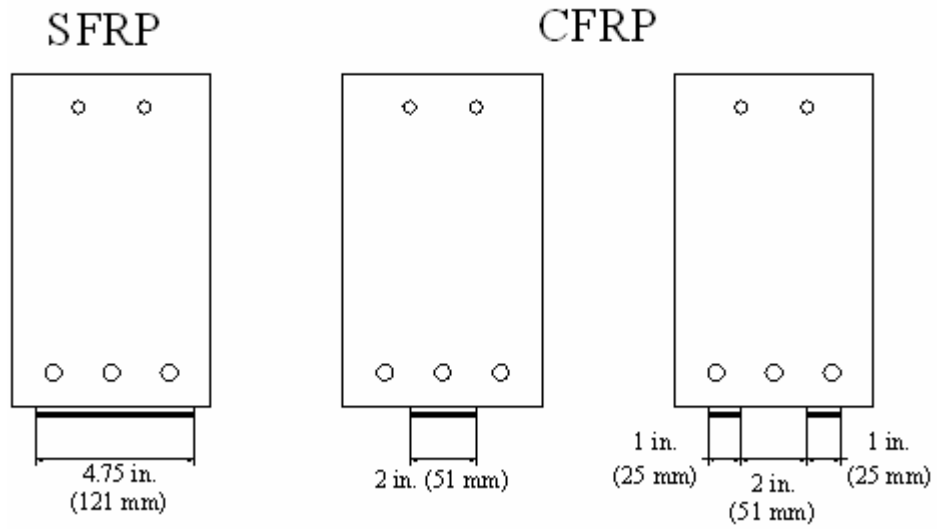


Figure 2.2 Retrofit details.



Figure 2.3 SFRP sheet and cord.
(Hardwire, 2002)

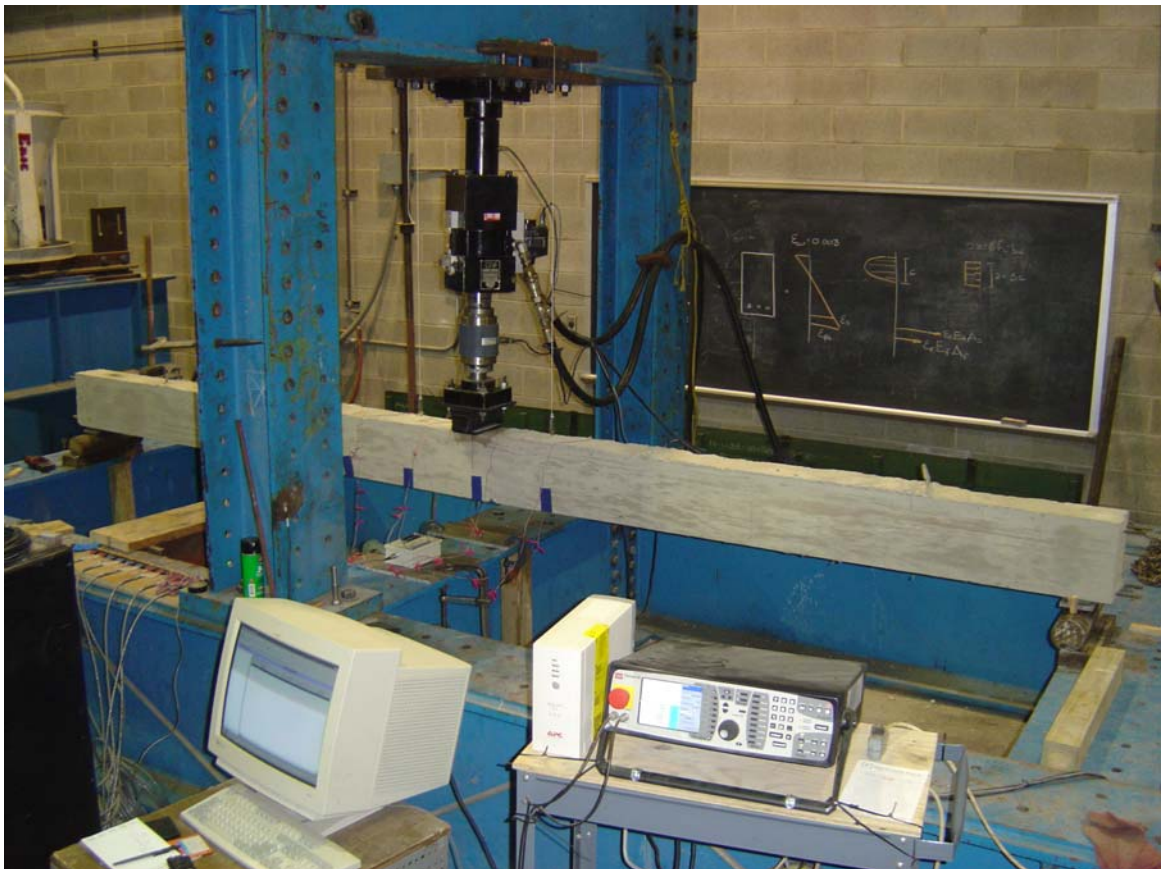


Figure 2.4 Test set-up.

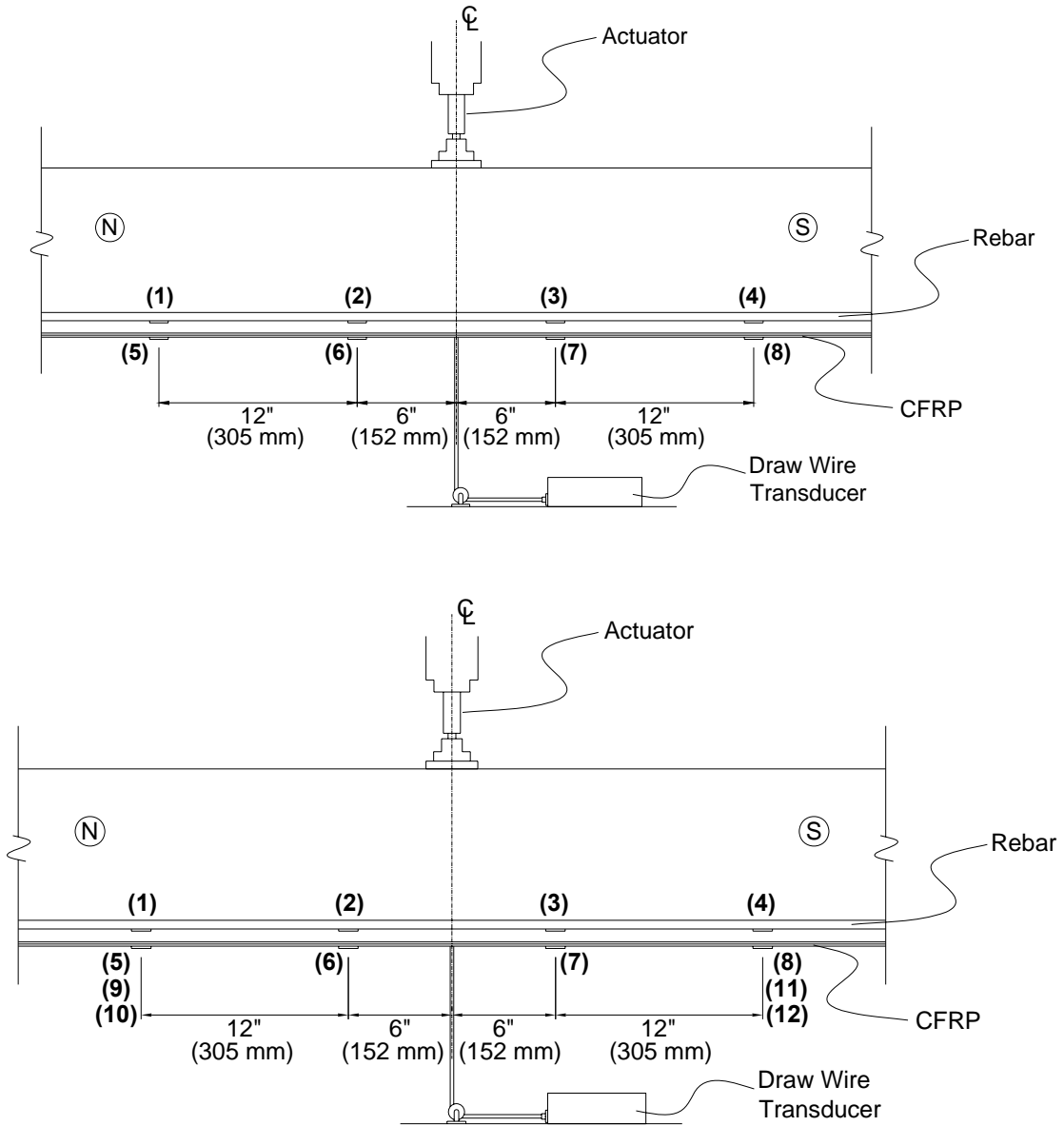


Figure 2.5 Instrumentation for specimens.
(Specimen SC on bottom)

3.0 TEST RESULTS AND TYPICAL SPECIMEN BEHAVIOR

This chapter reports the results of the test program and provides a discussion of the behavior of each test specimen.

3.1 TEST RESULTS

Figures 3.1 to 3.4 show the applied load versus midspan displacement for each SFRP Specimen plotted with the unretrofitted control specimen, Specimen C (reported by Reeve (2005)). The retrofit SFRP control, Specimen SC, is also repeated in each of these figures for comparison. For those specimens that underwent fatigue cycling, only intermittent fatigue cycles are shown as indicated in each Figure. For Specimen S4F, the final monotonic load cycle to failure is also shown. Figure 3.5 shows the damage accumulation, measured as the midspan deflection versus cycle number, of each test specimen. Figures 3.6 to 3.8 show the measured reinforcing bar and SFRP strains versus cycle number damage accumulation. In these figures, strains at each location are offset vertically by multiples of 2000 microstrain for clarity. Figure 3.9 shows the applied load versus reinforcing bar and SFRP strain for the retrofit control, Specimen SC. Figures 3.9(b) and 3.9(c) show the longitudinal strains measured across the width of the SFRP, at locations 18 in. (450 mm) to the north and south of midspan, respectively. Figure 3.10 shows the applied load versus reinforcing bar and SFRP strain for the runout portion of the

Specimen S4F test. Figures 3.11 to 3.18 are photographs of each test specimen as described further below.

A summary of key results for the fatigue specimens is presented in Table 3.1. A summary of the key results for the monotonic test, as well as the S4F monotonic runout test, are presented in Table 3.2. These tables also show data from companion CFRP-retrofit specimens reported by Reeve (2005) and Zorn (2006) as described in Section 2.1.

The following are descriptions for the data reported in Table 3.1.

b_f : width of S/CFRP strip

b : width of concrete substrate, equal to 6 inches (152 mm) in all cases.

age: age, in days, of the test specimen at time of testing with respect to date of cast.

cracking load: applied load at midspan at initiation of concrete cracking, determined by analyzing the time history of the reinforcing bar strains for each specimen.

The following parameters are reported for both $N = 2$ and $N = N_f$. Cycle $N = 2$ was used as this is the first cracked cycle. Cycle $N = N_f$ represents the last instrumented fatigue cycle and is defined in each case.

minimum applied load: the minimum midspan loading applied to the test specimen during one fatigue cycle (target = 1 kip (4.45 kN)).

deflection at minimum applied load: deflection at midspan at the minimum applied loading.

maximum reinforcing bar strain at minimum applied load: corresponding maximum reinforcing bar strain in the middle reinforcing bar at the minimum applied load.

maximum FRP strain at minimum applied loading: corresponding maximum S/CFRP strain at the minimum applied loading.

maximum applied load: the maximum midspan loading applied to the test specimen during one fatigue cycle (target changes depending on the specimen as described in Section 2.7).

deflection at maximum applied load: deflection at midspan at the maximum applied loading.

maximum reinforcing bar strain at maximum applied load: corresponding maximum reinforcing bar strain in the middle reinforcing bar at the maximum applied load.

maximum FRP strain at maximum applied load: corresponding maximum S/CFRP strain at the maximum applied loading.

range of applied load: the difference of the maximum applied load and the minimum applied load.

stress range in reinforcing bar: calculated by multiplying $E = 29000$ ksi (200 GPa) by the difference of the maximum and minimum reinforcing bar strains.

stress range in CFRP: calculated by multiplying $E = 22500$ ksi (155 GPa) by the difference of the maximum and minimum CFRP strains.

stress range in SFRP: calculated by multiplying $E = 10952$ ksi (75.5 GPa) by the difference of the maximum and minimum SFRP strains.

secant stiffness: apparent stiffness calculated by dividing the difference of the maximum and minimum applied load by the difference of the corresponding midspan deflections.

The following parameters are reported from any time during the fatigue cycling period; that is: $N \leq N_f$.

maximum observed strain in FRP: the greatest strain ever observed in the S/CFRP during the course of fatigue cycling. The strain in the reinforcing bar at the corresponding location, as well as the cycle number, are also reported.

initiation of S/CFRP debonding: the strain at which there is apparent debonding of the S/CFRP.

The following are descriptions for the data presented in Table 3.2 for the monotonic run-out tests.

load at initial yield of reinforcing: the applied load at midspan when the middle tensile reinforcing bar experiences its yield strain of 2140 microstrain (see Table 2.1).

load at general yield: the applied load at midspan when the specimen experienced general yield. This is defined as a significant change of load versus deflection with visible nonlinearity. In this case, there is a gradual degradation of stiffness. General yield was therefore determined from a bilinear idealization of the load-deflection curve. An illustrative example of this determination can be found in Chapter 3 of Reeve (2005).

deflection at general yield: midspan deflection when the specimen experienced general yield.

strain in S/CFRP at general yield: maximum strain in S/CFRP at time of general yield.

maximum load: maximum load experienced by the test specimen during monotonic testing.

ultimate load: either the load corresponding to failure of the specimen, or the post-peak load corresponding to 80% of the maximum load, whichever is greatest.

ductility: ratio of the midspan deflection at ultimate load to the midspan deflection at general yield.

maximum S/CFRP strain: the greatest strain in the S/CFRP observed. The strain in the middle reinforcing bar at the corresponding location is also indicated.

initiation of debonding: the S/CFRP strain at which debonding appears to occur.

All moments calculated in Tables 3.1 and 3.2 are midspan moments. They were calculated using the equation $M = PL/4$, where M is the moment, P is the applied midspan load, and L is the clear span (178.25 in (4527 mm)).

3.2 SPECIMEN BEHAVIOR

This section discusses the behavior of each specimen.

3.2.1 Specimen SC

Specimen SC was tested monotonically in displacement control to failure. Cracking occurred at 663 pounds (2.95 kN), which is comparable to the companion specimens tested by Reeve (2005) and Zorn (2006). The post-cracking stiffness was nearly identical to that of Specimen H2x1. Specimen SC exhibited a single large shear crack and accompanying longitudinal splitting at the level of the reinforcing steel as seen in Figure 3.11. Debonding initiated near the toe of the shear crack and propagated towards the nearest (south) support as shown in Figure 3.12. The SFRP did not debond completely, remaining bonded to the concrete near the south support. There was also significant concrete crushing at the point of load application. The ultimate capacity of Specimen SC was 10.65 kips (47.37 kN). Load versus midspan deflection can be seen in Figure 3.1. Load versus strain behaviors are shown in Figure 3.9.

3.2.2 Specimen S4F

Specimen S4F sustained 2,000,000 cycles of fatigue loading cycling from 1 kip (4.45 kN) to 5 kips (22.24 kN). The fatigue test was then stopped, and the specimen was tested monotonically to failure. This specimen may be considered to be “fatigue conditioned”. The initial stiffness of Specimen S4F was nearly identical to that of Specimen SC, as can be seen in Figure 3.2. Specimen S4F experienced little apparent damage throughout the fatigue conditioning. A “tap test” did not reveal any debonding following the 2,000,000 load cycles. Figure 3.2 shows how similar the load-deflection behavior of Specimen S4F was to that of Specimen SC to failure. Specimen S4F also exhibited a dominant shear crack with debonding initiating near the toe of the crack and propagating towards the nearest (south) support. Photographs in Figures 3.13 and 3.14 show this behavior. The ultimate capacity of Specimen S4F was 10.48 kips (46.62 kN). Load versus strain behaviors are shown in Figure 3.10.

3.2.3 Specimen S4.75F

Specimen S4.75F, cycled between applied loads of 1 kip (4.45 kN) and 5.75 kips (25.6 kN), failed due to a fatigue-induced reinforcing bar rupture. The stiffness of Specimen S4.75F was nearly identical to that of Specimen SC, as can be seen in Figure 3.3. The rupture of the west reinforcing bar became apparent after cycle 689,671. Following this cycle, the stiffness of the beam changed significantly, and there was a clear increase in midspan deflection. A shear crack also formed after the rupture. The reinforcing bar rupture was located directly at the toe of the shear crack. Figure 3.15 shows the shear crack, as well as the location of the reinforcing bar rupture. A tap test was done to locate any debonding of the SFRP. Debonding was only found

after the rupture, right at the location of the rupture. Figure 3.16 shows the reinforcing bar rupture. It is believed that the observed debonding was the result of the energy release of the rupture. The failure mode of Specimen S4.75F was fatigue-induced reinforcing bar rupture.

3.2.4 Specimen S5.5F

Specimen S5.5F, cycled between applied loads of 1 kip (4.45 kN) and 6.5 kips (28.9 kN), failed due to a fatigue-induced reinforcing bar rupture. The stiffness of Specimen S5.5F was nearly identical to that of Specimen SC, as can be seen in Figure 3.4. The rupture of the west reinforcing bar became apparent after cycle 286,306. Following this cycle, the stiffness of the beam changed significantly, and there was a clear increase in midspan deflection. The width of the flexural cracks directly under the loading increased significantly. Also, horizontal cracks were visible at the level of the reinforcing steel as can be seen in Figure 3.17. The test was continued until cycle 308,650, at which time the beam failed due to a large shear crack. The ruptured reinforcing bar was then visible, and can be seen in Figure 3.18. The failure mode of Specimen S5.5F was fatigue-induced reinforcing bar rupture.

Table 3.1 Summary of Fatigue Data.

SI Units (<i>kips, inches</i>)		CFRP					SFRP		
Beam ID:		CF	L2F	L2X1F	H2F	H2X1F	S4F	S4.75F	S5.5F
b _f /b:		na	0.333	0.333	0.333	0.333	0.792	0.792	0.792
adhesive type:		na	23	23	30	30	FX	FX	FX
age at start of fatigue test:	days	175	191	231	217	238	312	341	333
cracking load:	kips	0.68	0.68	0.69	0.67	0.69	0.69	0.66	0.69
cracking moment:	kip-in	30.2	30.3	30.7	30.0	30.8	30.8	29.5	30.8
at N = 2									
minimum applied load	kips	1.01	1.03	1.02	1.03	1.04	1.03	1.04	1.01
minimum applied moment	kip-in	44.9	45.8	45.8	46.1	46.3	46.2	46.6	45.2
deflection at minimum applied load	in	0.29	0.26	0.29	0.29	0.27	0.27	0.29	0.30
maximum reinforcing bar strain at minimum applied load	ue	747	633	622	610	633	520	601	663
maximum FRP strain at minimum applied load	ue	na	663	640	787	806	683	659	608
maximum applied load	kips	4.98	5.00	5.00	5.00	5.00	4.97	5.72	6.44
maximum applied moment	kip-in	222	223	223	223	223	222	256	288
deflection at maximum applied load	in	0.78	0.67	0.74	0.75	0.70	0.66	0.79	0.89
maximum reinforcing bar strain at maximum applied load	ue	1950	1668	1658	1606	1734	1465	1790	2094
maximum FRP strain at maximum applied load	ue	na	1758	1778	1997	2089	1783	1952	2151
range of applied load	kips	3.98	3.98	3.98	3.97	3.96	3.94	4.68	5.43
range of applied moment	kip-in	178	178	178	177	177	176	209	243
stress range in rebar	ksi	34.9	30.0	30.0	28.9	31.9	27.4	34.5	41.5
stress range in FRP	ksi	na	24.6	25.6	27.2	28.9	12.0	14.2	16.9
apparent stiffness between minimum and maximum load	kip/in	7.92	9.36	8.72	8.38	9.19	10.15	9.28	9.21
last recorded cycle before failure (N_f)		na	2000000	447695	1128006	2000000	2000000	689671	286306
at N = N_f or N = 2000000									
minimum applied load	kips	na	1.00	1.02	1.01	1.00	1.01	1.01	1.01

Table 3.1 (continued)

		CF	L2F	L2x1F	H2F	H2x1F	S4F	S4.75F	S5.5F
minimum applied moment	kip-in	na	45	45	45	45	45	45	45
deflection at minimum applied load (relative to zero load)	in	na	0.27	0.32	0.36	0.33	0.30	0.36	0.29
maximum reinforcing bar strain at minimum applied load	ue	na	607	641	598	628	513	578	660
maximum FRP strain at minimum applied load	ue	na	638	611	832	837	753	994	641
maximum applied load	kips	na	5.00	5.00	5.00	5.00	5.00	5.74	6.50
maximum applied moment	kip-in	na	223	223	223	223	223	256	290
deflection at maximum applied load (relative to zero load)	in	na	0.79	0.81	0.87	0.84	0.77	0.92	0.94
maximum reinforcing bar strain at maximum applied load	ue	na	1809	1790	1684	1881	1570	1870	2235
maximum FRP strain at maximum applied load	ue	na	1864	1819	2158	2279	2053	2114	2294
range of applied load	kips	na	4.00	3.98	3.99	4.00	3.99	4.73	5.48
range of applied moment	kip-in	na	179	178	178	179	178	211	245
stress range in rebar	ksi	na	34.9	33.3	31.5	36.3	30.7	37.5	45.7
stress range in FRP	ksi	na	27.6	27.2	29.8	32.4	14.2	12.3	18.1
apparent stiffness between minimum and maximum load	kip/in	na	7.69	8.07	7.86	7.58	8.64	8.39	8.38
any N									
maximum observed strain in FRP	ue	na	1873	1819	2158	2285	2047	2117	2294
corresponding (same location) rebar strain	ue	na	1809	1658	1684	1526	1566	1870	2018
cycle number		na	1698454	447695	1128006	1820072	1855904	268710	286306

Table 3.2 Summary of Monotonic Data.

SI Units (<i>kips, inches</i>)	CFRP								SFRP	
	Beam ID:	C	L2	L2x1	H2	H2x1	L2F	H2x1F	SC	S4F
b _f /b:	0	0.333	0.333	0.333	0.333	0.333	0.333	0.333	0.792	0.792
adhesive type:	na	23	23	30	30	23	30	FX	FX	
age at start of fatigue test:	144	157	161	163	165	191	238	327	312	
cracking load:	<0.66	0.66	0.63	0.64	0.64	0.68	0.69	0.66	0.69	
cracking moment:	<29.5	29	28	29	29	30	31	30	31	
load at initial yield of reinforcing(2140):	5.91	6.78	5.99	6.38	6.63	6.15	5.85	7.59	7.13	
moment at initial yield of reinforcing:	264.05	303	267	285	296	275	261	339	318	
deflection at initial yield of reinforcing:	0.980	1.000	0.842	0.948	0.893	0.92	0.94	1.03	1.02	
load at general yield:	6.96	8.61	9.08	8.80	9.20	8.88	9.49	9.6	8.84	
moment at general yield:	310.8	384	405	393	411	397	424	429	395	
deflection at general yield:	1.180	1.320	1.350	1.360	1.300	1.29	1.39	1.36	1.21	
maximum load:	6.98	9.96	10.23	9.79	10.15	10.23	10.19	10.65	10.48	
maximum moment:	311.7	445	457	437	453	457	455	476	468	
deflection at max load:	1.423	2.061	2.352	1.878	1.974	2.30	1.89	2.13	1.97	
least deflection from max to 80% max:	3.077	2.239	2.549	2.176	2.210	2.65	2.02	2.36	2.23	
displacement ductility:	2.61	1.70	1.89	1.60	1.70	2.06	1.45	1.74	1.84	
maximum observed strain in FRP:	na	6688	7878	6200	6863	7444	6970	7053	6974	
corresponding rebar strain:	15932	13167	6620	14812	6004	3238	13039	13877	13113	
maximum strain in FRP at time of max load:	na	6518	7872	6112	6853	7322	6875	6953	6551	
corresponding rebar strain:	2759	13124	6624	14663	6034	4171	13664	13645	12878	
strain in FRP at apparent initiation of debonding:	na	6688	7878	3550	3200	4301	3909	2978	3173	
corresponding rebar strain:	na	>15000	>15000	2680	2790	2898	2767	2679	2478	
max strain in FRP at time of general yield deflec:	na	3445	4681	3892	4253	3391	4318	3347	3291	
corresponding rebar strain:	na	3868	11877	7674	13085	7485	2727	2894	2688	

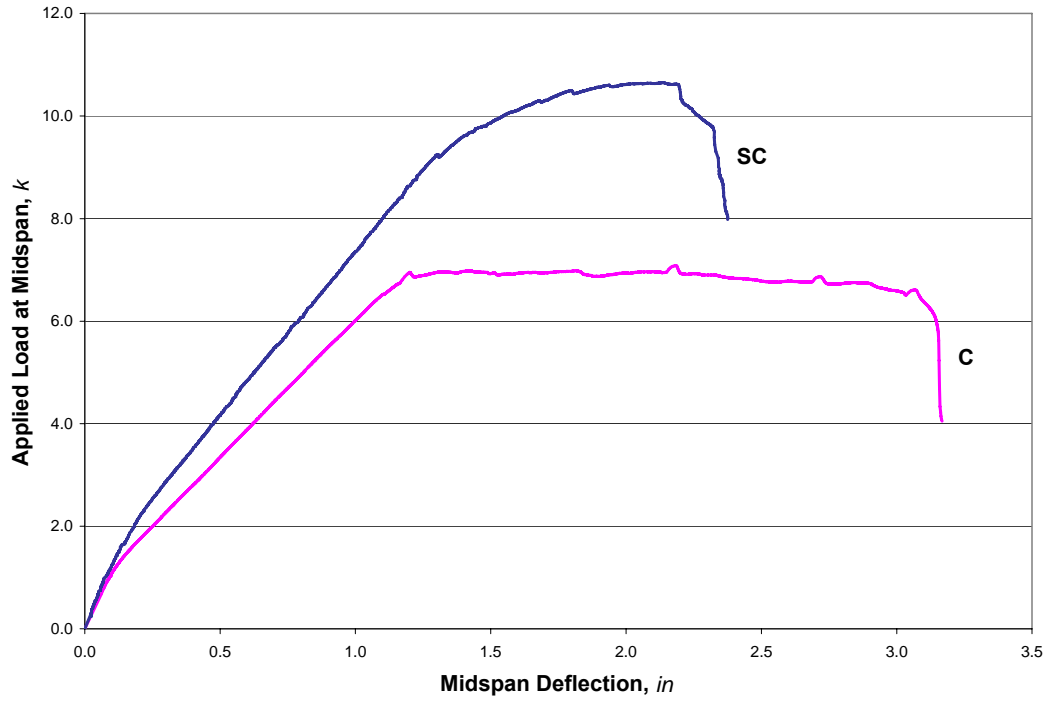


Figure 3.1 Test Specimens SC and C.

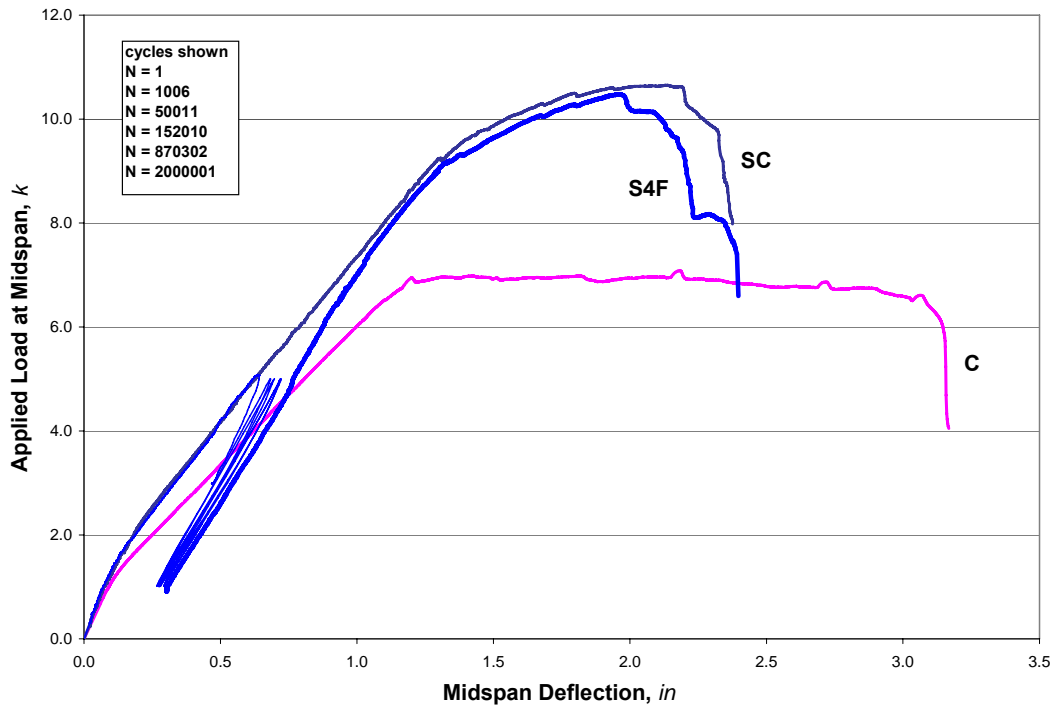


Figure 3.2 Specimens S4F, SC, and C.

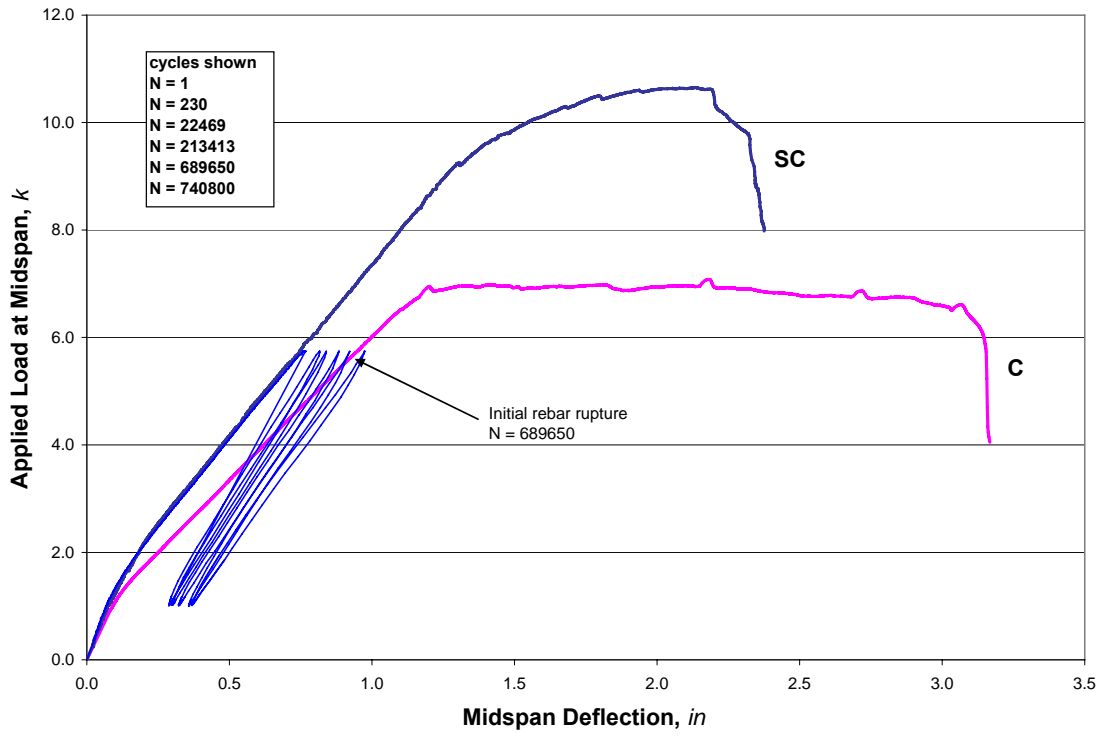


Figure 3.3 Specimens S4.75F, SC, and C.

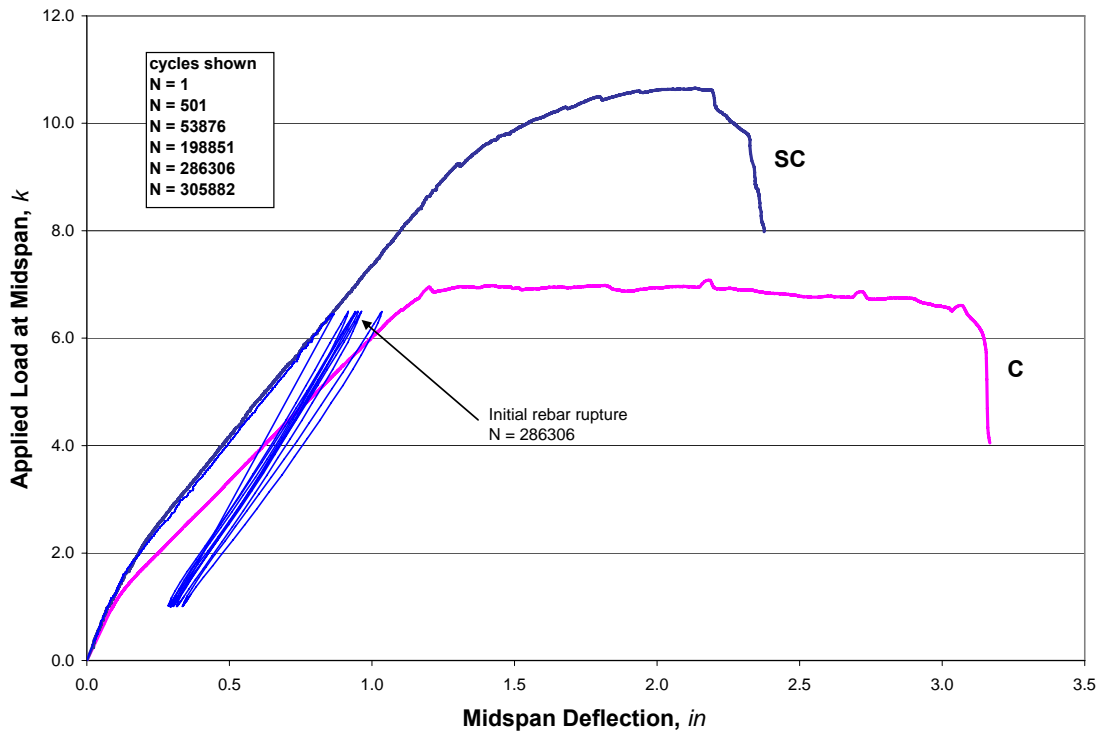


Figure 3.4 Specimens S5.5F, SC, and C.

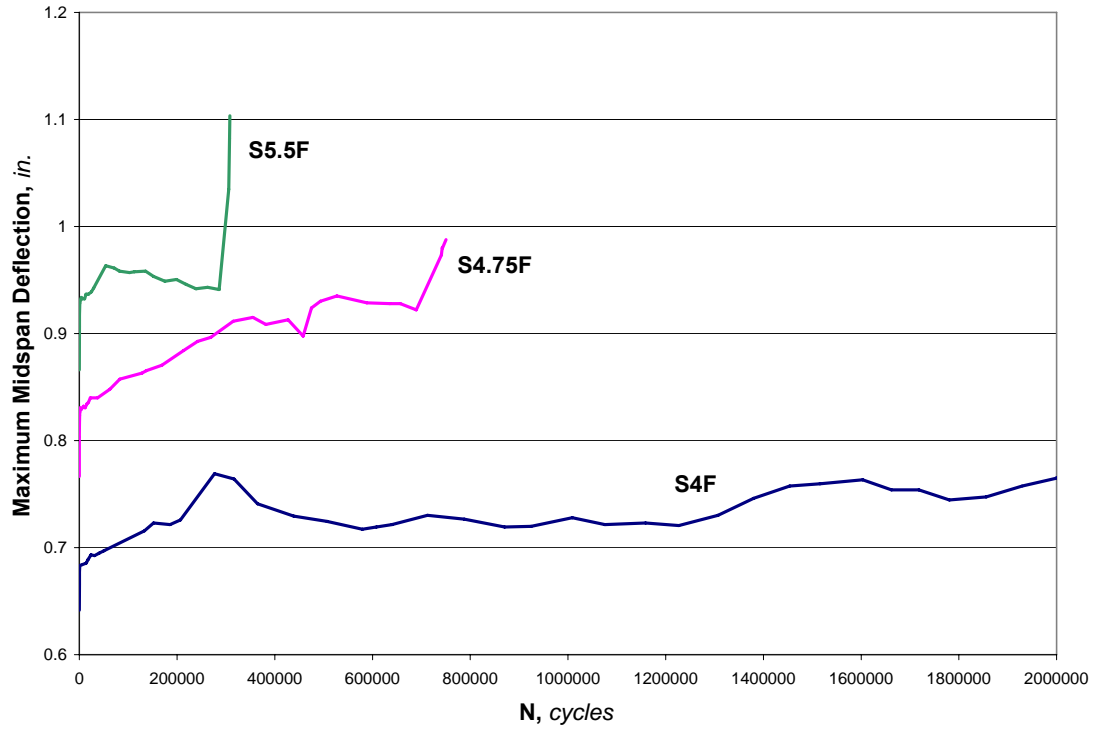


Figure 3.5 Midspan deflection accumulation curves.

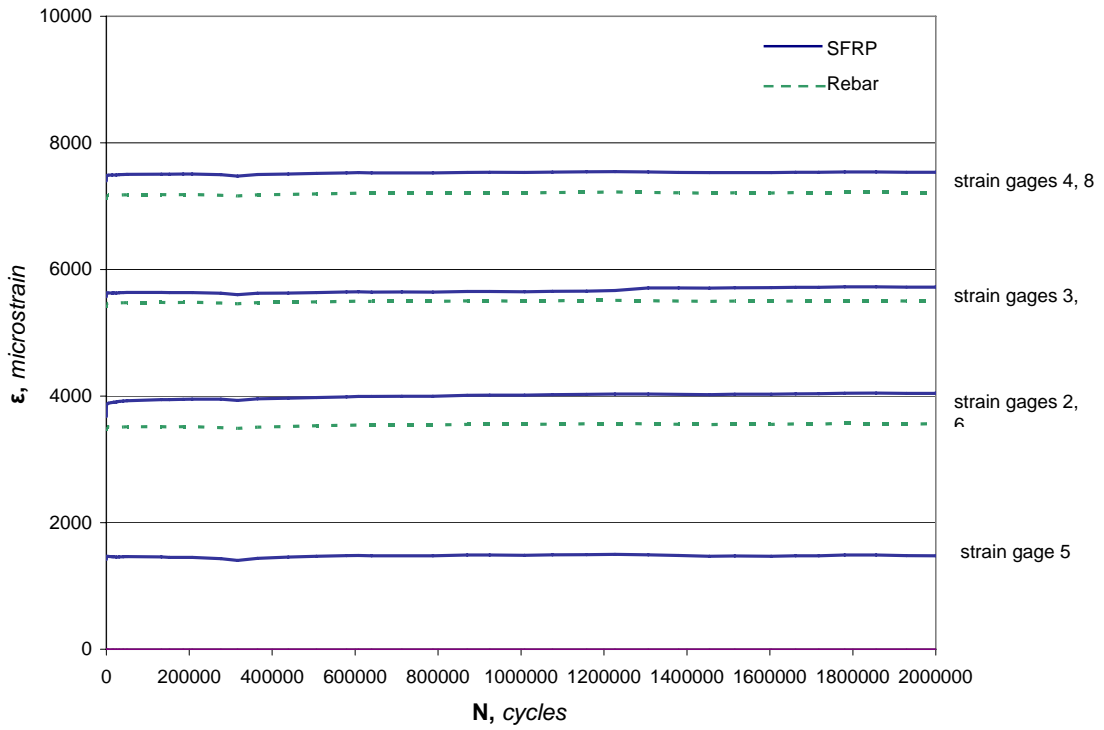


Figure 3.6 Strain accumulation curves for Specimen S4F (shifted vertically $2000 \mu\epsilon$).

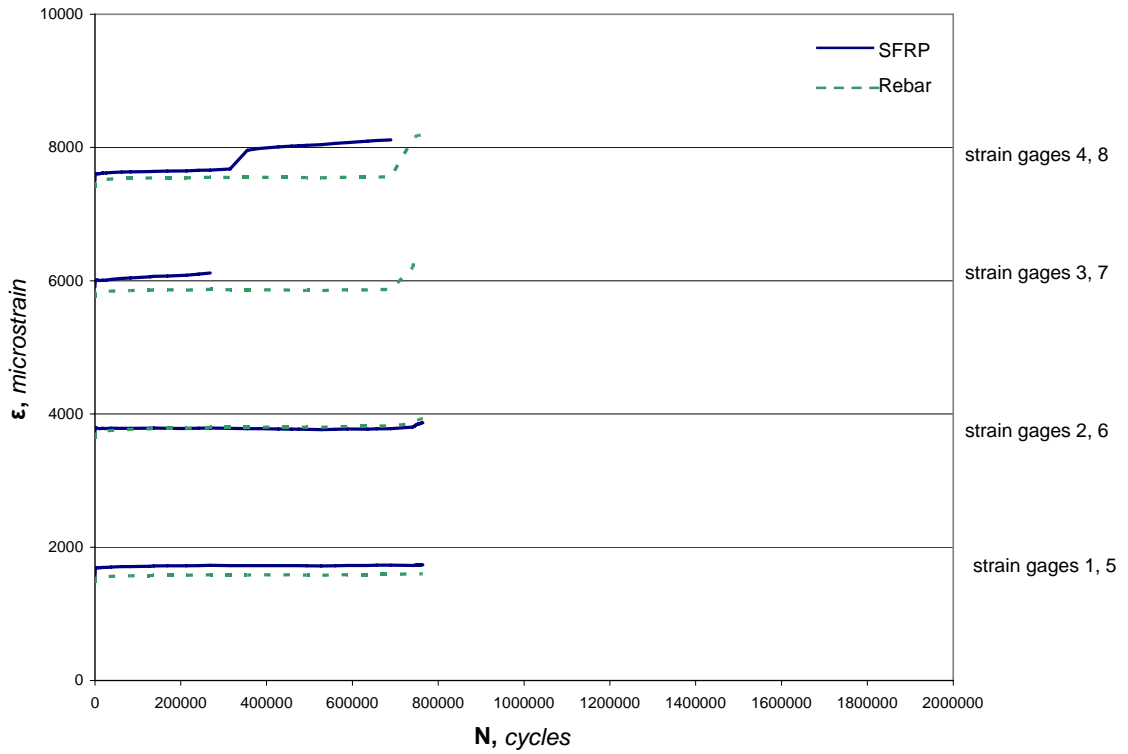


Figure 3.7 Strain accumulation curves for Specimen S4.75F (shifted vertically $2000 \mu\epsilon$).

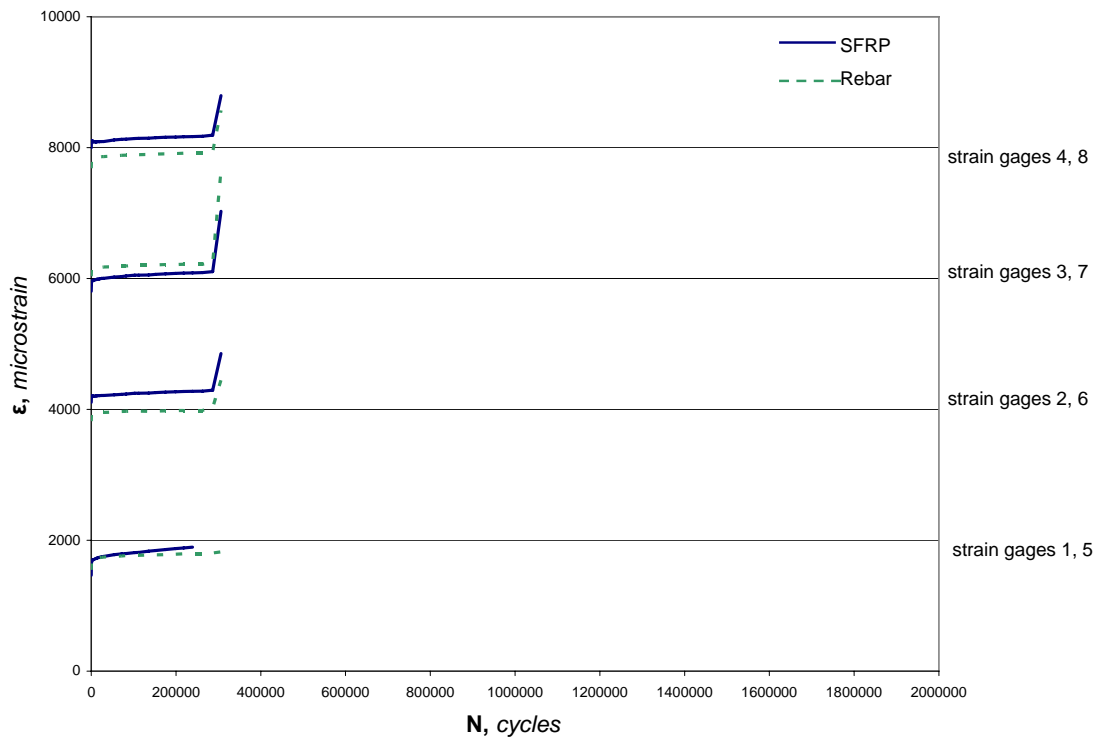


Figure 3.8 Strain accumulation curves for Specimen S5.5F (shifted vertically $2000 \mu\epsilon$).

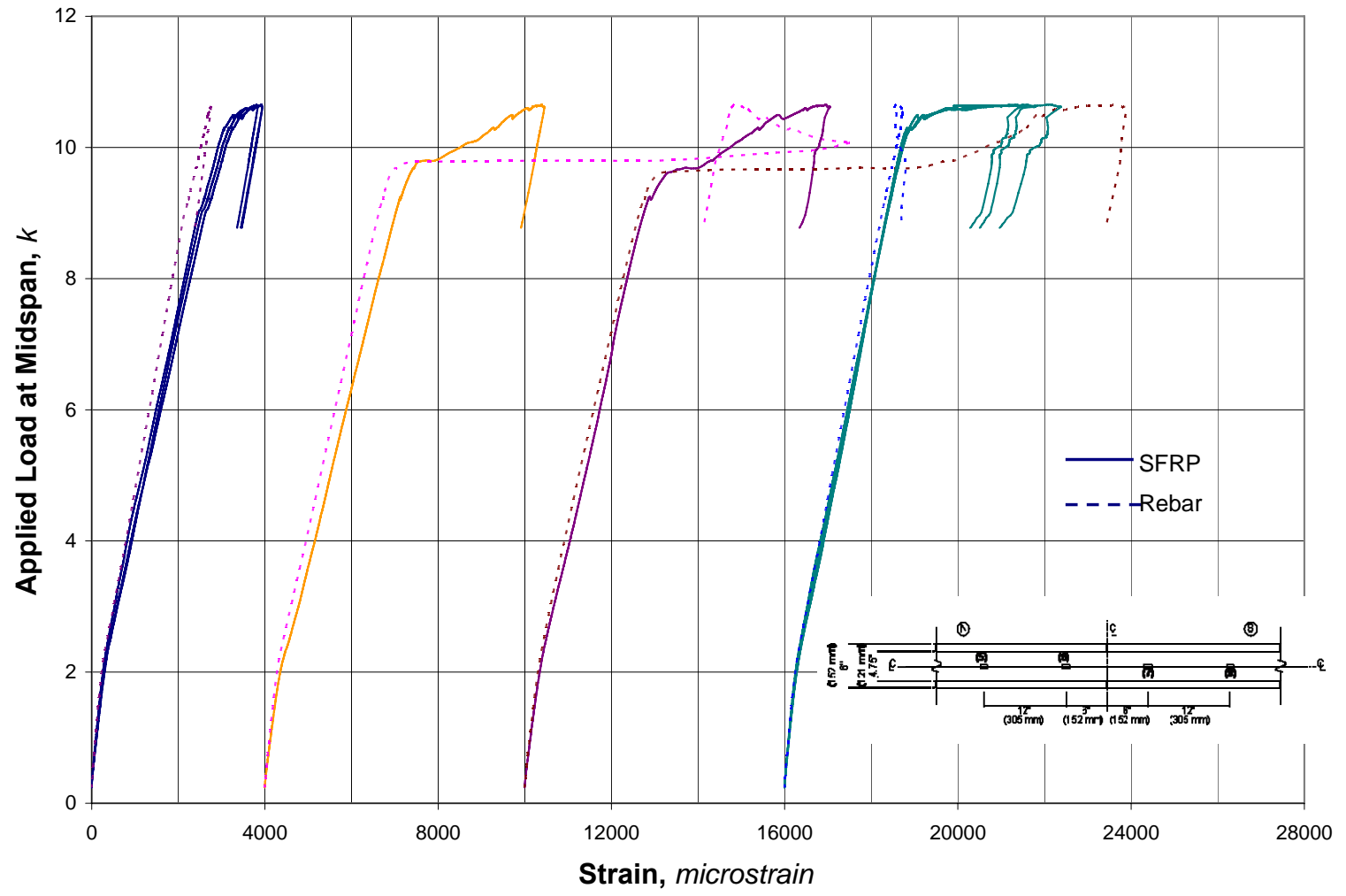


Figure 3.9(a) Load-strain behavior for Specimen SC (shifted horizontally).

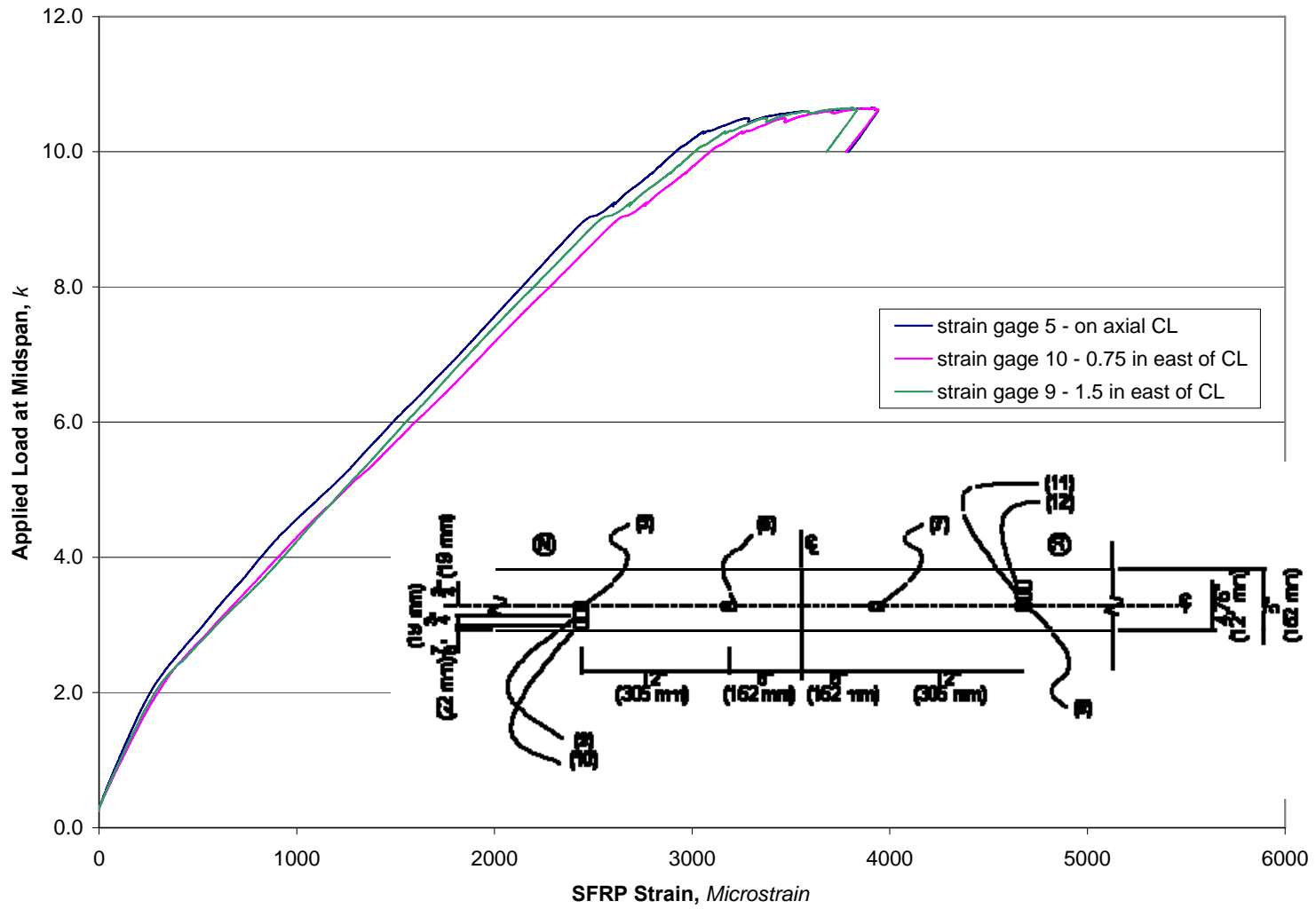


Figure 3.9(b) Test Specimen SC – North strain gages (9), (10), and (5).

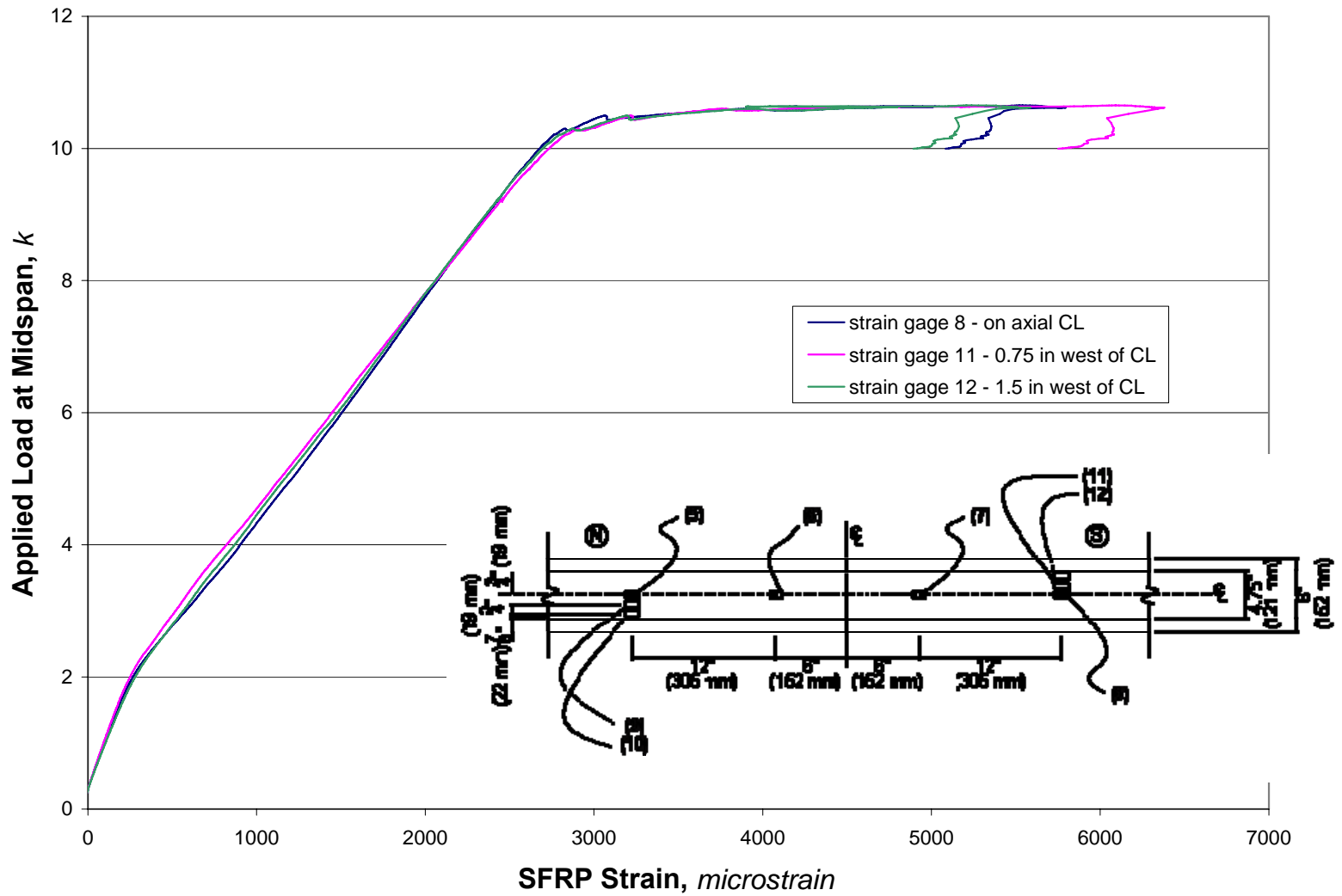


Figure 3.9(c) Test Specimen SC – South strain gages (8), (11), and (12).



Figure 3.11 Shear crack of Specimen SC (east side).



Figure 3.12 Debonding at toe of shear crack, Specimen SC (west side).



Figure 3.13 Shear crack on Specimen S4F (west side).



Figure 3.14 Debonding at toe of shear crack, Specimen S4F (west side).

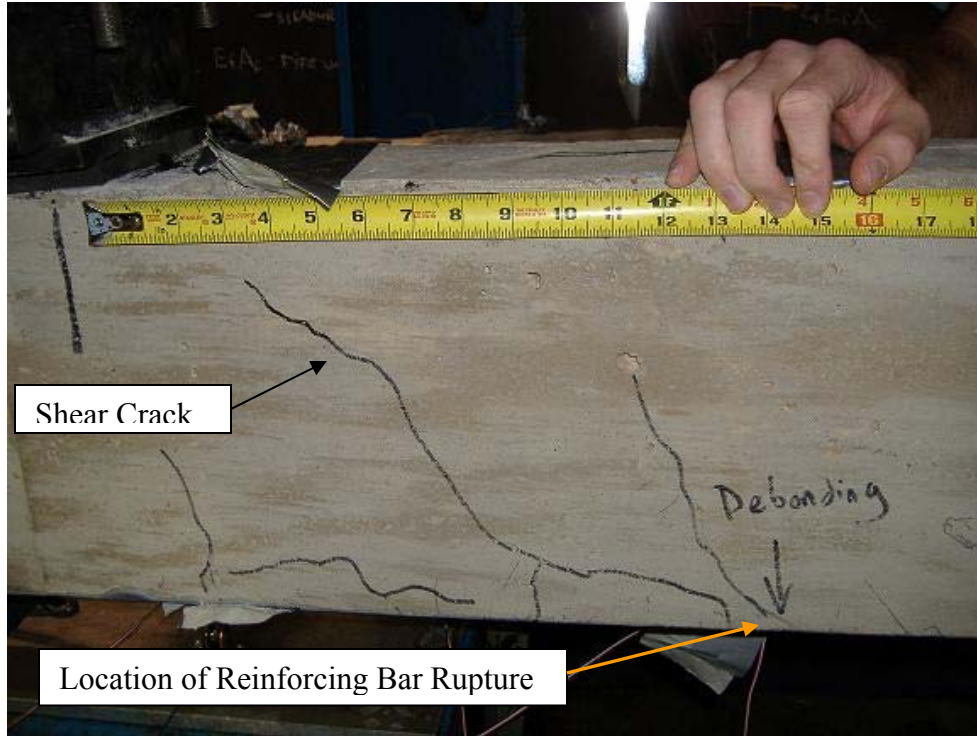


Figure 3.15 Specimen S4.75F after reinforcing bar rupture (west side).



Figure 3.16 Fatigue-induced reinforcing bar rupture, Specimen S4.75F.



Figure 3.17 Specimen S5.5F after reinforcing bar rupture (west side).



Figure 3.18 Fatigue-induced reinforcing bar rupture, Specimen S5.5F.

4.0 DISCUSSION OF EXPERIMENTAL RESULTS

This chapter reports interpretations of the experimental data reported in Chapter 3. The focus of this interpretation is to provide a comparison of SFRP with more conventionally used CFRP materials for retrofit of concrete beams in flexure.

4.1 COMPARISON OF MONOTONIC TEST SPECIMENS

Test specimen designation is outlined in Section 2.4. Figure 4.1 shows the load deflection plot for Specimen SC along with companion Specimens C, L2, L2x1, H2, and H2x1 reported by Reeve (2005). This plot allows a direct comparison of performance of an uncracked reinforced concrete beam retrofitted with SFRP to those retrofitted with an equivalent amount of CFRP (with respect to axial stiffness). A summary of key results for the monotonic tests is given in Table 3.2 and a summary of the ratios of these values to those of the control specimen is given in Table 4.1. Definitions for all key results are given in Section 3.1.

The cracking load for Specimen SC was nearly identical to that of the companion specimens tested by Reeve (2005). The load at general yield was slightly higher for Specimen SC when compared to the companion CFRP retrofits. The deflections were essentially the same. Specimen SC was able to achieve a slightly higher maximum load than the companion specimens.

Reeve concluded that the 2x1 specimens were nominally stronger and stiffer than the single 2 inch (50 mm) retrofits at general yield, indicating that multiple thinner strips may be preferable to fewer wider strips. This effect may explain why Specimen SC was slightly stronger and stiffer than the companion specimens, since the SFRP material is comprised of discrete thin cords rather than a more homogeneous continuum. Such an arrangement may allow a more uniform redistribution of stress in the transverse direction and minimize the stress raisor known to occur at the edges of bonded plates (Timoshenko and Goodier 1987, as reported by Quattlebaum 2003). The increased stiffness may also be a reflection of the SFRP system having an axial stiffness marginally larger than that of the CFRP specimen.

Normalized comparisons of Specimen SC with the companion specimens tested by Reeve (2005) and Zorn (2006) can be seen in Figures 4.2 through 4.5. These figures plot the ratio of the test specimen performance to that of the control Specimen C versus the equivalent flexural reinforcement ratio ($\rho_{\text{equivalent}}$) of the test specimen. The equivalent flexural reinforcement ratio is defined as follows:

$$\rho_{\text{equivalent}} = \frac{A_s}{bh} + \frac{A_f}{bh} \frac{E_f}{E_s} \quad (4.1)$$

where bh = gross area of concrete section

A_f = cross sectional area of SFRP or CFRP; $A_f = t_f b_f$

A_s = cross sectional area of existing internal tension steel reinforcement

E_f = modulus of SFRP or CFRP (see Table 2.2)

E_s = modulus of steel reinforcement, taken as 29000 ksi (200 GPa)

For all specimens in this study, the first term in Equation 4.1 (A_s/bh) is equal to 1%.

The SFRP specimens, and corresponding companion specimens, have an equivalent reinforcement ratio of 0.0114. Reeve and Zorn also tested CFRP retrofitted specimens with ratios

of 0.0107 and 0.0128. While these specimens are not used for comparison purposes with the SFRP specimens, they are included in the figures to illustrate the trends observed for the CFRP specimens. Figure 4.6 shows the FRP strain at the initiation of debonding for all specimens discussed.

Each of Figures 4.2 – 4.6 shows how Specimen SC is generally comparable to the CFRP companion specimens. In each case, other than debonding strain (Figure 4.6), Specimen SC performed marginally better than the companion specimens that used the high modulus adhesive (H-series specimens). As shown in Table 2.3, the FX-776 epoxy used for the SFRP specimens has properties that lie between the extremes of the low (L) and high modulus (H) adhesives used in the companion studies, although having properties closer to those of the high modulus adhesive. While Specimen SC performed slightly better than all companion specimens in terms of general yield load and maximum load, it was outperformed significantly by some companion specimens having low modulus adhesive (L-series) in terms of deflection and ductility. This reinforces the conclusion that adhesive stiffness has a significant contribution to the performance of a retrofit scheme (Reeve 2005).

Figure 4.6 shows how the debonding strain for Specimen SC was comparably lower than that observed for the CFRP specimens. This lower debonding strain is believed to result from the combination of a stiff adhesive and thinner adhesive bondline. Predicted debonding behavior is investigated later in this chapter.

4.2 COMPARISON OF FATIGUE TEST SPECIMENS

The fatigue behavior of the SFRP specimens is reported in this section. A comparison of the run-out portions of the tests is reported in section 4.3.

S-N data (S is stress range in the internal reinforcing steel and N is cycles to failure) from this study is plotted in Figures 4.7 and 4.8. Also shown in these figures are representative S-N relationships recommended for reinforcing steel tested in air (Moss 1980) and tested in flexural beams (CEB 1990). Run-out specimens are noted with arrows indicating that their fatigue life was not reached at the number of cycles (N) shown. All other specimens shown experienced fatigue-induced reinforcing bar rupture (FIRR). The control fatigue specimen, CF, was inadvertently loaded to failure during a power outage (Zorn, 2006) and is represented with an open circle and an arrow signifying that the actual fatigue life would have been somewhat greater than the 329,324 cycles reported.

The behavior of the three fatigue specimens having SFRP are predicted by the recommended relationship for reinforcing steel tested in flexural beams (CEB 1990) relatively well. Additionally, the SFRP specimens have an improved fatigue resistance as compared to the CFRP specimens – that is for a given stress range, S, the fatigue life, N, for the SFRP specimens is greater, or conversely, the SFRP specimens may withstand a greater S for a given fatigue life, N. Figure 4.8 includes data from a number of researchers. As can be seen the SFRP data generally falls near the lower boundary of the clustered data indicating a generally superior fatigue performance.

Figure 4.9 compares the stress range in the internal reinforcing steel at N=2 for different reinforcing ratios. All stresses are normalized by dividing by the stress range in the reinforcing steel observed for Specimen C. Specimen C was used for normalization since Specimen CF did

not experience applied loads large enough to be able to compare its performance to that of S4.75F and S5.5F. Figure 4.9 shows how the SFRP is equally as effective as the CFRP in reducing the stress range in the reinforcing steel. When the applied load was increased (S4F to S4.75F to S5.5F), the reduction in reinforcing bar stress range is diminished only nominally. All of the SFRP and CFRP data fell with a relatively small scatter in this performance measure.

4.2.1 Stress Range “Drift”

For the purpose of this study, as in the study performed by Zorn (2006), the stress range used for the S-N plot was taken from the second cycle, $N=2$. Typically, the first cycle, $N=1$, should be used; however, in this study, the first cycle was used to crack the beam, so it is expected to have a different response. Due to accumulated fatigue-induced damage, the stress range in the reinforcing steel was predicted to increase throughout the cycling process. Reasons for this increasing stress range, referred to as the “stress range drift” include: 1) the softening of the concrete under repeated compressive loads (Heffernan, 1997); and 2) the deterioration of the SFRP-to-concrete bond with cycling resulting a redistribution of stress to the internal reinforcing steel (Harries et al., 2007).

In the SFRP specimens reported in this study, the reinforcing steel stress increases between 9% and 12% from $N=2$ to $N=N_f$ as reported in Table 4.2. The steel stress increases are comparable to those of the companion CFRP specimens. Of the SFRP specimens that had a fatigue-induced rebar rupture (FIRR), the stress increases were 9% and 10%. Of the comparable CFRP specimens that exhibited FIRR, the stress increase was 9% and 11%. The run-out specimens had stress range increases that were higher, ranging from 12% to 16%. In this case, the additional cycles result in greater degradation despite a lower rate of stress range increase

(Table 4.2). The rate of stress range increase and thus the final stress range increase for the SFRP run-out Specimen S4F was lower than comparable values for the CFRP run-out Specimens L2F and H2x1F (Table 4.2).

Figure 4.7 demonstrates the effect of using $N=N_f$ for the value of S on the S-N curve. The result is an upwards shift of each point (increased S , as discussed above). This shift is generally proportional to the fatigue life and is unaffected by other parameters investigated (Zorn, 2006).

Figure 4.10 shows the same S-N data for SFRP specimens and CFRP specimens as shown in Figure 4.7 only with the data sorted by the different epoxy systems used. No clear trends are present although the SFRP data appears more uniform and thus representable by a traditional S-N relationship (such as that of CEB 1990). More data points are needed to investigate if different adhesive systems result in different degradations in performance. Figure 4.10 does show, however, that Specimen S4F (the run-out SFRP specimen) reduced the stress in the steel more than any of the comparable CFRP specimens that were subjected to the same loading. This is a further indication that SFRP is able to outperform CFRP in fatigue.

4.2.2 Secant Stiffness

Another measure of the degradation of a specimen due to fatigue cycling is the secant stiffness. This is defined as the slope of the load-deflection relationship obtained during cycling. This slope is calculated as the difference of the maximum and minimum loads during each cycle divided by the corresponding difference in deflection. Table 4.2 demonstrates how the degradation is relatively consistent for all of the SFRP specimens. Specimen S4F had a final stiffness that was 85% that of the cracked secant stiffness determined at $N=2$. Specimens S4.75F

and S5.5F each degraded to 90% and 91%, respectively. This behavior generally corresponds to that reported for the CFRP specimens.

Figure 4.11 plots the cycle number versus secant stiffness for the three fatigue SFRP specimens. This figure demonstrates how the degradation of the stiffness is relatively consistent and similar for all three specimens, despite the large differences in applied loading. Figure 4.12 compares the secant stiffness degradation of the SFRP specimens to that of the companion CFRP specimens. The degradation is similar in all cases. This reaffirms Zorn's conclusion that adhesive properties do not have a large effect on the degradation of beam stiffness behavior. Also, the figure demonstrates how SFRP is a reasonable alternative to CFRP in this respect. It should be noted that Specimen S4F is the most important specimen for comparison, as it was the only one that had the same applied loading as the CFRP specimens.

4.3 COMPARISON OF FATIGUE RUN-OUT SPECIMENS

The following section reports on the fatigue run-out Specimen S4F. It also compares its performance to that of the monotonic Specimen SC and those specimens tested by Reeve and the run-out specimens tested by Zorn.

Specimen S4F was a fatigue run-out specimen. That is, it sustained 2,000,000 cycles of fatigue loading and was subsequently loaded monotonically to failure, as described in section 2.7.2. The companion specimens that were run-out specimens from Zorn were Specimens L2F and H2x1F. These specimens are considered "fatigue conditioned."

4.3.1 Effect of Fatigue Cycling on Debonding Strain

Figure 4.6 compares the strain at the initiation of debonding for each monotonic test with the corresponding run-out companion specimen. This figure shows how the fatigue conditioning had little effect on the debonding strain for the SFRP specimens. This is an indication that the relatively stiff FX-776 is an acceptable epoxy system for SFRP when fatigue loading is a concern. These results reinforce the findings of Zorn, where the softer (low modulus) adhesive specimens showed a significant decrease in debonding strains, and the stiffer (high modulus) adhesive specimens remained apparently unaffected by fatigue conditioning. Regardless of terminology, it should be noted that all of the adhesives used are classified as stiff structural adhesives. The L-series, low modulus adhesive is simply softer by comparison.

4.3.2 Effect of Fatigue Cycling on Other Parameters

Figures 4.2 through 4.5 also show how Specimen S4F compared to Specimen SC. In every case, Specimen SC performed marginally better than its fatigue conditioned partner. However, none of the parameters reported appeared to be significantly degraded following the 2,000,000 cycles of fatigue conditioning.

Figure 4.2 and Figure 4.3 show the observed general yield and maximum load versus reinforcement ratio, respectively. While the general yield decreased more for Specimen S4F when compared to the CFRP run-outs, it still fell into the comparable scatter. While Specimen S4F had a slightly lower ultimate capacity than Specimen SC, it still was higher than all of the comparable CFRP specimens and fell within the expected variability associated with testing

concrete specimens. Again, this is further confirmation that SFRP is a reasonable alternative to CFRP.

Figure 4.4 plots the deflection at ultimate load versus reinforcement ratio, while Figure 4.5 plots the ductility deflection. In both cases, the fatigue conditioning had a slight degrading effect on the behavior of the SFRP specimens. Nonetheless, the scatter of data still fit well within the comparable CFRP specimens. The data actually seems to fit right between the data points for the lower modulus adhesive and the higher modulus adhesive. This is important, because the stiffness of the FX-776 used with the SFRP was between the values for the L and H adhesives used by Reeve and Zorn. This is a further reflection of the conclusion that softer adhesives exhibit marginally improved displacement ductility over stiffer adhesives.

Figure 4.13 plots load versus displacement for Specimen S4F. Also shown are Specimen SC and the companion run-out Specimens L2F and H2x1F. The figure shows how Specimen S4F had a permanent set before the final monotonic load cycle reflecting the permanent deformation associated with accumulated fatigue damage. This behavior is reflected in all fatigue specimens. Specimen S4F was slightly stiffer than Specimen L2F. When compared to Specimen SC, Specimen S4F showed only marginal reductions in performance

4.4 PREDICTED DEBONDING BEHAVIOR

Reeve (2005) analyzed the current recommended models for determining the critical strain at which debonding is likely, ϵ_{fub} . This value is used in design as a limiting value for FRP strain (and thus stress) above which debonding is assumed to control behavior. Since debonding is a brittle failure mode, in design, the FRP strain is kept below ϵ_{fub} . Figure 4.14 shows the

current ACI (2002) equation for maximum allowable strain, a model shown to have good agreement with experimental data recommended by Teng et al. (2004), and a model recommended by the ACI Task Group on Bond (2006) for adoption into the forthcoming version of ACI 440.2R (currently ACI, 2002).

ACI 440.2R (ACI, 2002) provides the following equation for the maximum allowable FRP strain to mitigate debonding:

$$\varepsilon_{fub} = \kappa_m \varepsilon_{fu} \quad (4-1)$$

Where ε_{fu} is the design rupture strain of the FRP and κ_m is as follows:

$$\kappa_m = \begin{cases} \frac{1}{60\varepsilon_{fu}} \left(1 - \frac{nE_f t_f}{2,000,000} \right) \leq 0.90 & \text{for } nE_f t_f \leq 1,000,000 \text{ lb/in.} \\ \frac{1}{60\varepsilon_{fu}} \left(\frac{500,000}{nE_f t_f} \right) \leq 0.90 & \text{for } nE_f t_f > 1,000,000 \text{ lb/in.} \end{cases} \quad \text{(US Units)} \quad (4-2)$$

$$\kappa_m = \begin{cases} \frac{1}{60\varepsilon_{fu}} \left(1 - \frac{nE_f t_f}{360,000} \right) \leq 0.90 & \text{for } nE_f t_f \leq 180,000 \text{ N/mm} \\ \frac{1}{60\varepsilon_{fu}} \left(\frac{90,000}{nE_f t_f} \right) \leq 0.90 & \text{for } nE_f t_f > 180,000 \text{ N/mm} \end{cases} \quad \text{(SI Units)} \quad (4-3)$$

Where n = number of FRP plies

E_f = FRP modulus of elasticity

t_f = FRP thickness

The ACI equation is a function only of the stiffness of the FRP material and its thickness and neglects other factors observed to affect debonding behavior including substrate concrete material and adhesive properties.

Teng et al. (2004) recommend the following equation to mitigate debonding:

$$\varepsilon_{fub} = \alpha k_b k_L \sqrt{\frac{\sqrt{f_c'}}{E_f n t_f}} \quad (4-4)$$

$$\text{Where } k_b = \sqrt{2 - \frac{b_f}{b} / 1 + \frac{b_f}{b}} \quad (4-5)$$

The Teng equation includes parameters such as number of layers of FRP, concrete strength, and the b_f/b ratio. This equation is plotted twice in Figure 4.14, as the comparable CFRP specimens had a b_f/b ratio of 0.333, and the SFRP specimens had a b_f/b ratio of 0.792. Teng recommends that a value of $\alpha = 1.1$ (SI units) should be used. The value of k_L is taken as unity based on the assumption that the available bond length exceeds that which is required to fully develop the FRP – a condition easily satisfied in beam applications.

Also plotted is an equation recommended by the ACI Task Group on Bond (2006). This equation is based on the Teng equation but consolidates all empirical factors into a single value of α . The Task Group (2006) determined that including a k_b factor did not affect the predictive capability of the equation. Additionally, as a design equation, clauses are recommended that ensure the k_L must be taken as unity.

$$\varepsilon_{fub} = \alpha \sqrt{\frac{f_c'}{n E_f t_f}} \quad (4-6)$$

Where the value of $\alpha = 0.42$ in SI units (f_c' in MPa) and $\alpha = 0.083$ in US units (f_c' in psi). This equation falls just above the Teng equation for b_f/b of 0.792 plotted in Figure 4.14.

It can be seen that the ACI (2002) equation is generally non-conservative for the material systems considered while the proposed Task Group (2006) is reasonable for the CFRP material reported.

The SFRP debonding behavior appears to be a non-conservative outlier when shown in this manner. In all other respects, the SFRP is comparable to its equivalent CFRP companion

specimens. It is proposed that the $nE_f t_f$ term in Equations 4.2, 4.4 and 4.6, while appropriate for the relatively homogeneous FRP materials must be modified for use with SFRP. This modification should reflect an equivalent behavior between the materials.

SFRP relies on a larger width, b_f , to achieve a retrofit with an equivalent axial stiffness compared to CFRP. Therefore, SFRP has a $E_f t_f$ stiffness that is comparably lower. However, this $E_f t_f$ value is comparable to GFRP applications. The difference is that SFRP has a higher modulus while being thinner than GFRP. This suggests that only using the properties of E_f and t_f are not enough to model debonding behavior.

An acceptable solution for this study may be to take advantage of how the SFRP system has an equal stiffness compared to the CFRP system in terms of area, $E_f t_f b_f$. For instance, if one were to divide the axial stiffness of the SFRP by the width of the comparable CFRP, the resulting larger normalized $E_f t_f$ value will be a better indication for limiting strain in the SFRP. The limitation of this method is that it only works for this specific application in this specific manner. It gives no guidance as to whether the SFRP should be normalized to an equivalent stiffness of CFRP, GFRP, or high modulus CFRPs.

Table 4.1 Analysis of key results summary for monotonic and runout specimens.

Specimen:	SC	S4F	L2F	H2x1F	L2	L2x1	H2	H2x1
ratio of general yield load to Specimen C general yield load:	1.38	1.27	1.28	1.36	1.24	1.30	1.26	1.32
ratio of maximum load to Specimen C maximum load:	1.53	1.50	1.47	1.46	1.43	1.47	1.40	1.45
ratio of max load deflection to Specimen C max load deflection:	1.50	1.38	1.62	1.33	1.45	1.65	1.32	1.39
ratio of ductility deflection to Specimen C ductility deflection:	0.77	0.72	0.86	0.66	0.73	0.83	0.71	0.72

Table 4.2 Measures of fatigue behavior.

	Fatigue Life	ratio of final (N_f) to initial ($N = 2$) stress range	average rate of change of stress range with cycling	ratio of final (N_f) to initial ($N = 2$) secant stiffness	average rate of change of stiffness with cycling
			ksi/100k cycles		kip/in/100k cycles
S4F	>2,000,000	1.12	0.16	0.85	-0.08
S4.75F	689,671	1.09	0.43	0.90	-0.13
S5.5F	286,306	1.10	1.46	0.91	-0.29
L2F	>2,000,000	1.16	0.24	0.82	-0.08
L2x1F	447,695	1.11	0.73	0.92	-0.15
H2F	1,128,006	1.09	0.23	0.94	-0.05
H2x1F	>2,000,000	1.14	0.22	0.82	-0.08

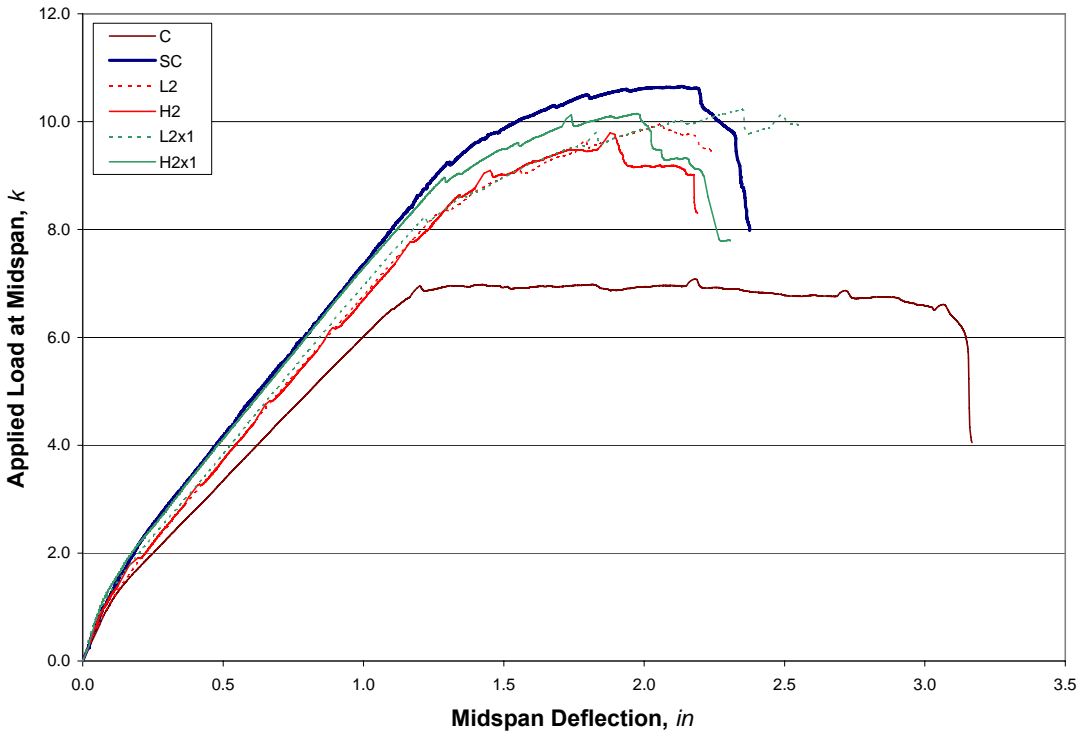


Figure 4.1 Load vs. deflection for monotonic tests.

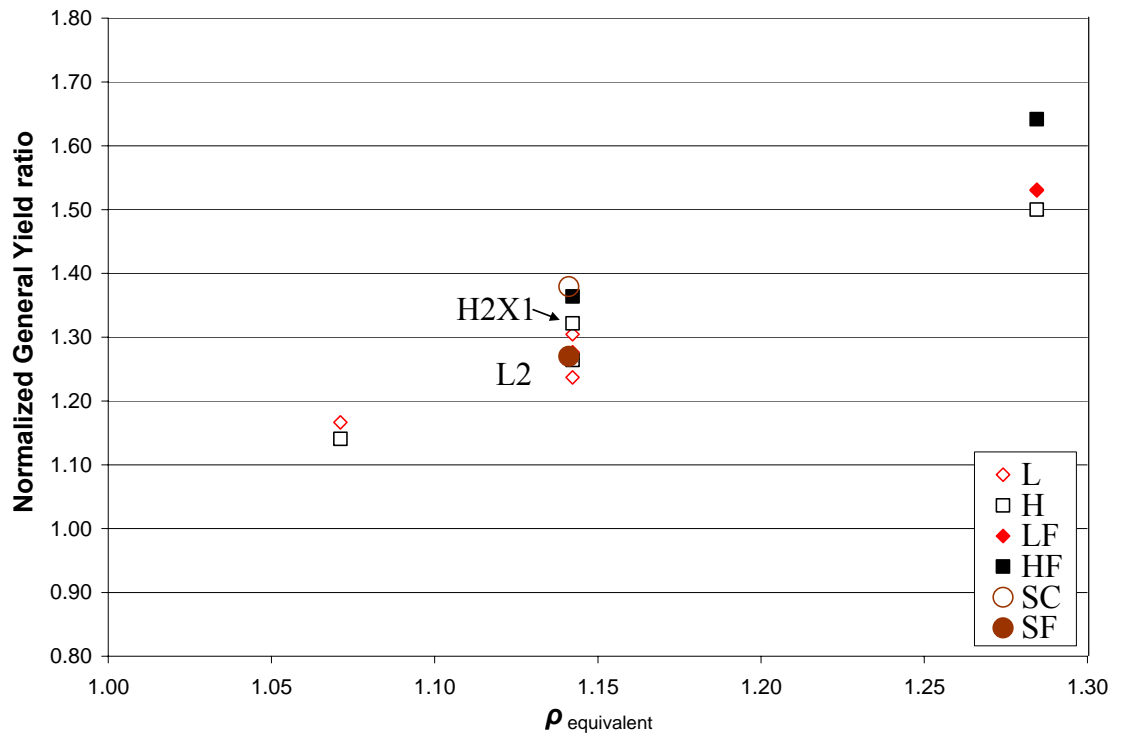


Figure 4.2 SFRP vs. CFRP, general yield load.

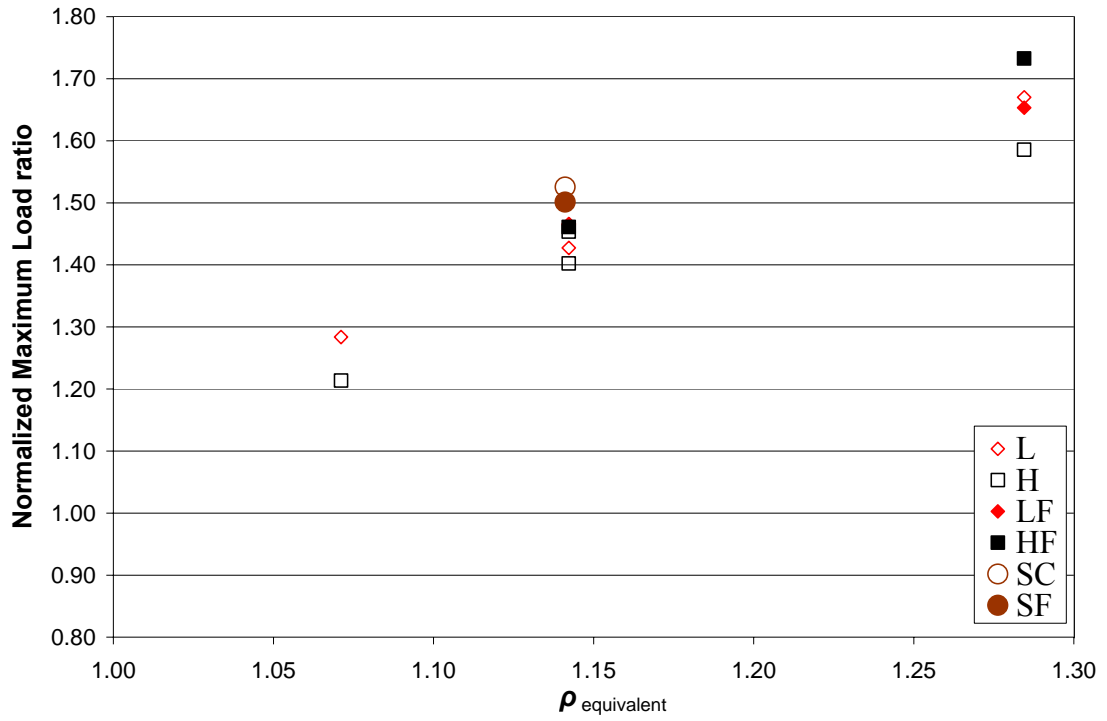


Figure 4.3 SFRP vs. CFRP, maximum load capacity.

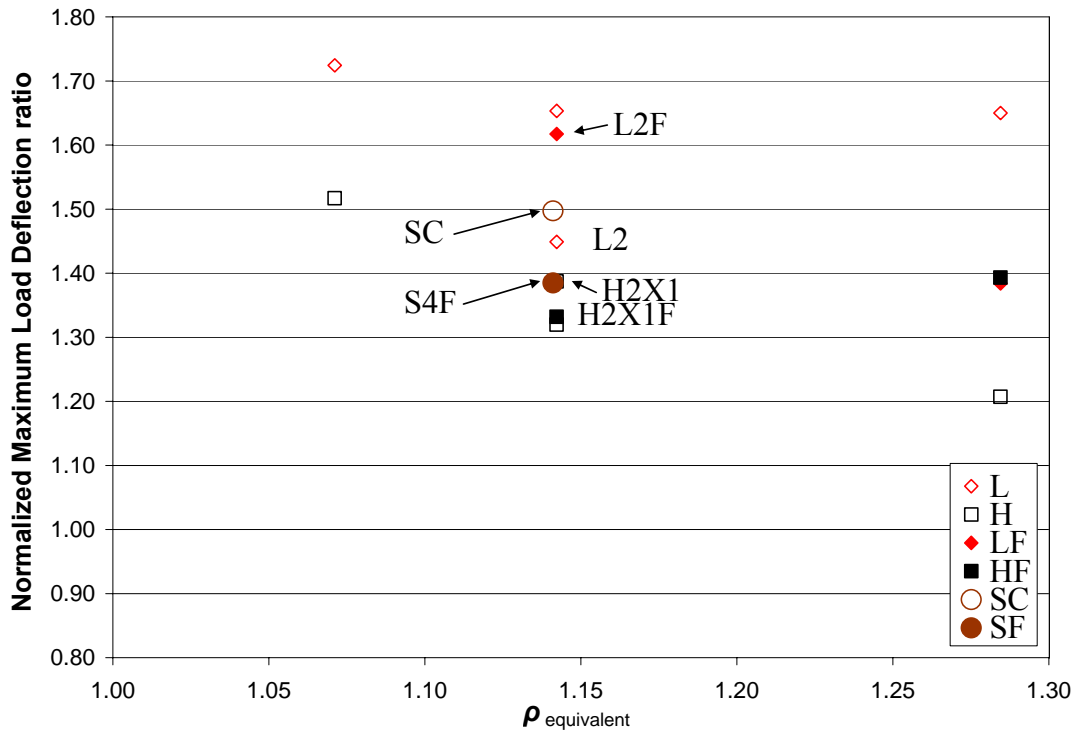


Figure 4.4 SFRP vs. CFRP, deflection at maximum load.

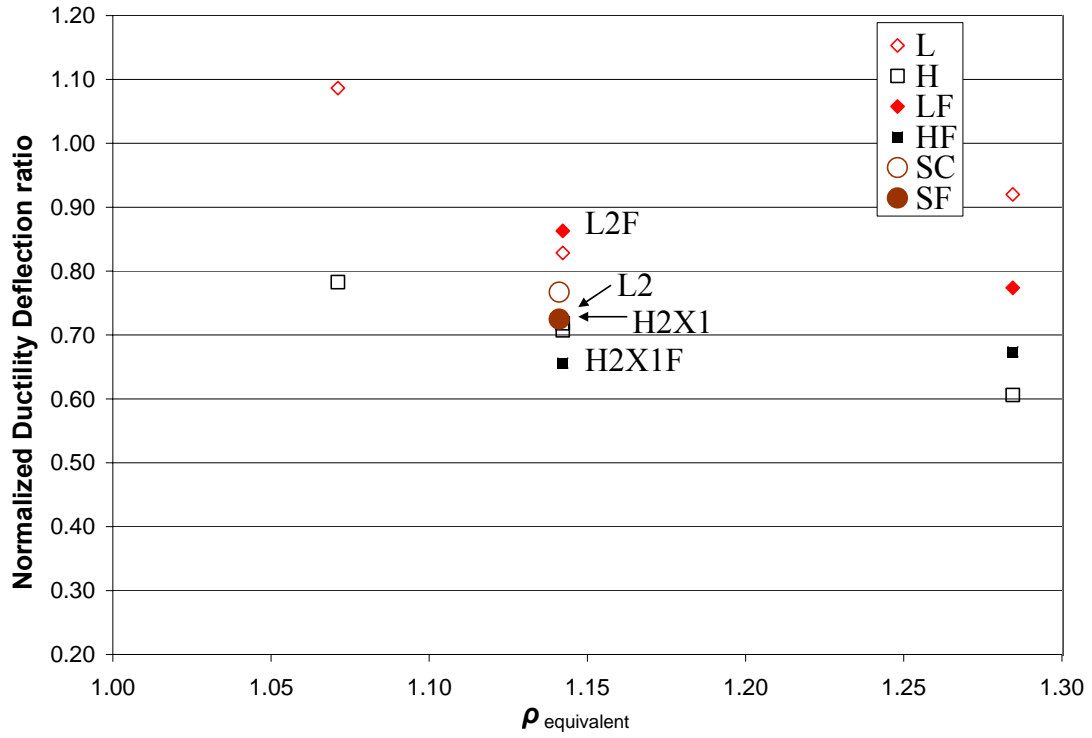


Figure 4.5 SFRP vs. CFRP, ductility deflection.

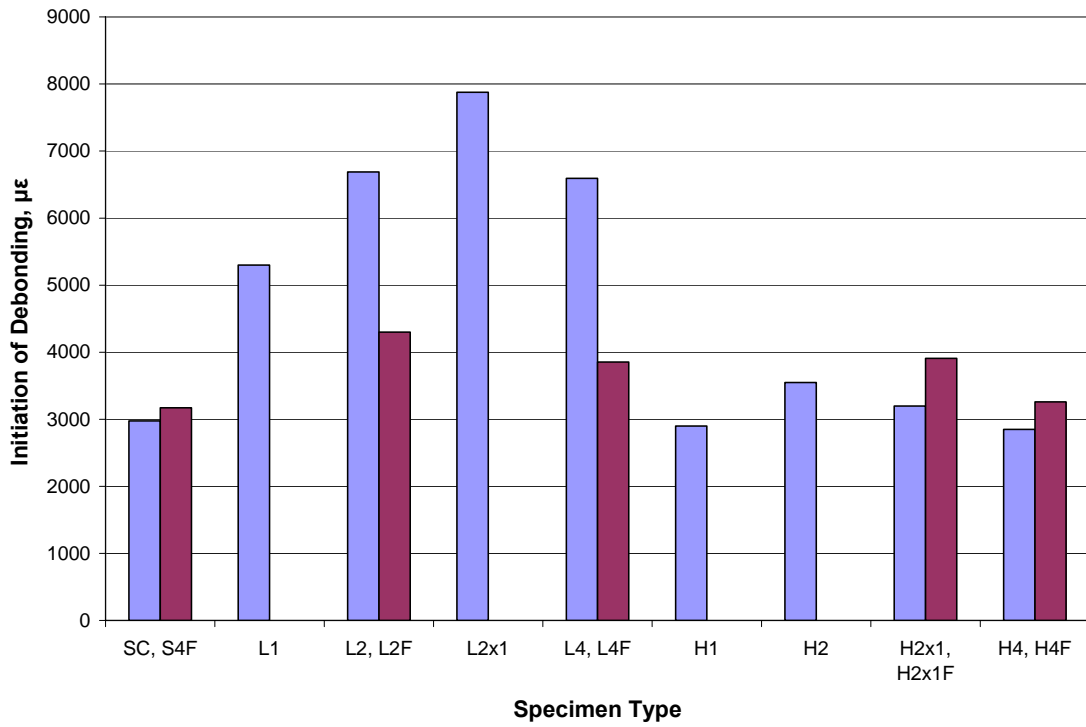


Figure 4.6 SFRP vs. CFRP, strain at apparent initiation of debonding.

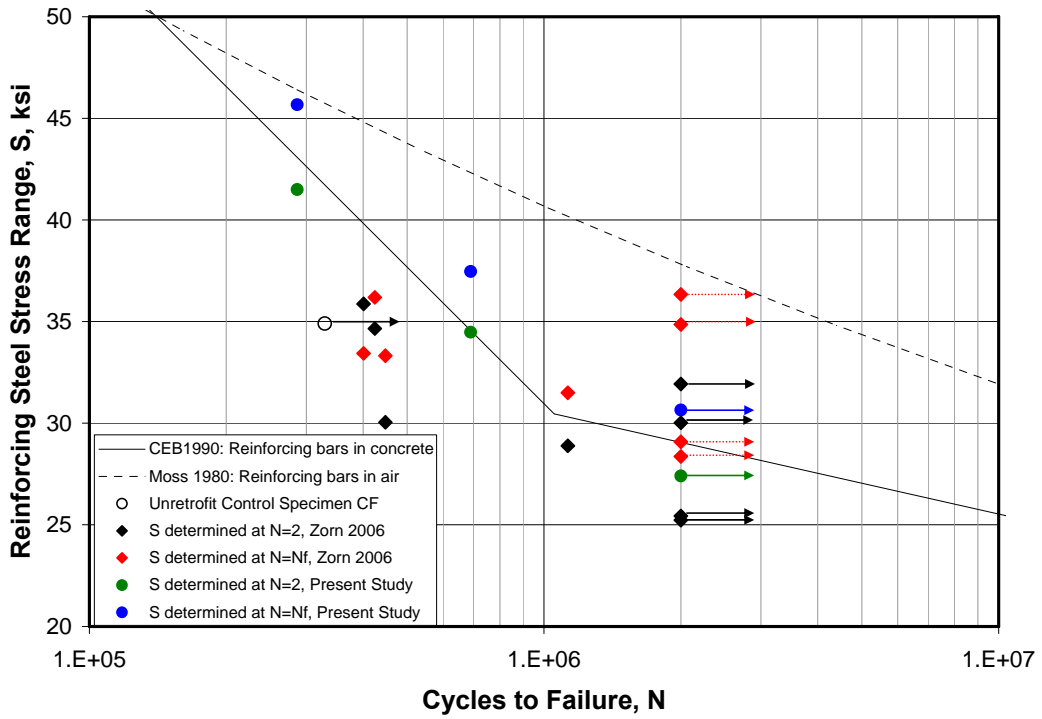


Figure 4.7 S-N data determined at $N=2$ and $N=N_f$ for SFRP and CFRP.

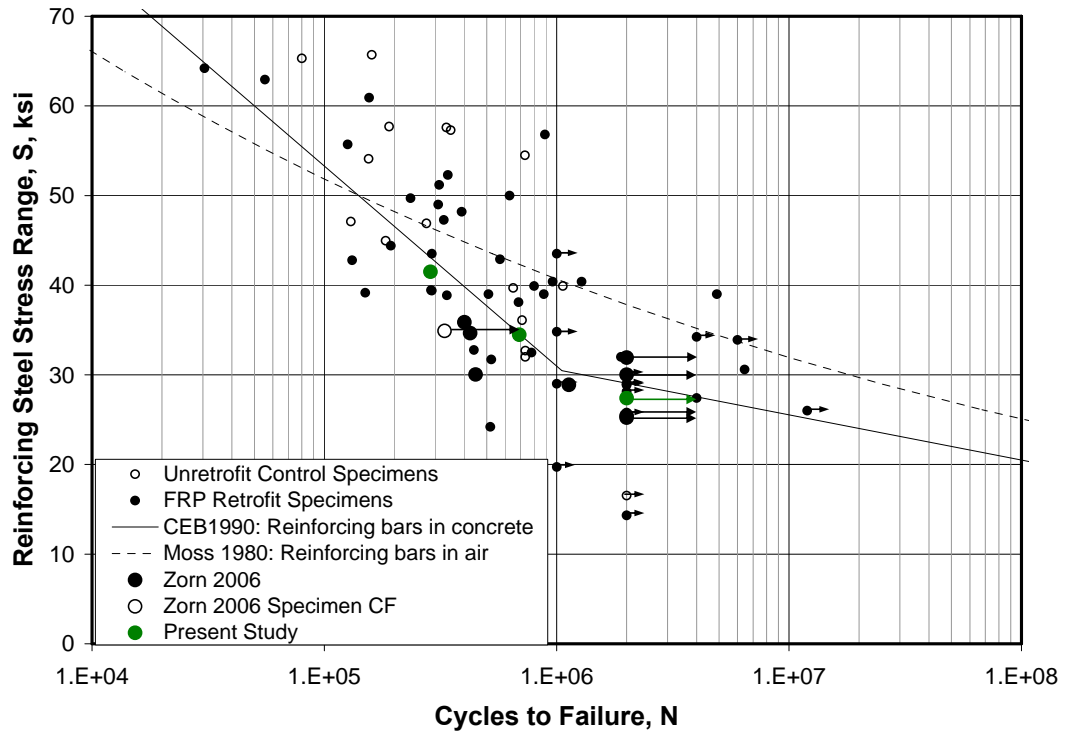


Figure 4.8 S-N data for SFRP specimens with database compiled by Zorn (2006).

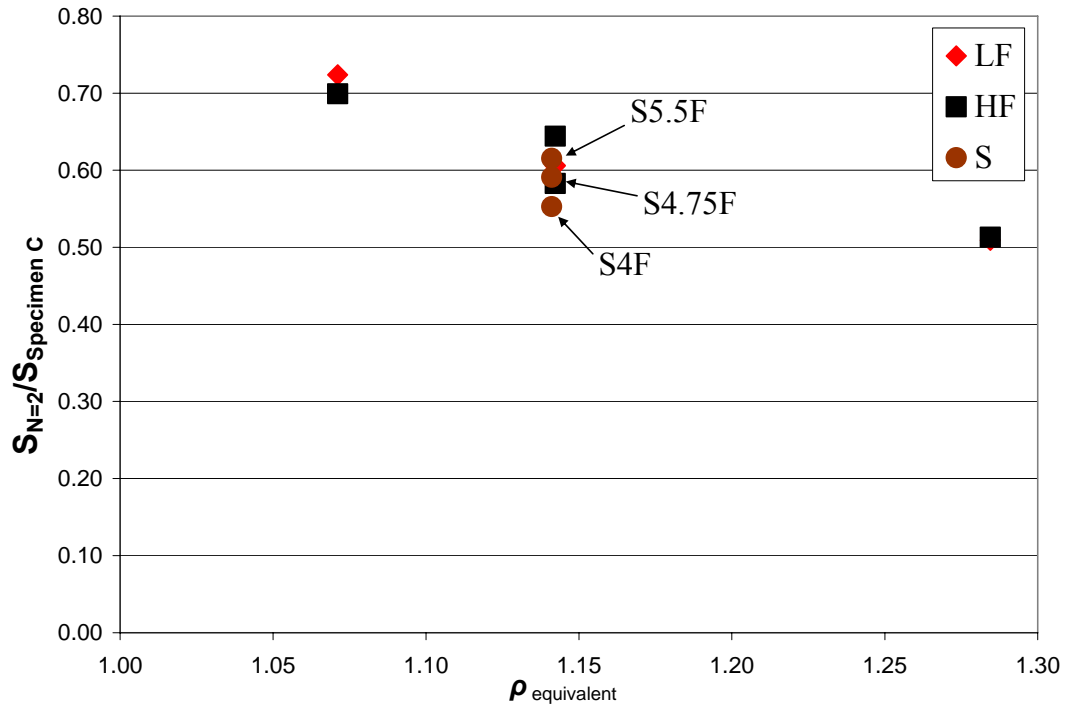


Figure 4.9 SFRP vs. CFRP, effect on fatigue stress range at N = 2.

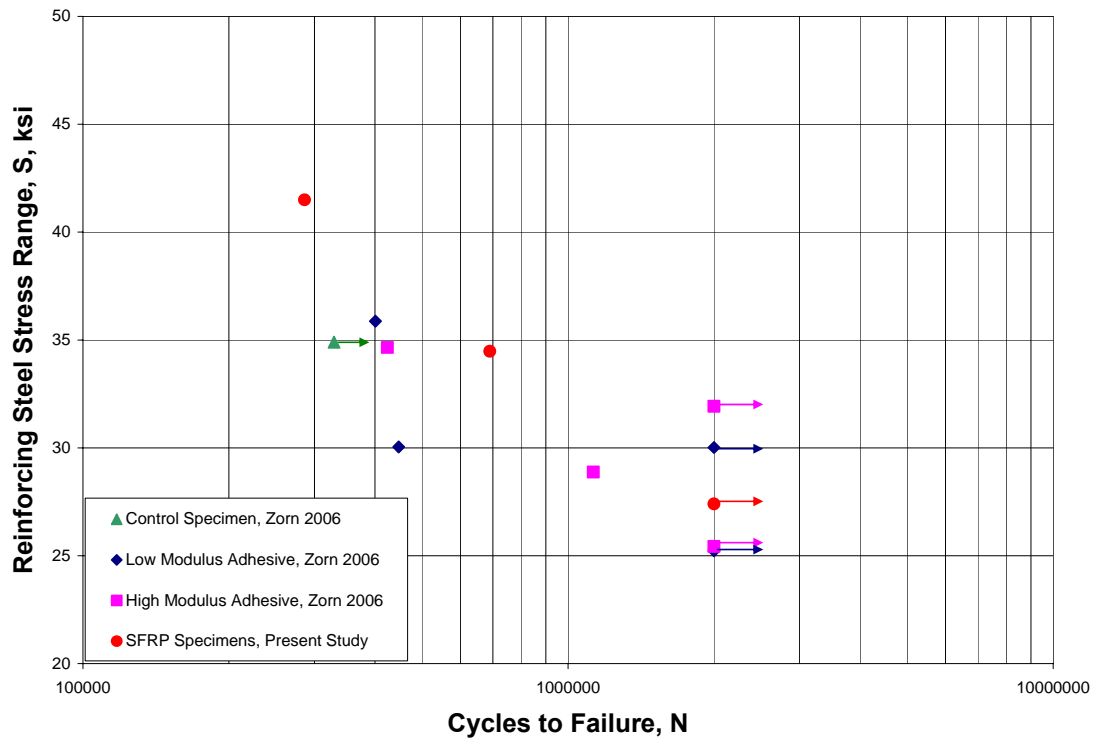


Figure 4.10 S-N data comparing different adhesives.

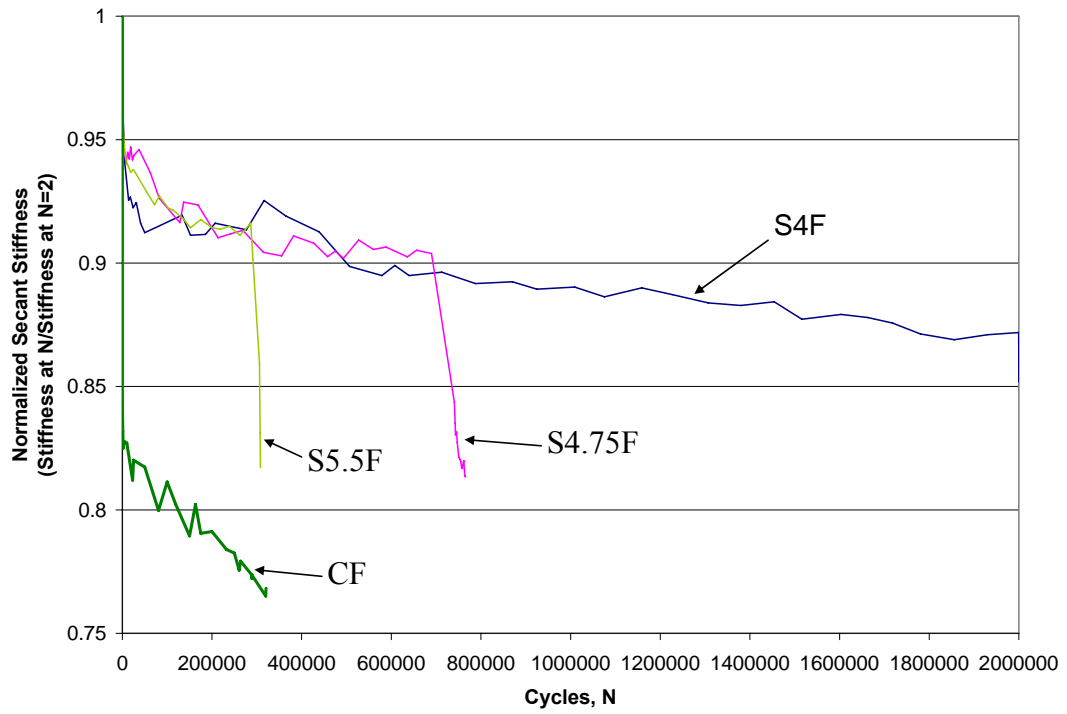


Figure 4.11 Stiffness degradation with fatigue cycling for SFRP specimens.

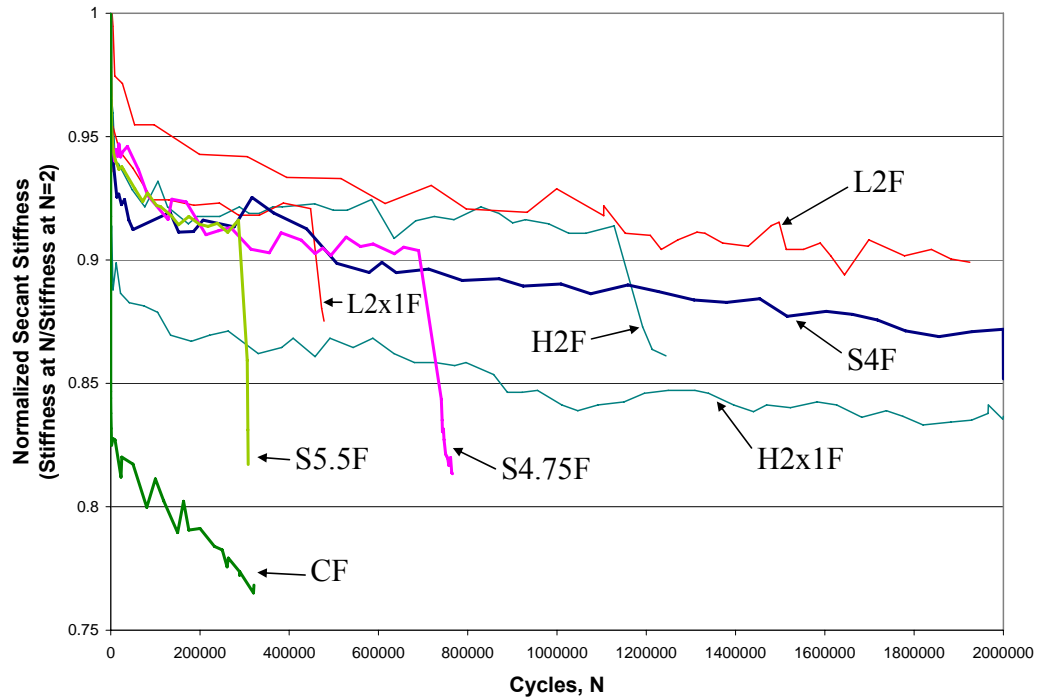


Figure 4.12 SFRP vs. CFRP, stiffness degradation with fatigue cycling.

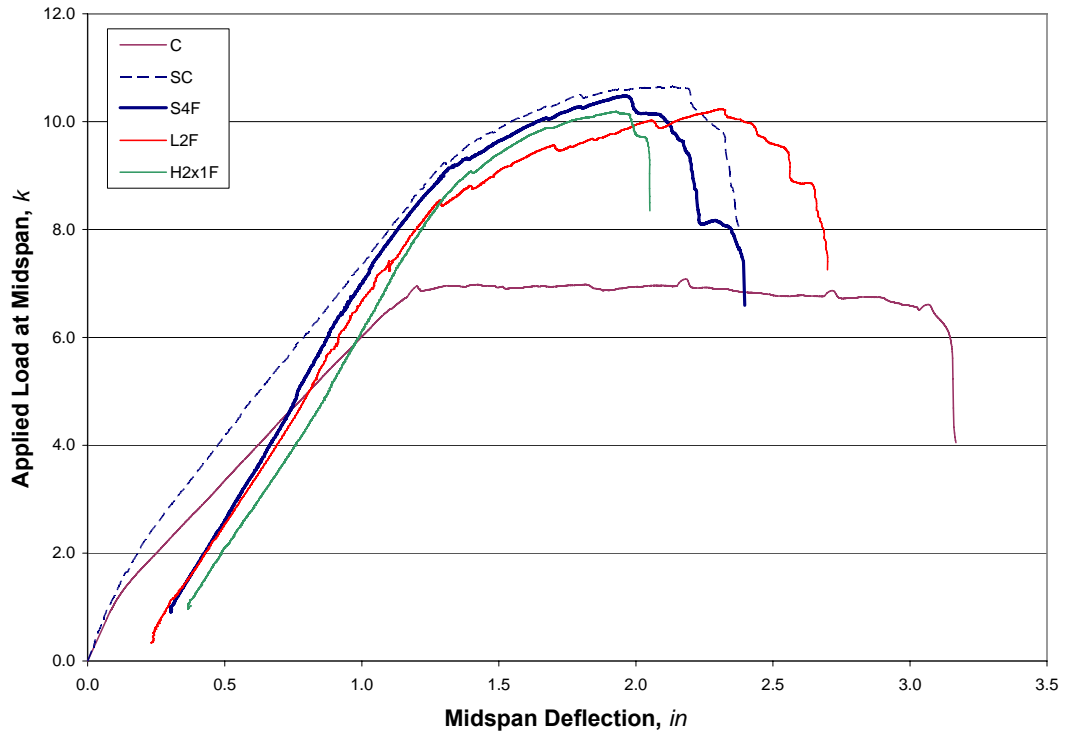


Figure 4.13 Load vs. deflection for all runout specimens.

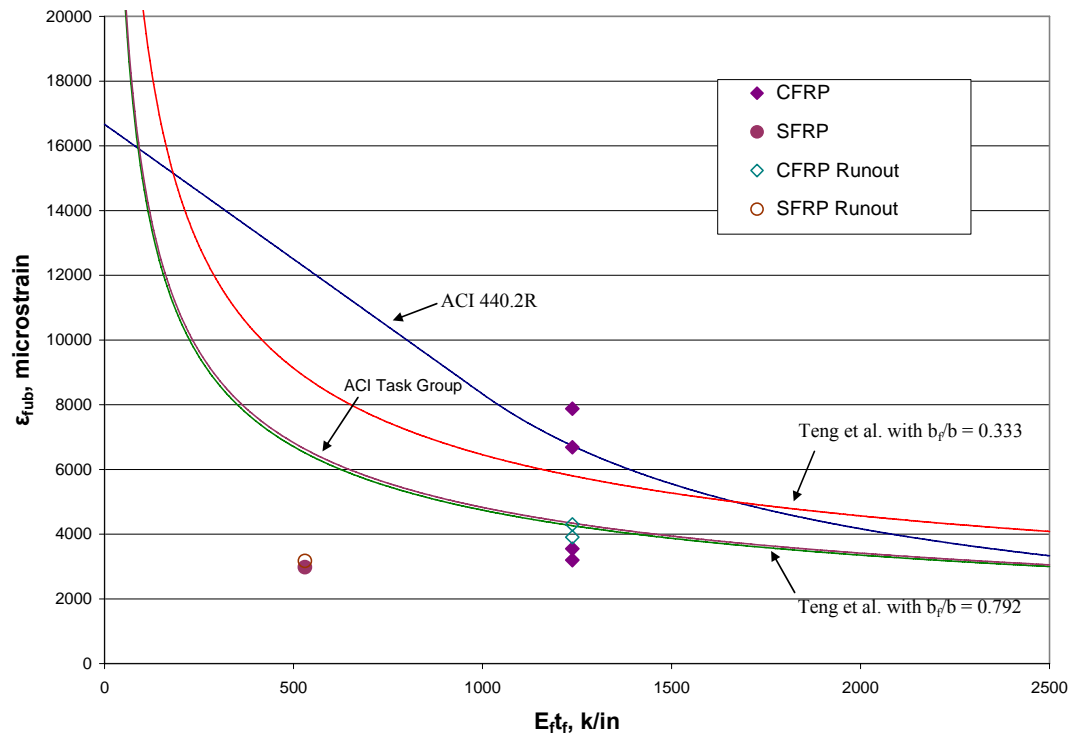


Figure 4.14 Strain vs. $E_f t_f$.

5.0 SUMMARY, CONCLUSIONS, AND RECOMMENDATIONS

This chapter reports and discusses conclusions of the experimental program. A summary of the test procedure and continuing needs for future work is also presented.

5.1 SUMMARY OF TEST PROGRAM

Four test specimens were tested, each 10 in. (254 mm) deep, 6 in. (152 mm) wide, and 186 in. (4730 mm) long. All four specimens were retrofitted with the same amount and type of steel fiber reinforced polymer (SFRP). The width of SFRP used was such that it had the same axial stiffness as companion specimens retrofitted with 2 in. (51 mm) wide carbon fiber reinforced polymer (CFRP) strips. Unretrofit control specimens were also tested. All reinforced concrete beams had three #4 longitudinal steel reinforcing bars as the primary flexural reinforcement resulting in a steel reinforcement ratio of 1.0%.

The SFRP, supplied by Hardwire, LLC, was precut to a width of 4.75 in. (121 mm) and a length of 172 in. (4369 mm). The cord type was 3x2-23-12, which has 23 cords per inch. Each cord is made of 5 individual high strength wires. The adhesive used to bond the SFRP to the concrete substrate was FX-776, a high modulus epoxy-based structural adhesive recommended by Hardwire.

The beam specimens were supported over a simply supported clear span of 178.5 in. (4537 mm) and tested under mid-point bending. Specimen SC was tested monotonically to failure in displacement control and can be compared to the companion monotonic specimens (L2, L2x1, H2 and H2x1) and the unretrofit Specimen C, all tested by Reeve (2005). Specimens S4F, S4.75F, and S5.5F were tested under cyclic loading until failure (S4.5F and S5.5F) or 2,000,000 cycles (S4F). The cyclic load used was a sinusoidal wave with a frequency of not more than 1.7 Hz. The range of the applied midspan load for Specimen S4F was 1 kip (4.45 kN) to 5 kips (22.24 kN); for Specimen S4.75F: 1 kip (4.45 kN) to 5.75 kips (25.58 kN); and for Specimen S5.5F: 1 kip (4.45 kN) to 6.5 kips (28.91 kN). Specimen S4F sustained 2,000,000 load cycles without failure; at this point the fatigue test was terminated and a monotonic test to failure was performed. The SFRP fatigue specimens can be compared to the companion fatigue specimens (L2F, L2x1F, H2F and H2x1F) and the unretrofit Specimen CF, all tested by Zorn (2006).

5.2 CONCLUSIONS

The primary objective of this work is to assess the applicability of well-established design guidance for GFRP and CFRP (ACI 2002) for SFRP. Thus the following conclusions are provided in this context.

Both monotonic specimens, SC and run-out S4F, exhibited intermediate crack induced debonding behavior. Debonding was the primary mode of failure for these two specimens. Specimens S4.75F and S5.5F both failed during fatigue cycling at $N_f = 689671$ and $N_f = 286306$,

respectively. The failure mode for these specimens was fatigue-induced reinforcing steel rupture.

The following conclusions have been drawn from this work:

1. On the basis equivalent axial stiffnesses (that is the product $E_f t_f b_f$), the SFRP retrofits behaved comparably to the companion CFRP retrofits in terms of general yield, maximum load, deflection at maximum load, and deflection ductility. Thus the behavior of SFRP and its design is similar that of CFRP.
2. With respect to Conclusion 1, the manufacturer reported effective material properties for SFRP are suitable for use in design.
3. The exception to Conclusions 1 and 2 is that the guidance provided for the mitigation of debonding of GFRP or CFRP was not apparently appropriate to apply directly to SFRP using effective material properties. This is discussed further in the following section.
4. The SFRP specimens performed better than comparable CFRP specimens in terms of fatigue performance. At equal internal steel stress ranges, SFRP specimens achieved a longer fatigue life. At equal applied load ranges, Specimen S4F affected a greater reduction of stress in the internal reinforcing steel than any of the CFRP companion specimens. This is believed to indicate superior bond performance at the stress ranges considered. The superior performance is hypothesized to result from the improved mechanical bond resulting from the twisted wires embedded within the epoxy system.
5. Two million cycles of applied load (fatigue conditioning) had only marginal effects on the performance of Specimen S4F. General yield, maximum load, deflection at maximum load, and ductility were all shown to only degrade very slightly from Specimen SC to S4F. The SFRP strain at the initiation of debonding of Specimen S4F was observed to be slightly higher than Specimen SC, indicating the fatigue cycling had little effect on this performance

parameter. This reinforces Conclusion 4 and indicates that SFRP is desirable in service load level fatigue environments.

6. The degradation of secant stiffness with fatigue loading was essentially the same for all SFRP specimens up to the point of fatigue failure. The degradation was also comparable to that of the CFRP specimens tested by Zorn (2006). This also is an indication of sound bond being maintained during fatigue cycling.
7. Stress range drift in the internal steel reinforcement should be considered when designing a bonded SFRP (or G/CFRP) retrofit that will have to perform in a fatigue environment. Provided debonding is mitigated, fatigue life is shown (in this study and others) to be governed by fatigue-induced reinforcing steel rupture. Stress ranges in the primary internal steel reinforcement were observed to increase from 9% to 12% as the fatigue loading progressed from $N = 2$ to $N=N_f$.
8. The data from the fatigue tests presented fit generally within the expected scatter of fatigue data and corresponds quite well with the equation recommended by CEB (1990) for the S-N behavior of reinforcing bars embedded in concrete.
9. Conclusions 4 through 8 are believed to reflect the fact that a wider width of SFRP material is needed to affect a retrofit equivalent to a CFRP retrofit (considering the discrete CFRP strip and SFRP sheet products presently available). The wider width results in decreased interfacial stresses and thus improved fatigue behavior with no evidence of debonding for the relatively high stress ranges tested in this program.
10. It is believed that a thinner and more uniform adhesive bondline was obtained with the SFRP system (resulting because the adhesive may be displaced through the relatively open SFRP

material). This may account for the marginally improved global beam behavior and the apparent earlier onset of debonding.

11. The FX-776 adhesive appeared to perform well with the SFRP. No evidence of incompatibility or adhesive or cohesive failure in the SFRP system was observed.
12. Similar to all bonded FRP applications, locating the termination of the SFRP close to the supports at each end of the beam successfully mitigated end peel debonding.
13. With the exception of debonding mitigation (discussed in following section), the design guidance provided by ACI 440.2R (2002) appears to be applicable to the SFRP material tested.

5.2.1 Debonding of SFRP

Based on both the current (ACI 2002) and proposed (ACI Task Group 2006) recommendations for FRP strain to mitigate debonding, the SFRP tested performed poorly; exhibiting debonding failures at strains substantially below the limits recommended to mitigate debonding.

Current and proposed recommendations include FRP properties in their limit calculations as the product of FRP modulus, E_f and thickness, t_f . Using SFRP effective properties, $E_f t_f$ is relatively small. Indeed, SFRP values of $E_f t_f$ are comparable to those calculated for GFRP applications. GFRP differs from SFRP in that GFRP has a relatively low modulus and is relatively thicker in order to make up the value of $E_f t_f$. SFRP properties, on the other hand are reversed; SFRP is relatively thin and has a higher modulus. The observed difference in behavior between SFRP and G/CFRP suggests that the interaction between modulus and thickness is not sufficient to model debonding behavior. The empirically derived equations for limiting strain

may simply be an artifact of the fact they were generally developed using only two material systems, GFRP and CFRP. Additionally, most GFRP systems have very similar properties (as do most CFRP systems) and thus little parametric variance is considered.

It is noted that in this present study, considering the product of SFRP modulus and *area*, $E_f t_f b_f$ and normalizing by the width of the CFRP application (for which the limiting strain equations were developed) yields an improved, and believed to be appropriate, calculation for limiting strain.

5.3 RECOMMENDATIONS

This work has shown that the current and proposed ACI recommendations for calculating critical strain is non-conservative when using SFRP. Some recommendations for future study include:

1. Currently, equations for determining FRP stress/strain limits to mitigate debonding are functions of E_f and t_f . SFRP has a relatively high E_f and low t_f with respect to GFRP materials although the materials have similar $E_f t_f$ values. This may be the reason SFRP debonding strains were apparently low in relation to established empirical equations. Future research should be done on FRP systems having a greater variance of material properties and geometries to investigate this behavior.
2. SFRP is still relatively untested compared with GFRP or CFRP; additional testing over a range of parameters should be conducted to establish more definitive relationships than are possible in the limited study reported here.

3. The debonding strains reported in this work are lower bound values. This is because the debonding is only assessed at discrete points (the gages) and therefore the debonding strain *during propagation* rather than at *initiation* is recorded. Based on fracture toughness (and analogous to friction), it takes greater energy to initiate debonding than to propagate it. Because the gages are discretely located, their recorded strains reflect propagation rather than initiation. Future work needs to be performed that can capture the actual initiation phase of debonding and study how the debonding propagates.

This study has shown how SFRP is a comparable alternative to CFRP in all ways except in predicting debonding failure. Improved methods and equations for predicting debonding are necessary since SFRP retrofits will have a greater width, b_f , which is not included in any current debonding equations.

APPENDIX A

KEY RESULTS FROM REEVE (2005) AND ZORN (2006)

Table A.1 Summary of Key Results from Reeve (2005).

		C	L1	L2	L2X1	L4	H1	H2	H2X1	H4
b _f /b		0	0.17	0.33	0.33	0.67	0.17	0.33	0.33	0.67
adhesive type		na	SikaDur 23 (L)				SikaDur 30 (H)			
age at start of test	days	144	154	157	161	228	162	163	165	170
cracking load	kips	<0.66	0.62	0.66	0.63	0.75	0.55	0.64	0.64	0.65
cracking moment	kip-in	<30	28	29	28	33	25	29	29	29
load at initial yield of reinforcing	kips	5.91	6.05	6.78	5.99	7.31	6.16	6.38	6.63	8.44
moment at initial yield of reinforcing	kip-in	264	270	303	267	326	275	285	296	377
deflection at initial yield of reinforcing	in	0.98	1.07	1.00	0.84	1.46	0.98	0.95	0.89	1.08
load at general yield	kips	6.96	8.12	8.61	9.08	10.68	7.94	8.80	9.20	10.44
moment at general yield	kip-in	311	363	384	405	477	355	393	411	466
deflection at general yield	in	1.18	1.35	1.32	1.35	1.49	1.32	1.36	1.30	1.40
maximum load	kips	6.98	8.96	9.96	10.23	11.65	8.47	9.79	10.15	11.07
maximum moment	kip-in	312	400	445	457	520	378	437	453	494
deflection at max load	in	1.42	2.45	2.06	2.35	2.34	2.16	1.88	1.97	1.72
deflection at ultimate load (80% max)	in	3.08	3.34	2.24	2.55	2.84	2.41	2.18	2.21	1.86
displacement ductility		2.61	2.48	1.70	1.89	1.91	1.82	1.60	1.70	1.33
maximum observed strain in FRP	ε _μ	na	8370	6688	7878	6595	6466	6200	6863	4813
corresponding rebar strain	ε _μ	15932	n.r.	13167	6620	15337	12414	14812	6004	9952
maximum strain in FRP at time of max load	ε _μ	na	8218	6518	7872	6462	6160	6112	6853	4787
corresponding rebar strain	ε _μ	2759	11559	13124	6624	14422	12446	14663	6034	9947
strain in FRP at initiation of debonding	ε _μ	na	5300	6688	7878	4540	2900	3550	3200	2850
corresponding rebar strain	ε _μ	na	2600	n.r.	n.r.	2990	2300	2680	2790	2500

Table A.2 Summary of Key Results from fatigue tests of Zorn (2006).

		CF	L1F	L2F	L2X1F	L4F	H1F	H2F	H2X1F	H4F
b_f/b		na	0.167	0.333	0.333	0.667	0.167	0.333	0.333	0.667
adhesive type		na	SikaDur 23 (L)				SikaDur 30 (H)			
age at start of fatigue test	days	175	184	191	231	274	210	217	238	253
cracking load	kips	0.68	0.66	0.68	0.69	0.67	0.67	0.67	0.69	0.73
cracking moment	kip-in	30	29	30	31	30	30	30	31	32
N = 2										
minimum applied load	kips	1.01	1.04	1.03	1.02	1.04	1.02	1.03	1.04	1.01
minimum applied moment	kip-in	45	46	46	46	46	45	46	46	45
deflection at minimum applied load	in	0.29	0.27	0.26	0.29	0.22	0.32	0.29	0.27	0.21
maximum rebar strain at minimum applied load	$\mu\epsilon$	747	717	633	622	523	700	610	633	474
maximum FRP strain at minimum applied load	$\mu\epsilon$	na	647	663	640	548	815	787	806	506
maximum applied load	kips	4.98	5.00	5.00	5.00	5.00	4.99	5.00	5.00	5.00
maximum applied moment	kip-in	222	223	223	223	223	223	223	223	223
deflection at maximum applied load	in	0.78	0.76	0.67	0.74	0.59	0.81	0.75	0.70	0.62
maximum rebar strain at maximum applied load	$\mu\epsilon$	1950	1954	1668	1658	1393	1895	1606	1734	1351
maximum FRP strain at maximum applied load	$\mu\epsilon$	na	1869	1758	1778	1479	2127	1997	2089	1428
range of applied load	kips	3.98	3.96	3.98	3.98	3.96	3.98	3.97	3.96	3.99
range of applied moment	kip-in	178	177	178	178	177	178	177	177	178
stress range in rebar	ksi	34.9	35.9	30.0	30.0	25.2	34.7	28.9	31.9	25.4
stress range in FRP	ksi	na	27.5	24.6	25.6	20.9	29.5	27.2	28.9	20.7
secant stiffness	kip/in	7.92	7.85	9.36	8.72	10.59	8.09	8.38	9.19	9.53
last recorded cycle before failure (N_f)		na	400892	2000000	447695	2000000	424422	1128006	2000000	2000000
failure mode during fatigue cycling			FIRR ¹	run-out	FIRR ¹	run-out	FIRR ¹	FIRR ¹	run-out	run-out

N = N_f, or N = 2000000										
minimum applied load	kips	na	1.12	1.00	1.02	1.00	1.02	1.01	1.00	1.00
minimum applied moment	kip-in	na	50	45	45	45	46	45	45	45

Table A.2 (continued)

		CF	L1F	L2F	L2x1F	L4F	H1F	H2F	H2x1F	H4F
deflection at minimum applied load	in	na	0.36	0.27	0.32	0.29	0.42	0.36	0.33	0.30
maximum rebar strain at minimum applied load	$\mu\epsilon$	na	679	607	641	508	714	598	628	527
maximum FRP strain at minimum applied load	$\mu\epsilon$	na	659	638	611	518	912	832	837	556
maximum applied load	kips	na	5.00	5.00	5.00	5.00	5.00	5.00	5.00	5.00
maximum applied moment	kip-in	na	223	223	223	223	223	223	223	223
deflection at maximum applied load	in	na	0.88	0.79	0.81	0.74	0.95	0.87	0.84	0.77
maximum rebar strain at maximum applied load	$\mu\epsilon$	na	1832	1809	1790	1511	1962	1684	1881	1505
maximum FRP strain at maximum applied load	$\mu\epsilon$	na	1980	1864	1819	1545	2327	2158	2279	1638
range of applied load	kips	na	3.88	4.00	3.98	4.00	3.98	3.99	4.00	4.00
range of applied moment	kip-in	na	173	179	178	179	178	178	179	179
stress range in rebar	ksi	na	33.4	34.9	33.3	29.1	36.2	31.5	36.3	28.4
stress range in FRP	ksi	na	29.7	27.6	27.2	23.1	31.8	29.8	32.4	24.3
secant stiffness	kip/in	na	7.29	7.69	8.07	8.64	7.43	7.86	7.58	8.37
any N										
maximum observed strain in FRP	$\mu\epsilon$	na	1988	1873	1819	1545	2327	2158	2285	1638
corresponding rebar strain	$\mu\epsilon$	na	1792 ³	1809	1658	1511 ²	1962 ²	1684	1526	1263
cycle number		na	342629	1698454	447695	2000000	424422	1128006	1820072	2000000
strain in FRP at initiation of debonding	$\mu\epsilon$	na	n.o.	n.o.	n.o.	n.o.	n.o.	n.o.	n.o.	1565
corresponding rebar strain	$\mu\epsilon$	na	n.o.	n.o.	n.o.	n.o.	n.o.	n.o.	n.o.	1552
cycle number		na	n.o.	n.o.	n.o.	n.o.	n.o.	n.o.	n.o.	118213

¹ FIRR = fatigue-induced reinforcing bar rupture

² strain gage #2 was lost so gage #3 was reported

³ strain gage #3 was lost so gage #2 was reported

n.o. = not observed

Table A.3 Summary of Key Results from run-out monotonic tests of Zorn (2006).

		L2F	L4F	H2x1F	H4F
b _f /b		0.333	0.667	0.333	0.667
adhesive type		SikaDur 23 (L)		SikaDur 30 (H)	
age at start of fatigue test	days	191	274	238	253
cracking load	kips	0.68	0.67	0.69	0.73
cracking moment	kip-in	30	30	31	32
load at initial yield of reinforcing	kips	6.15	7.51	5.85	7.61
moment at initial yield of reinforcing	kip-in	275	335	261	340
deflection at initial yield of reinforcing	in	0.92	1.03	0.94	1.06
load at general yield	kips	8.88	10.66	9.49	11.43
moment at general yield	kip-in	397	476	424	510
deflection at general yield	in	1.29	1.42	1.39	1.59
maximum load	kips	10.23	11.54	10.19	12.10
maximum moment	kip-in	457	515	455	540
deflection at max load	in	2.30	1.97	1.89	1.98
deflection at ultimate load (80% max)	in	2.65	2.38	2.02	2.07
displacement ductility		2.06	1.68	1.45	1.30
maximum observed strain in FRP	μ ϵ	7444	5807	6970	5860
corresponding rebar strain	μ ϵ	3238	9916	13039	10885
maximum strain in FRP at time of max load	μ ϵ	7322	5180	6875	5860
corresponding rebar strain	μ ϵ	4171	9897	13664	10885
strain in FRP at initiation of debonding	μ ϵ	4301	3854	3909	3260
corresponding rebar strain	μ ϵ	2898	2706	2767	2767

REFERENCES

American Concrete Institute (ACI) Committee 440 (2002). *ACI 440.2R-02 Guide for the Design and Construction of Externally Bonded FRP Systems for Strengthening Concrete Structures*. 45pp.

American Concrete Institute (ACI) Committee 440 Task Group on Bond of Externally Bonded FRP (2006). *Current Recommendations and Guidelines for Mitigating Debonding Failures in Adhesively Bonded, Externally Applied FRP Applications*. (K. Harries, chair) Committee Report.

Barton, B., Wobbe, E., Dharani, L.R., Silva, P., Birman, V., Nanni, A., Alkhrdaji, T., Thomas, J., and Tunis, G. (2005). "Characterization of reinforced concrete beams strengthened by steel reinforced polymer and grout (SRP and SRG) composites." *Materials Science and Engineering A*, Vol. 412, No. 1, pp 129-136.

Casadei, P., Nanni, A., Alkhrdaji, T., and Thomas, J. (2005). "Performance of Double-T Prestressed Concrete Beams Strengthened with Steel Reinforced Polymer." ACI Special Publication, Volume SP-230-44, pp 763-778.

Casadei, P., Nanni, A., and Ibell, T. (2005). "Development and Validation of Steel Reinforced Polymer (SRP) for Strengthening of Transportation Infrastructures." University of Missouri-Rolla Center for Infrastructure Engineering Studies, UTC R94, 64pp.

Comité Euro-International du Béton (1990). *CEB/FIB Model Code 1990*. Thomas Telford, London. 437pp.

Figeys, W., Schueremans, L., Brosens, K., and Van Gemert, D. (2005). "Strengthening of Concrete Structures using Steel Wire Reinforced Polymer." ACI Special Publication, Volume SP-230-43, pp 743-762.

Fox Industries Engineered Products (2002). Technical Product Data Sheet. <http://www.foxind.com/datasheet.asp?sheet=231>, accessed December 1, 2005.

Fyfe Company LLC (2005). Technical Product Data Sheet. <http://www.fyfeco.com/products/misc.html>, accessed December 1, 2005.

Gallagher, Brian (2005). "Restoring Our Heritage", *Revitalization Magazine*, May 2005, pp 11-13.

Hardwire. (2002). "What is Hardwire?", www.hardwirellc.com, Pocomoke City, Maryland.

Harries, K.A. and J. Aidoo (2005). "Deterioration of FRP-to-Concrete Bond Under Fatigue Loading." *International Symposium on Bond Behaviour of FRP in Structures*, Hong Kong, International Institute for FRP in Construction, 2005.

Harries, K.A., Zorn, A., Aidoo, J. and Quattlebaum, J., (2007). Deterioration of FRP-to-Concrete Bond Under Fatigue Loading. *Advances in Structural Engineering Special Issue on Bond Behaviour of FRP in structures* (in press).

Harries, K.A., Zorn, A., and Reeve, B. (2006). "Effect of Adhesive Modulus on the Monotonic and Fatigue Behavior of Externally Bonded CFRP Strips", *Proceedings of the Third International Conference on FRP Composites in Civil Engineering (CICE 2006)*, December 13-15 2006, Miami, Florida, USA, paper #26.

Heffernan, P.J. (1997). *Fatigue Behaviour of Reinforced Concrete Beams Strengthened with CFRP Laminates*, Ph.D. Dissertation, Department of Civil Engineering, Royal Military College of Canada, Kingston, Ontario.

Helgason, T. and Hanson, J.M. (1974). "Investigation of Design Factors Affecting Strength of Reinforcing Bars-Statistical Analysis", *Abeles Symposium on Fatigue of Concrete*, SP-41 ACI, pp 107-138.

Huang, X., Birman, V., Nanni, A., and Tunis, G. (2005). "Properties and Potential for Application of Steel Reinforced Polymer and Steel Reinforced Grout Composites." *Composites Part B: Engineering*, Volume 36, Issue 1, pp 73-82.

International Concrete Repair Institute (1997). *Concrete Surface Profile Chips*. ICRI, Sterling, VA.

Kim, Y.J., Fam, A., Kong, A., and El-Hacha, R. (2005). "Flexural Strengthening of RC Beams Using Steel Reinforced Polymer (SRP) Composites." ACI Special Publication, Volume SP-230-93, pp 1647-1664.

Lopez, A., and Nanni, A. (2005). "Strengthening of a Reinforced Concrete Bridge with Externally Bonded Steel Reinforced Polymer", *FRP International*, Volume 2, Issue 3, pp 15-18.

Lu, B., Silva, P., Nanni, A., and Baird, J. (2005). "Retrofit for Blast-Resistant RC Slabs with Composite Materials." ACI Special Publication, Volume SP-230-76, pp 1345-1360.

Mallet, G. (1991). *Fatigue of Reinforced Concrete*. Transportation and Road Research Laboratory (TRRL) State of the Art Review / 2, London, U.K.

- Matana, M., Galecki, G., Maerz, N., Nanni, A. (2005). "Concrete Substrate Preparation and Characterization Prior to Adhesion of Externally Bonded Reinforcement." *International Symposium on Bond Behaviour of FRP in Structures*, Hong Kong, pp 133-139.
- Matana, M., Nanni, A., Dharani, L., Silva, P., and Tunis, G. (2005). "Bond Performance of Steel Reinforced Polymer and Steel Reinforced Grout." *International Symposium on Bond Behaviour of FRP in Structures*, Hong Kong, pp 125-132.
- Moss, D.S. (1980). "Axial Fatigue of High Yielding Reinforcing Bars in Air," Transport and Road Research Laboratory, *Report SR622*.
- Oehlers, D.J. (2005). "Generic Debonding Mechanisms in FRP Plated Beams and Slabs", *Proceedings of the International Symposium on Bond Behavior of FRP in Structures*, December 7-9, 2005, Hong Kong, pp 561-566.
- Pecce, M., Ceroni, F., Prota, A., and Manfredi, G. (2006). "Response Prediction of RC Beams Externally Bonded with Steel-Reinforced Polymers." *ASCE Journal of Composites for Construction*, Vol. 10, No. 3, pp 195-203.
- Prota, A., Tan, K., Nanni, A., Pecce, M., and Manfredi, G. (2006). "Performance of RC Shallow Beams Externally Bonded with Steel Reinforced Polymer." *ACI Structural Journal*, Vol. 103, No. 2, pp 163-170.
- Quattlebaum, J.B. (2003). *Comparison of Three CFRP Flexural Retrofit Systems under Monotonic and Fatigue Loads*, MS Thesis, University of South Carolina Department of Civil and Environmental Engineering, Columbia, SC.
- Reeve, B.Z. (2005). *Effect of Adhesive Stiffness and CFRP Geometry on the Behavior of Externally Bonded CFRP Retrofit Measures Subject to Monotonic Loads*. MS Thesis, University of Pittsburgh Department of Civil and Environmental Engineering, December 2005.
- Sika Corporation (2005). Technical Product Data Sheet. <http://www.sikaconstruction.com/con/con-prod-name.htm#con-prod-Sikadur23LoModGel>, accessed December 1, 2005.
- Steel-Belted Reinforcement Product Meets Blast-Resistance Need. (2004). *Journal of Failure Analysis and Prevention*, Vol. 4, No. 6.
- Teng, J.G., Smith, S.T., Yao, J. and Chen, J.F. (2001). "Intermediate Crack Induced Debonding in RC Beams and Slabs," *Construction and Building Materials*, Vol. 17, No. 6-7, pp 447-462.
- Teng, J.G., Lu, X.Z., Ye, L.P. and Jiang, J.J. (2004). "Recent Research on Intermediate Crack Induced Debonding in FRP Strengthened Beams." *Proceedings of the 4th International Conference on Advanced Composite Materials for Bridges and Structures*, Calgary 2004.

Tilly, G.P., and Moss, D.S. (1982). “Long Endurance Fatigue of Steel Reinforcement”, *IABSE Reports, International Association for Bridge and Structural Engineering*, 37, Zurich, Switzerland, pp 229-238.

Timoshenko, S.P and Goodier, J.N. (1987 reissue) *Theory of Elasticity*, 3rd edition.

Wobbe, E., Silva, P., Barton, B.L., Dharani, L.R., Birman, V., Nanni, A., Alkhrdaji, T., Thomas, J., and Tunis, G. (2004). “Flexural Capacity of RC beams externally bonded with SRP and SRP”, *Proceedings of the Society for the Advancement of Materials and Process Engineering*, Symposium, Long Beach, CA.

Zorn, A. (2006). *Effect of Adhesive Stiffness and CFRP Geometry on Behavior of Externally Bonded CFRP Retrofit Measures Subject to Fatigue Loads*. MS Thesis, University of Pittsburgh Department of Civil and Environmental Engineering, March 2006.